2013-07-31

Study of Interactions between DNA and Gold Nanoparticles for Biosensor Applications

Jiaqi Zou
University of Miami, jiaqizou@gmail.com

UNIVERSITY OF MIAMI

STUDY OF INTERACTIONS BETWEEN DNA AND GOLD NANOPARTICLES FOR BIOSENSOR APPLICATIONS

By

Jiaqi Zou

A DISSERTATION

Submitted to the Faculty
of the University of Miami
in partial fulfillment of the requirements for
the degree of Doctor of Philosophy

Coral Gables, Florida

August 2013

UNIVERSITY OF MIAMI

A dissertation submitted in partial fulfillment of
the requirements for the degree of
Doctor of Philosophy

STUDY OF INTERACTIONS BETWEEN DNA AND GOLD NANOPARTICLES FOR BIOSENSOR APPLICATIONS

Jiaqi Zou

Approved:

_____
Na Li, Ph.D.
Assistant Professor
Department of Mechanical
& Aerospace Engineering

_____
M. Brian Blake, Ph.D.
Dean of the Graduate School

_____
Weiyong Gu, Ph.D.
Professor
Department of Mechanical
& Aerospace Engineering

_____
Hongtan Liu, Ph.D.
Professor
Department of Mechanical
& Aerospace Engineering

_____
Chun-Yuh Charles Huang, Ph.D.
Assistant Professor
Department of Biomedical Engineering

ZOU, JIAQI (Ph.D., Mechanical Engineering)

Study of Interactions between DNA and Gold Nanoparticles for Biosensor Applications (August 2013)

Abstract of a dissertation at the University of Miami.

Dissertation supervised by Assistant Professor Na Li.
No. of pages in text. (108)

Optical biosensors that utilize unmodified Gold nanoparticles (GNPs) and nucleic acid probes are one of the most popular biosensors, thanks to the unique colorimetric and fluorescent properties of GNPs. These biosensors are based on the interactions between GNPs, DNA probes, and target molecules. As a result, their performance is dependent on the relative binding strength between DNA probes, GNPs, and target molecules. However, there is no systematic study on the thermodynamics and kinetics of interactions between DNA and GNPs. Moreover, there is no accessible tool for biomedical researchers to quantitatively study the interactions between DNA probes and target molecules, which could be DNA or other molecules. The current work consists of experimental study of the interactions between DNA and GNPs, as well as computational study of the interactions between DNA and target molecules.

Systematic investigations on both thermodynamics and kinetics of interactions between DNA molecules and GNPs have been conducted. In the thermodynamics study, we developed titration experiments based on critical coagulation concentration (c.c.c.). To study the sequence dependency of DNA molecules, we used nucleobases, ribonucleosides, deoxynucleosides, deoxynucleoside monophosphate, deoxynucleoside

triphosphates, and homo-oligonucleotides with 15 nucleotides (nt). We found that DNA molecules with bases thymine (T) have the weakest binding strength to GNPs, which is due to the lack of amine groups in T as indicated by previous studies. To study the length dependency of DNA molecules, we used homo-oligonucleotides of different lengths, ranging from 5 nt to 100 nt. It was found that shorter DNAs generally bind to GNPs stronger compared to longer DNAs. To study the difference of single-stranded DNA (ssDNA) and double-stranded DNA (dsDNA), we used dsDNA in different conformations. It was discovered that single-stranded DNA (ssDNA) binds to GNPs much stronger than double-stranded DNA (dsDNA). In addition, dsDNA with overhangs or mismatches bind to GNPs differently than completely complementary dsDNA. In kinetics study, we developed fluorescent experiments based on fluorescent quenching effect of gold surfaces on fluorophores. To study the kinetics and effect of salt on the interactions between DNA and GNPs, we used 15mer homo-oligonucleotides and two sets of completely complementary dsDNA. It was observed that the longer the incubation time and/or the higher the NaCl concentration, the more DNAs bind to GNPs. We also found that the binding kinetics and the effect of salt is sequence dependent.

To provide a user-friendly tool to quantitatively study interactions between DNA and target molecules, a thermodynamics based computational model was implemented with two Microsoft® Excel spreadsheets that utilized macros and visual basic applications (VBA). One spreadsheet is for up to three DNA molecules and the other spreadsheet is for up to two DNA molecules and one non-nucleic acid molecule. We have extensively tested and verified the two spreadsheets under various situations.

The results of this work could be used to optimize the design of biosensors based on GNPs and nucleic acid probes, thus improving on selectivity and sensitivity of these biosensors.

ACKNOWLEDGEMENTS

I would like to extend my sincere gratitude and appreciation to my Ph.D. dissertation advisor and chair of the committee, Dr. Na Li for her patient guidance, practical advice, multiple revisions, and consistent encouragement throughout the work. There is a quiet force in her sweet smile, which gives me power through my Ph.D. study. I am very proud and lucky to have her as my academic advisor.

My thanks also go to Dr. Weiyong Gu and Dr Hongtan Liu of Department of Mechanical & Aerospace Engineering, and Dr. Chun-Yuh Charles Huang of Department of Biomedical Engineering, University of Miami, for accepting the invitation as my dissertation committee members, as well as their helpful suggestions and advice.

I would like to thank the Department of Mechanical & Aerospace Engineering and Dr. Na Li for providing the full financial support for four years.

I would like to thank all the other faculty and staff members in the Department of Mechanical & Aerospace Engineering.

Finally, I would like to give my deepest sense of gratitude to my family members for their constant love, understanding and support.

Jiaqi Zou

August 2013

CONTENTS

LIST OF TABLES

LIST OF FIGURES

Chapter 1 Introduction

1.1 Biosensors

1.1.1 What is Biosensor

Biosensor-related research has been through explosive growth over the last several decades [1]. Biosensors are generally defined as analytical devices, used for the detection of an analyte [2]. A biosensor is made of a bio-recognition component, biotransducer component, electronic system, processor and display (Figure 1-1) [3]. The objective of the design of a biosensor is to provide quick, convenient testing [4].

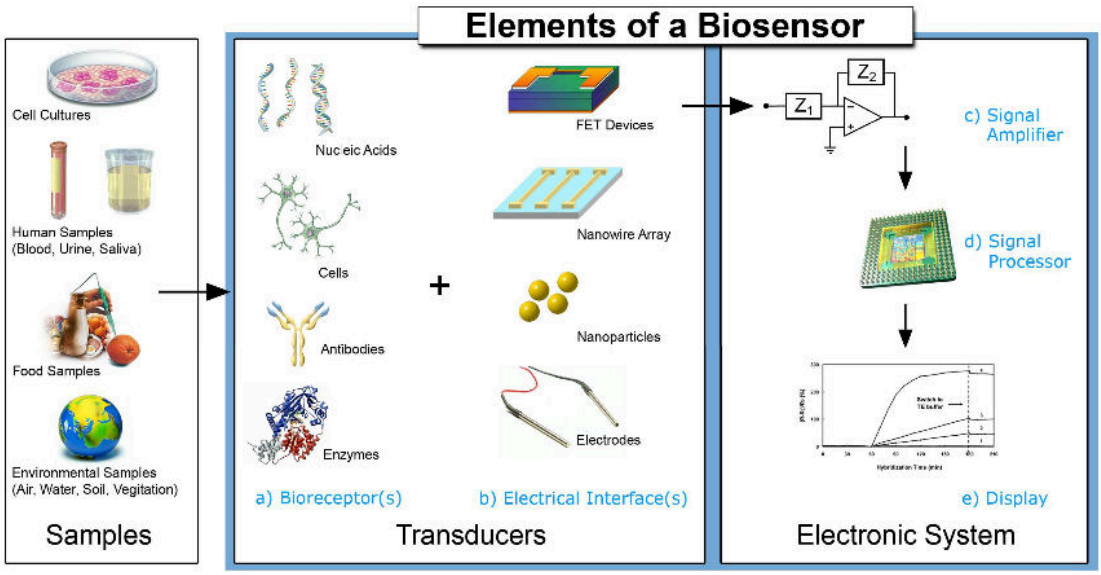

Figure 1-1 Elements and selected components of a typical biosensor [3].

There are numerous potential applications of biosensors. A common example of commercial biosensor is glucose monitor, which monitors glucose level in diabetes patients. In addition, environmental applications include detection of pesticides and river water contaminants, such as heavy metal ions like mercury, lead and cadmium [5]. Also

there is remote sensing of airborne bacteria like the sensing pathogens [6]. Some applications are for the discovery and evaluation of biological activity of new drug compounds [7]. Furthermore, applications could be used to detect toxic metabolites such as mycotoxins [8].

1.1.2 Types of Biosensors

There are five major types of biosensor by measured property: electrochemical biosensors, electrical biosensors, mass sensitive biosensors, thermal biosensors, and optical biosensors. Electrochemical biosensors measure the change in current or voltage. Electrical biosensors measure change in surface conductivity or electrolyte conductivity. Mass sensitive biosensors measure the change of resonant frequency. Thermal biosensors measure the heat of reaction or heat of absorption. Optical biosensors measure change in light adsorption or photon count for a luminescent or fluorescent output. Optical biosensors are the most popular type of biosensors [9].

Optical biosensors are powerful alternative to conventional analytical techniques due to their particularly high sensitivity, specificity, small dimension and cost effectiveness [10, 11]. Some optical biosensors are based on the phenomenon of surface plasmon resonance (SPR) [12, 13]. Other optical biosensors are essentially based on the changes in absorbance or fluorescence. Nanobiosensors are those using nanomaterial, such as gold and silver nanoparticles [14].

1.2 Gold Nanoparticles (GNPs) Based Optical Biosensor

Gold has been used in a variety of situations through human history [15]. The unique optical, electrical and electrochemical properties of gold nanoparticles can be utilized in biosensor applications [16-18]. Over the last decade, there have been a lot of important developments for the application of GNPs in detection of nucleic acids or other molecules, based on the optical property of Au NPs [19, 20].

One of the unique properties is its colorimetric property. Aggregation of GNPs changes the color of colloid solution from deep red to violet or deep blue [21-23]. The extinction spectrum of gold nanoparticles depends on particle size, particle shape, particle aggregate morphology, and dielectric environment of the medium [17, 21, 24-29]. Figure 1-2 shows TEM images and extinction spectra of gold nanoparticles in various size and shape [30].

The other unique optical property is its fluorescence quenching effect on fluorescent dye caused by foster transfer [31]. The effect of GNPs on dye depends on distance. Usually within the distance of 0-5 nm, most of the fluorescence intensity would be quenched [32]. The quenching effect decreases with the cube of the distance between the metal surface and the fluorescent dye [33]. Under lager distance there is an increase in the radiative decay rate at a larger distance of the fluorescent dye [32]. Under larger distances enhancement of the strength is observed.

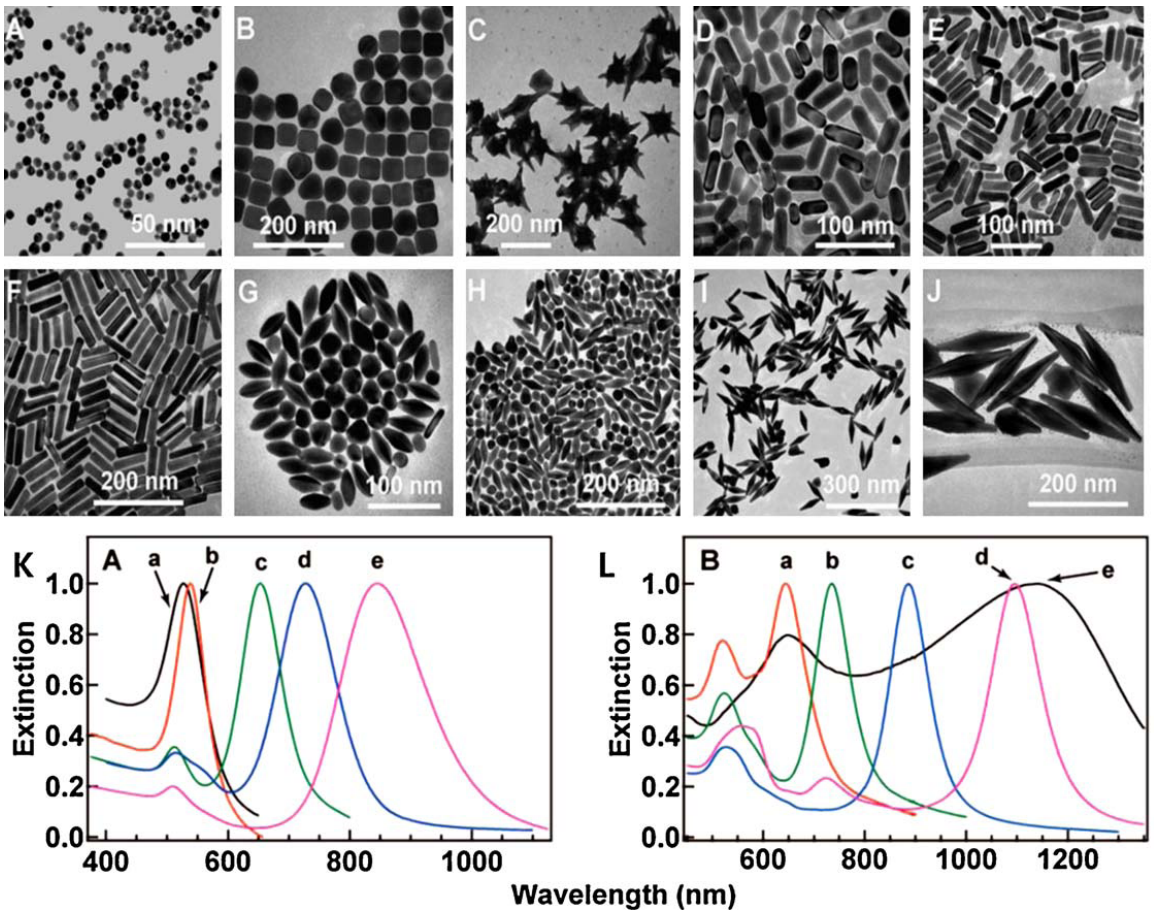

Figure 1-2 TEM images and the extinction spectra of GNPs [30].

1.2.1 Colloid Stability Theory

Gold nanoparticles that are used in our study are in colloid status. The stability of colloids is based on pair potential. The pair potential is composed of attractive van der Waals and repulsive electrostatic potential. It is the basis of the DLVO (Derjaguin, Landau, Verwey and Overbeek) [34-36] theory for colloid stability. Under the assumptions that the particle separation is small compared with diameter and electric double layer is small [37], the pair potential is determined by

$$V = V_A + V_R = -\frac{Aa}{12h} + 2\pi\varepsilon_r\varepsilon_0 a\psi_0^2 ln[1 + \exp(-\kappa h)] \qquad (1\text{-}1)$$

where, V is total interaction energy, V_A is Van der Waals attraction energy, VR is electrostatic potential energy, A is the Hamaker constant, h is the smallest distance between surfaces of two particles, a is particle radius, ε_r is the dielectric constant of the medium (80 for water), ε_0 (8.85E-12 $F*m^{-1}$) is electric permittivity of free space, ψ_0 is surface potential, and κ is reciprocal of Debye length

$$\kappa = \left[\frac{1000e^2 N_A(2I)}{\varepsilon_r \varepsilon_0 kT}\right]^{1/2} \quad (1\text{-}2)$$

where e (1.602E-19Q) is electric charge of electron, N_A (6.02E+23) is Avogadro number with value of, I is ionic strength, k (1.38E-23 $m^2*kg*s^{-2}*k^{-1}$) is Boltzmann constant and T is temperature in Kelvin.

The electrostatic repulsion depends on the stern potential and the thickness of the electric double layer, κ^{-1}. Moreover, counter-ion would affect the thickness of the electric double layer. Various factors would affect the stability if we assume the attraction potential remains the same. For example, surface charge, salt type and salt concentration. The larger the surface charge is, the more stable the colloid is. In addition, the higher the concentration of salt added to the solution, the less time the colloid solution would remain stable [38]. A typical curve for total potential in different salt concentration is plotted (Figure 1-3) for GNPs with radius of 6.5 nm (a=6.5 nm), Hamaker constant of 1.94E-19J (A = 1.94E-19J), and surface potential is -50 mV (ψ_0 = -0.05V). Curve a, b and c represents the potential with different salt concentration. The salt concentrations for curve a, b and c are 0.01M, 0.053M and 1M. Primary maximum of total potential energy increase with decrease of salt concentration, this barrier to aggregation only make the

solution stabilized kinetically. Therefore, the larger the barrier the longer the colloid system would remain stable.

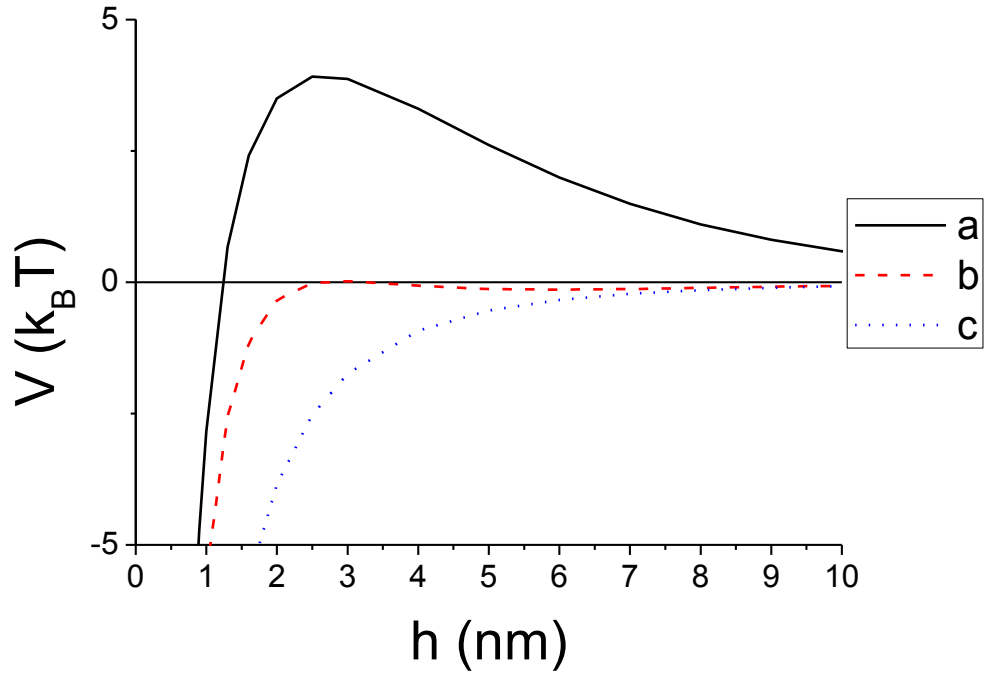

Figure 1-3 Effect of salt concentration on total potential. The potential was plotted in units of k_BT [39]. (a) 0.01M NaCl (b) 0.053M NaCl (c) 1M NaCl

As shown in Figure 1-3, curve a represents the condition while surface charge density is high, electrolyte concentration is low and potential barrier is high, which means the colloid is kinetically stable. Curve b represents the potential barrier is equal to zero, at this condition the colloid would coagulate fast thus very unstable. Curve c represents the condition while there is no potential barrier, which results in very fast coagulation of the colloid. In curve b there is a point at which the potential energy barrier opposing coagulation just disappears. It is usually called the critical coagulation concentration (c.c.c.). An estimate of the c.c.c. can be obtained by from pair potential equation. As we could see from the curve b, when the potential energy barrier just disappears we have:

$$V = V_A + V_R = 0 \tag{1-3}$$

$$\frac{d(V)}{dh} = \frac{d(V_A + V_R)}{dh} = 0 \tag{1-4}$$

And at that point κh=1 [36]. Substituting this value into equations (1-1), (1-2) and (1-3) under assumptions that electric double layer is smaller than distance between particles, the distance between particles are smaller than diameter of the particle, and surface potential is smaller than 25 mV,

$$c.c.c. = \frac{0.039\pi^2 \varepsilon_r^3 \varepsilon_0^3 \psi_0^4 kT}{A^2 e^2 N_A} \tag{1-5}$$

1.2.2 Biosensors Based on Unmodified GNPs and Nucleic Acid Probes

The gold nanoparticle based colorimetric and fluorescent method for DNA and other molecules detection have been widely reported in recent years. [20, 40, 41]. For nucleic acid detection, the target recognition is based on the principle of complementary base paring, adenine (A) to thymine (T) and cytosine (C) to guanine (G) in DNA [42]. For non-nucleic acid detection, the target recognition is based on the binding of target molecule to aptamer. Aptamers are short DNA or RNA oligonucleotides that can bind with high affinity and specificity to a specific target molecule. The target molecules could be of wide range, organic or inorganic, such as metal ions, drugs, proteins or other molecules [43, 44]. Aptamers show a very high affinity, specificity and resolution to their targets [45]. Aptamers would fold into a different structure when bind with their target

molecule. [46]. In other words, they are no longer single-stranded nucleic acids when bound with target molecules [47].

For nucleic acids detection, Li and coworkers [48] found that ssDNA and dsDNA have different propensities to adsorb on gold nanoparticles. As shown in Figure 1-4A, without target ssDNA, the colloid remains to be pink. With target, solution would form double stranded DNAs leads to aggregation and tuned the solution into blue. Similarly, Kim and coworkers [49] reported a fluorescent detection method for DNA (Figure 1-4B). With target, double stranded DNA would form and fluorescence intensity would not be quenched. Without target, fluorescence intensity would be quenched.

A B

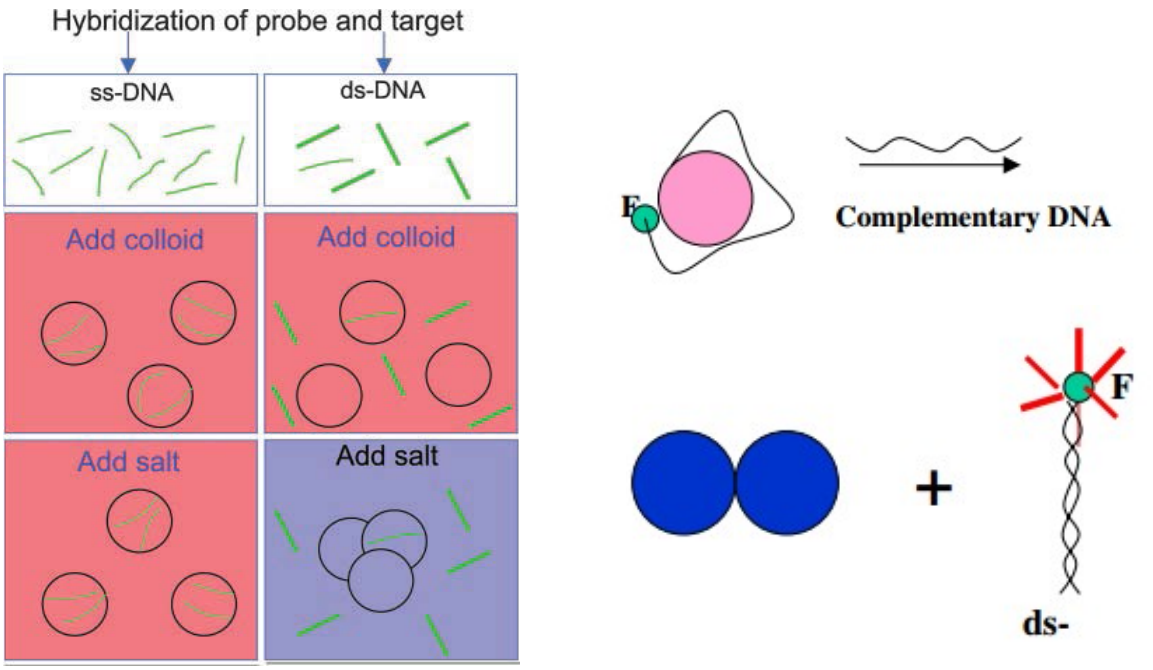

Figure 1-4 Applications of GNP-based biosensor using nucleic acids for the detection of dsDNA using (A) Colorimetric method [48], and (B) Fluorescent method [49].

For detection of non-nucleic acids, Wang and coworkers [50] demonstrated that color changes of unmodified gold nanoparticles can be used to probe K^+ (Figure 1-5A). With target, the formation of G-quartets would not stabilize GNPs. Without target, single stranded aptamer would stabilize GNPs. Similarly, Wang and coworkers reported a gold nanoparticle-based aptamer target binding readout for ATP assay, (Figure 1-5B) [51]. With ATP, ATP would bind with aptamer and ssDNA probe would stabilize GNPs. Without ATP, aptamer and ssDNA probe would form into dsDNA thus not able to stabilize GNPs.

A B

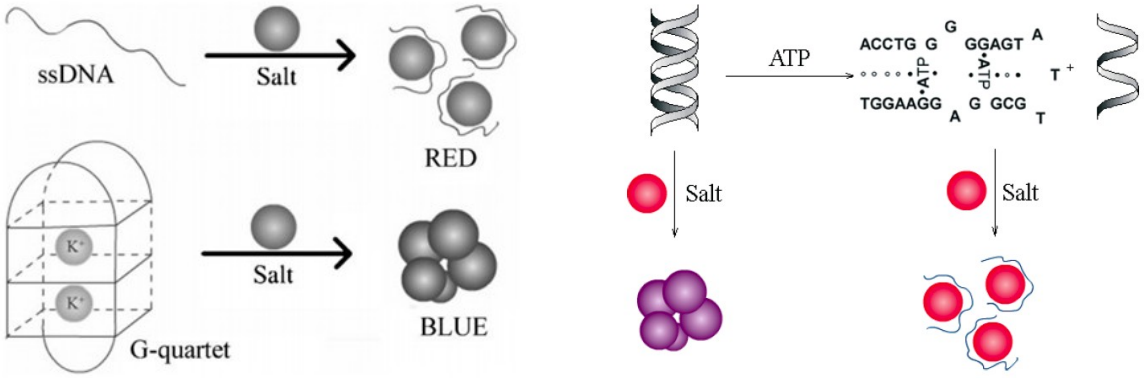

Figure 1-5 Applications of GNP-based biosensor using nucleic acids (A) Colorimetric detection for K^+ [50] (B) Colorimetric detection for ATP [51]

1.3 Objectives of the Dissertation

These biosensors are based on interactions between DNA, GNPs and target molecules. It is the interactions, thermodynamically and kinetically, of the probe to target molecule binding reaction and probe to GNPs binding reaction that is the essential component in performance of the biosensor [52].

The goal of this work is to help the design of biosensors that are based on the interactions between DNA and GNPs. Therefore, there are two objectives:

1. Experimental study of interactions between DNA and GNPs

Some works have been reported on the interactions between DNA and GNPs. Nevertheless, disagreement exists among their methods and results. Most of the studies are not systematic. Therefore, we will conduct systematical experimental investigation on the interactions between DNA in different formations (nucleobase, nucleoside, nucleotide, oligonucleotide, completely matched dsDNA, dsDNA with overhangs and dsDNA with mismatches) and GNPs, thermodynamically and kinetically. Effect of incubation time and salt concentration on interactions between ssDNA and dsDNA will be investigated. Methods we will use include colorimetric method and fluorescent method. This work would aid the design of biosensors based on GNPs and DNA probes.

2. Computational study of interactions between DNA and target molecules

Some literatures have been reported related to the studying of the interactions between DNA and target molecules. However, none of these methods is accessible to researchers who are not familiar with thermodynamic theory and even for those with adequate knowledge, complicated and tedious math could be a hinder to them. Therefore, we will develop two thermodynamic modeling tools based on Microsoft® Excel and Visual Basic Applications. This tool will allow quantitatively study on the interactions between nucleic acid species and nucleic acid species or the interactions between nuclei acids species and non-nucleic acid species.

Chapter 2 Experimental Study of Interactions between GNPs and Nucleobases, Nucleosides and Nucleotides

2.1 Literature Review and Introduction

Some researchers have reported the interactions between GNPs and nucleosides, nucleotides and nucleobases by various techniques, such as UV-vis spectra [53, 54], heats of desorption [55], transmission electron microscopy (TEM) [56], isothermal titration calorimetry (ITC) [54] and so on [53, 57]. Table 2-1 shows a list of literature on interactions between gold and nucleobase, deoxynucleoside, ribonucleoside, deoxynucleoside monophosphate and deoxynucleoside triphosphate. These studies are not systematic. Most of the studies only focus on either nucleobases or nucleosides or nucleotides. The results from them are not comparable with each other due to difference on experimental system. Therefore, the objective of this chapter is to conduct systematic investigation on the thermodynamics of the interactions between GNPs and nucleobase, nucleoside and nucleotide, using one experimental system.

Table 2-1 List of literature on interactions between gold and nucleobase, nucleoside, and nucleotide.

Literature	Method	Gold	Nucleic acid	Ranking
Gourishankar, 2004 [54]	UV-spectra and Isothermal titration (ITC)	6.5 nm GNPs	Base and PNA monomers	C>G>A>T
Yang, 2007 [57]	Melting transition measurements	5 nm GNPs	mononucleotides	A>G>C>T
Demers, 2002 [55]	Heats of desorption	Gold thin films	Bases	G>A>C>T
Zhao, 2007 [56]	UV-spectroscopy Transmission electron microscopy (TEM)	10 nm GNPs	mononucleotides	A>C>G~T
			Bases and nucleosides	G>A>C>T

2.2 Materials and Methods

2.2.1 Materials

Chemicals are purchased from SIGMA-ALDRICH® (St. Louis, Missouri, United States) if not otherwise specified. 1 X buffer is composed of 0.1xPBS, 15 mM NaCl and 5 mM KCl. Powder of deoxynucleoside monophosphates (-20 °C), nucleobases (25 °C), deoxynucleosides (4 °C), and ribonucleosides (4 °C) were dissolved in deionized water. 10mM deoxynucleoside triphosphates (-20 °C) stock solution (30 mM Trizma-HCl, 50mM NaCl and 10mM $MgCl_2$) were diluted using 1 X buffer (0.1xPBS, 15 mM NaCl and 5 mM KCl). The names and abbreviates for nucleobases, nucleosides and nucleotides are listed in following table.

Table 2-2 Names and abbreviates for nucleobases, nucleosides and nucleotides

Name	Abbreviate
Nucleobase	A, C, G, T
Ribonucleoside	r(A), r(C), r(G), r(T)
Deoxynucleoside	d(A), d(C), d(G), d(T)
Deoxyucleoside monophosphate	NMP (AMP, CMP, GMP, TMP)
Deoxyucleoside triphosphate	NTP (ATP, CTP, GTP, TTP)

2.2.2 Synthesis and Characterization of GNPs

Gold nanoparticles were synthesized using citrate reduction method first reported by Turkevich and coworkers [58]. 10.0 mM hydrogen tetrachloroaurate stock solution was prepared by dissolving 0.2 g $HAuCl_4.3H_2O$ in 50 mL deionized water to make stock solution of gold (III) ions and then stored in a brown bottle. 1% trisodium citrate was prepared by dissolving 0.5 g $Na_3C_6H_5O_7.2H_2O$ (sodium citrate) in 50 mL deionized water. During the synthesis 50 mL of 1.0 mM $HAuCl_4$ (ten times dilution of 10.0 mM stock) was added to an Erlenmeyer flask on a stirring hot plate. Then a magnetic stir bar was added and the solution was brought to a boil, while temperature was maintained at 200°C and the stirring speed was set to 500 RPM. To the boiling solution, 5 mL of a 1% solution of trisodium citrate was added. Stirring was continued until the solution turned into deep red. Then GNPs solution was filtered by 0.2 μm filters and stored at 4 °C.

Several methods were used to characterize GNPs. Based on measurement of extinction spectra [59] taking synergy 2 Multi-Mode Microplate Reader (manufactured by BioTek® Instruments, Winooski, Vermont, United States), the size was determined around 13.8 nm and the concentration was determined around 11 nM. Dynamic light scattering (DLS) [60-62] and electrophoretic light scattering (ELS) were performed by Delsa™Nano C (manufactured by Beckman Coulter, Pasadena, California, United States), the size was determined around 21 nm and zeta potential was determined around -50 mV. The NaCl concentration in the GNPs solution was calculated to be 10 mM based on law of mass conservation. The pH value of the GNPs solution was determined around 6 by pH paper.

2.2.3 Critical Coagulation Concentration (c.c.c.) Based Titration Experiments

Firstly, 1000 μL GNPs was mixed with 500 μL nucleotide dilution and incubated for 48 hours. Secondly, 40 μL per well of the mixture was loaded into 96 well half-area plate, which is manufactured by Greiner Bio-One® (Monroe, North Carolina, United States). Thirdly, 40 μL NaCl in various concentrations were added into those mixtures and incubated for 5 minutes. Lastly, absorbance at 520 nm and 650 nm was scanned by Synergy 2 Multi-Mode Microplate Reader. All experiments were carried out under room temperature (25 °C).

The result of titration was plotted as final NaCl concentration verse ratio of absorbance at 650 nm and 650 nm (A_{650}/A_{520}). Final NaCl concentration includes NaCl in GNP, NaCl in dilution and NaCl added. The value of A_{650}/A_{520} of each sample was subtracted by the control group with deionized water added instead of NaCl. A typical plot for 22,500 nM GTP we got from titration experiment was shown in Figure 2-1. The equation that we used is the Langmuir EXT1 in Origin®.

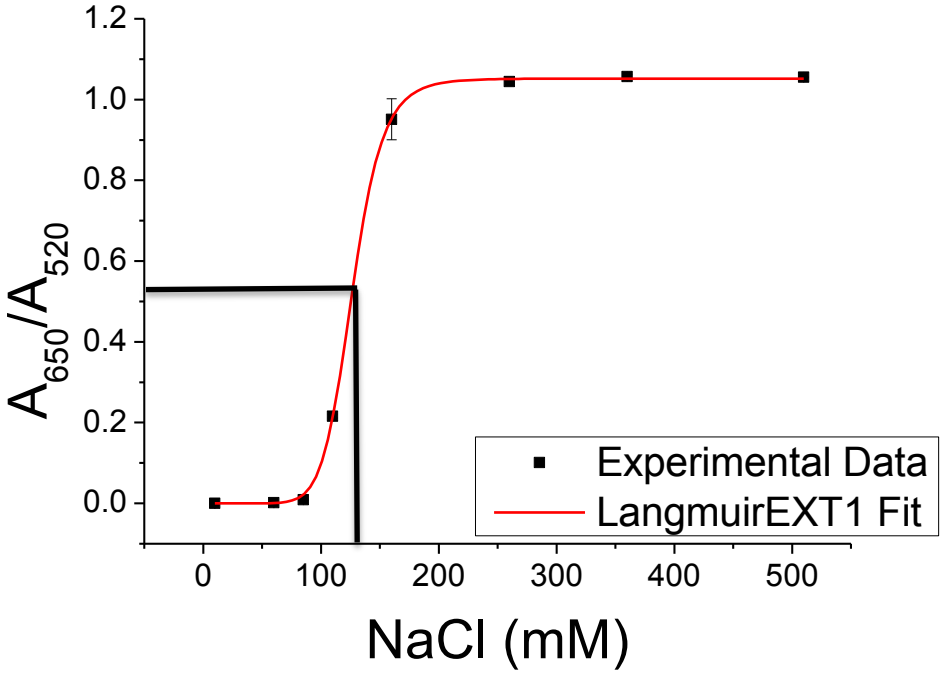

Figure 2-1 Determination of c.c.c. in salt titration experiment for 22,500 nM GTP.

The result of titration was fitted by Langmuir EXT1 in Origin®:

$$y = \frac{abx^{1-c}}{1 + bx^{1-c}} \tag{2-1}$$

Here y is A_{650}/A_{520}, x is NaCl concentration, a, b and c are constants. a is the maximum of A_{650}/A_{520}. c.c.c. is the NaCl concentration where the aggregation rate is determined only by diffusion and could establish the stabilization of colloid. Here we define c.c.c. is the NaCl concentration where the A_{650}/A_{520} is at the half of a. That is,

$$y = \frac{abx^{1-c}}{1 + bx^{1-c}} = \frac{a}{2} \tag{2-2}$$

from which we get,

$$x = c.c.c. = b^{\left(\frac{-1}{1-c}\right)} \quad (2\text{-}3)$$

In this chapter, the c.c.c. value that we defined is not the true c.c.c. value in Chapter 1. Instead, it a characteristic parameter to indicate the stabilizing effect of nucleotide on GNPs.

2.2.4 Determination of Dissociation Constant

The dissociation constant (K_D) is commonly used to describe the affinity, or binding strength, between one molecule and another molecule or surface. Binding strengths are influenced by non-covalent intermolecular interactions between the one molecule and another molecule or surface such as hydrogen bonding, electrostatic interactions, hydrophobic and Van der Waals forces [63, 64].

The original Langmuir equation relates the coverage or adsorption of molecules on a solid surface to gas pressure or concentration of a medium above the solid surface at a fixed temperature [65]. We found that the original Langmuir equation could not describe absorption behavior we observed. Instead, we found that the absorption formula for the dilute solutions on energetically heterogeneous solids [66, 67] named Freundlich Langmuir isotherm [68] describes adsorption behavior we observed very well. Dissociation constant is the concentration of molecule, at which half the binding sites are occupied.

$$y = \frac{abx^{1-c}}{1 + bx^{1-c}} \quad (2\text{-}4)$$

where y is the experimental data that reflect the extent of molecule bound to GNPs. x is concentration of molecules. a, b and c are constants. For molecules that destabilize GNPs, such as nucleobases and nucleosides, y is A_{650}/A_{520}. For nucleotide molecules that stabilize GNPs, such as nucleotides and DNAs, y is c.c.c.. a is a constant which indicates the maximum of y, b is a constant depends on the adsorption energy and c is the heterogeneity parameter characteristic for a given adsorption system.

Dissociation constant is the concentration of molecule, at which half the binding sites are occupied.

and $$y = \frac{abx^{1-c}}{1 + bx^{1-c}} = \frac{a}{2} \quad (2\text{-}5)$$

we get $$x = K_D = b^{\left(\frac{-1}{1-c}\right)} \quad (2\text{-}6)$$

Two examples are shown in Figure 2-2. Figure 2-2A is K_D of d(T) fitted from A_{650}/A_{520}. Figure 2-2B is K_D of GMP fitted from c.c.c.. The equation that used to fit the curve is Langmuir EXT1 equation in Origin®. The value of A_{650}/A_{520} and c.c.c. could represent the ability of molecules of aggregating or stabilizing GNPs. The smaller the K_D the stronger the binding is.

A

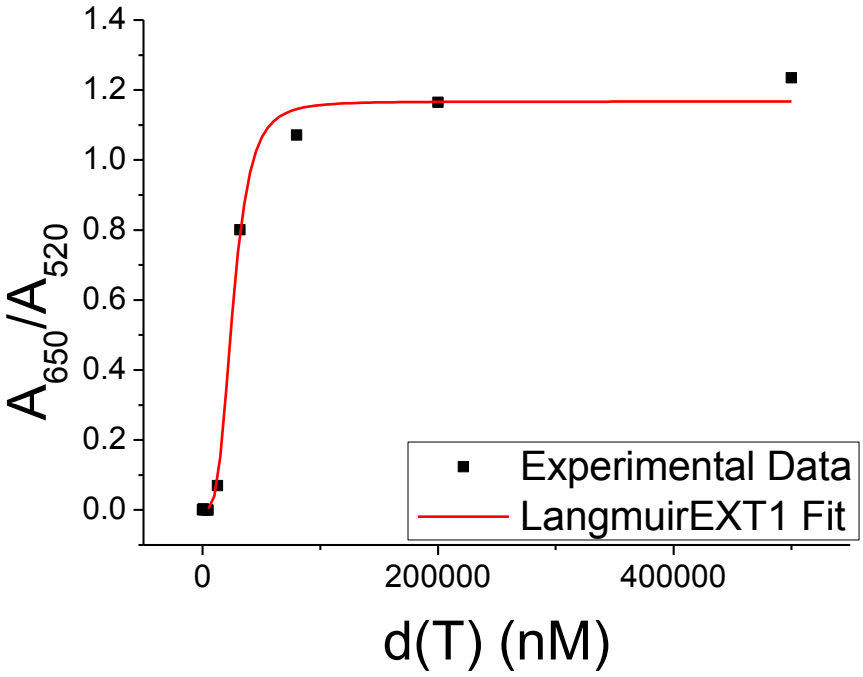

B

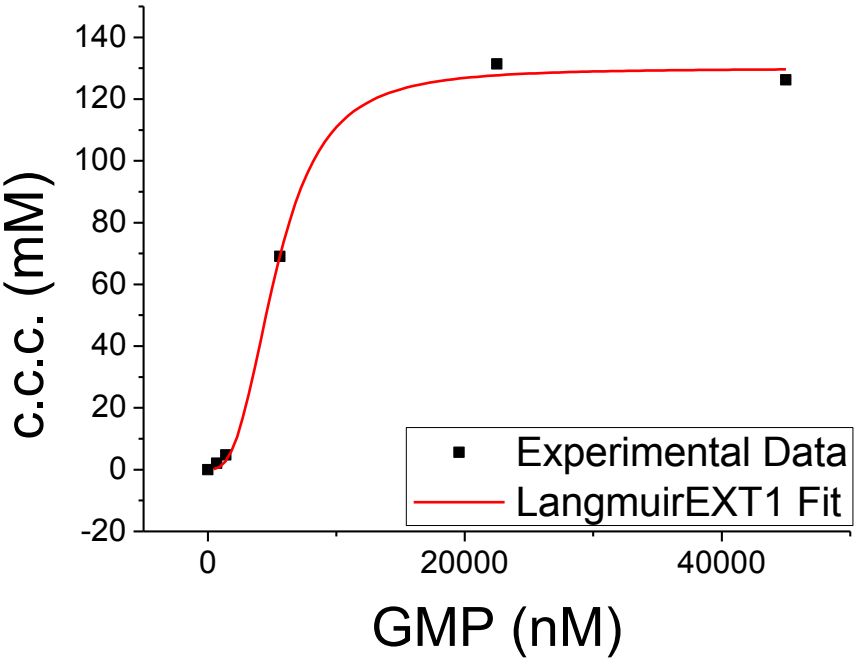

Figure 2-2 Determination of dissociation constant (K_D) for d(T) and GMP.

2.3 Results and Discussion

2.3.1 Interactions of GNPs with Nucleobase and Nucleoside

Nucleobase, nucleoside and nucleotide could bind to GNPs surfaces through amine groups of nucleobases [54]. However, due to its lack of strongly negatively charged phosphate backbone as nucleotide, it would not prevent GNPs from aggregation. On the contrary, nucleobase and nucleoside would aggregate GNPs upon mixing. Therefore, we did colorimetric experiments to investigate the binding of different nucleobases, deoxynucleosides and ribonucleosides to GNPs by comparing their ability of aggregating GNPs.

In this study, UV-vis spectroscopy was conducted to characterize the absorbance spectrum of GNPs aggregated by nucleobases, deoxynucleosides and ribonucleosides. First, 40 μL sample was added to 40 μL GNPs. Later, the absorbance at wavelength 650 nm and 520 nm was scanned. We use the value of adsorption dividend ratio at wavelength of 650 nm to 520 nm (A_{650}/A_{520}) would to reflect color of GNPs. A typical experiment of 64 μM nucleobases mixed with GNPs was shown in Figure 2-3. It clearly shows that A, C and G binds to GNPs surfaces more rapidly than T, and the slowest is U.

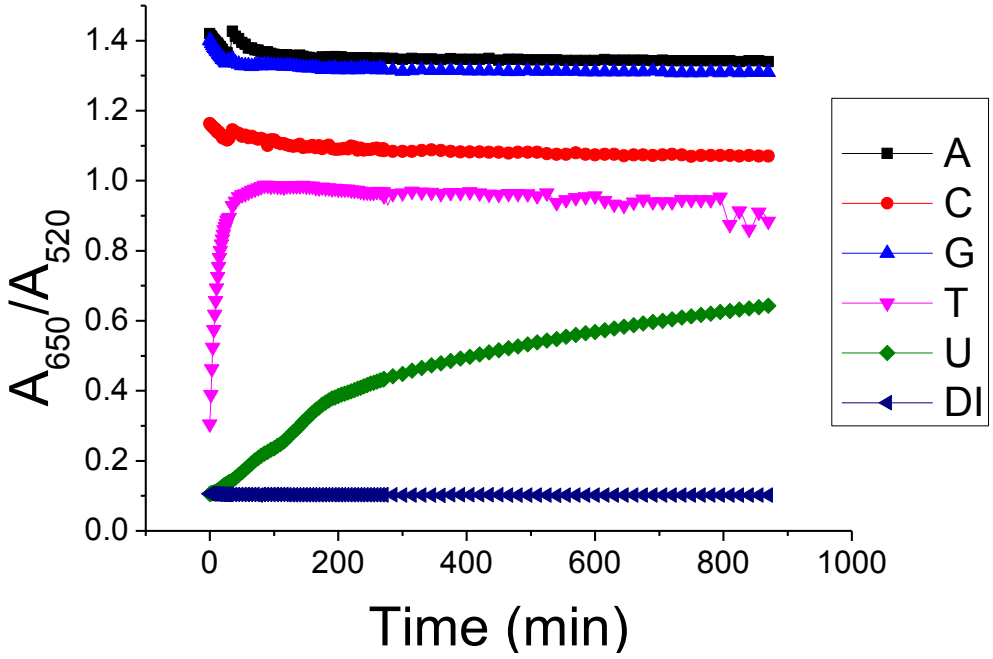

Figure 2-3 Absorbance of GNPs with 64 μM nucleobase.

To figure out the base dependency on binding strength of bases, deoxynucleoside and ribonucleoside to GNPs, K_D were fitted. As shown in Figure 2-4A, the absorbance ratio of absorbance at 650 nm to 520 nm is detected upon the mixing of GNPs to bases at 1 hour, and then from there dissociation constants were fitted. As a result, binding strength is base dependent between nucleobases, nucleosides and nucleotides. For bases, the binding strength to GNPs ranking from high to low is A>C>G>T>U. For deoxynucleosides, the binding strength to GNPs ranking from high to low is C~G>A>T. However, for ribonucleosides, the binding strength to GNPs ranks from high to low is C~G>A>U. The results are of some difference compared to the results reported by others on the ranking of A, C and G (C>G>A>T for bases [54], G>A>C>T for bases [55], G>A>C>T for bases and nucleosides [56]). The difference could be caused by the reaction time, detection method, etc. Instead of differences between our studies other others, our study and others indicate that base T binds to GNPs surfaces the weakest. It is

probably due to its absence of an amine group [54]. Besides, concentration at the point when A_{650}/A_{520} of which is 95% of its maximum are presented in Figure 2-4B. This variable indicates the concentration needed to nearly saturate the surface of GNPs. The trend has high similarity with the trend of K_D. It suggests that K_D could also give us a clue of how many molecules are needed to fully occupy the surface of GNPs. It suggests that, the higher the K_D, the more molecules are needed to fully occupy the surface of GNPs.

A

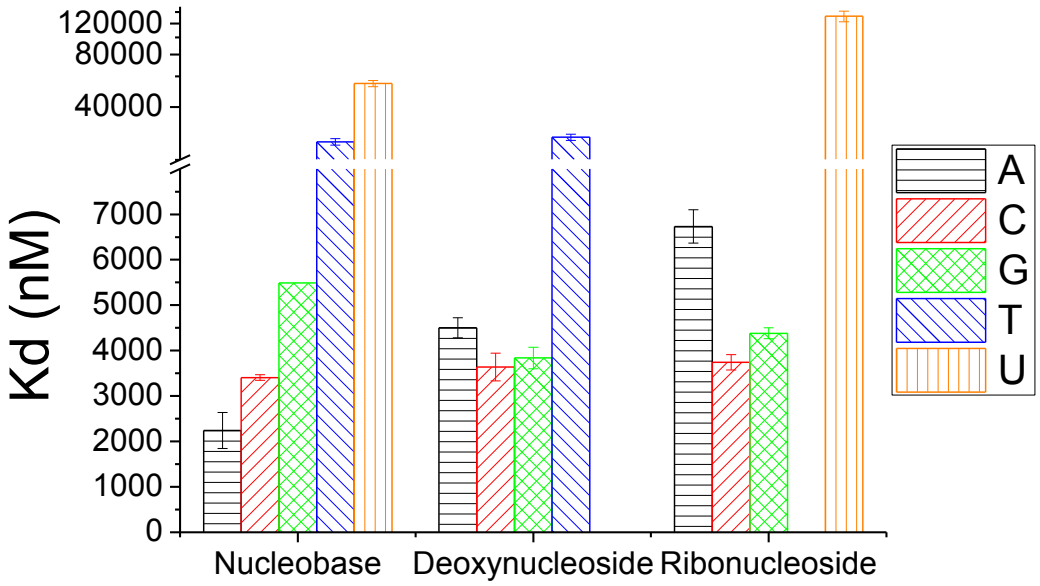

B

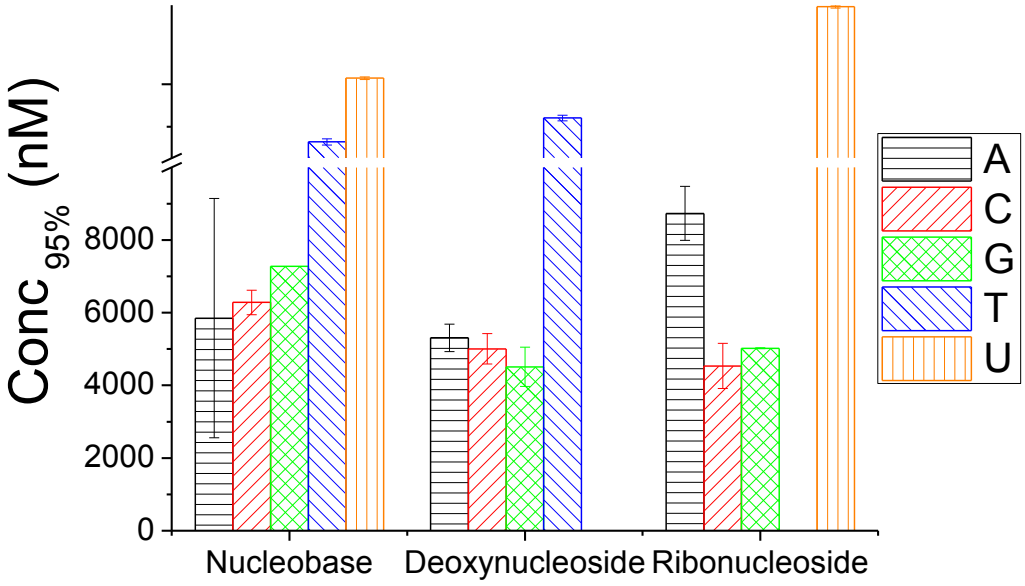

Figure 2-4 (A) K_D of nucleobases, deoxynucleosides, and ribonucleosides mixed with GNPs for 1 hour. (B) Nucleobase concentration at 95% of the maximum A_{650}/A_{520}.

Table 2-3 List of K_D (nM) in Figure 2-4A

	A	C	G	T	U
Nucleobase	2242.602	3405.793	5491.513	25391.28	54568.69
Deoxynucleoside	4504.268	3637.771	3838.906	26956.28	
Ribonucleoside	6733.517	3743.823	4380.99		132233.6

It was observed that when the base concentration is high enough, the increasing of base concentration would no longer change the color of GNPs. Because spectrum reflects the structure of GNPs [69], the result in Figure 2-5 suggests that the GNPS aggregated by different bases have different structures. In addition, the maximum of A_{650}/A_{520} (which is the constant 'a' in the fitting of K_D in Figure 2-4A) and the wavelength at maximum OD in Figure 2-5 were compared in Table 2-4. It was found that the more the wavelength

peak shifts, the smaller the constant ‘a’ is. This means that the constant ‘a’ in the fitting equation could reflect the structure of the aggregated GNPs in this experiment. Consider the scanning of spectrum takes long time so we used the maximum of A_{650}/A_{520} to indicate the structure of aggregated GNPs.

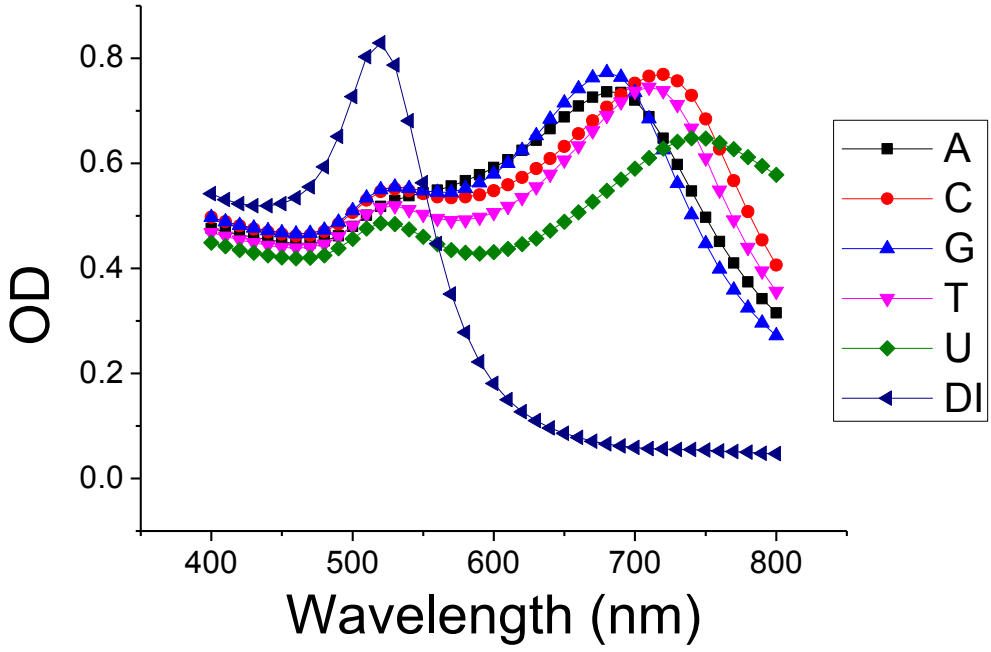

Figure 2-5 UV-vis spectrum of GNPs mixed with very high concentration (500 mM) nucleobases for 15 minutes.

Table 2-4 Comparison of maximum A_{650}/A_{520} in Figure 2-4 and wavelength at max OD in Figure 2-5.

Nucleobases	A	C	G	T	U
Maximum A_{650}/A_{520}	1.275	0.996	1.214	1.014	0.950
Wavelength (nm) at max OD	680	720	680	710	740

2.3.2 Interactions of GNPs with Nucleotide

In this section, the binding strength of NMP and NTP to GNPs was investigated. These two kinds of molecules would stabilize GNPs due to their negatively charged backbones. Experimental results are shown in Figure 2-6. TMP and TTP are barely able to stabilize GNPs and as a result cannot be fitted for c.c.c. or K_D. When concentrations are the same, for example, 5.6 μM, we could observe several things. For NMP, the c.c.c. value of AMP is much higher than CMP and GMP. For NTP, the c.c.c. value of ATP is higher than CTP and followed by GTP. While as in Figure 2-6B, we could find that, for NMP, the K_D of AMP is the smallest, followed by CMP and GMP. This ranking agrees with the ranking of c.c.c.. c.c.c. value has a positive correlation to the ability of preventing GNPs from aggregation. Furthermore, NMP show higher binding strength to GNPs than NTP. It could be explained by the difference between NMP and NTP on the number of phosphate. NTP could better stabilize GNPs because it has two more phosphates than NMP. However, more phosphates would hinder the binding of other molecules to GNP surfaces. Besides, NTP stock solutions have high salt concentration itself. The stabilization ability is composed of two parts: the binding strength to GNPs and the effect of each bound molecule. Therefore, the number of molecules bound to GNPs is the dominate factor. We could conclude that the binding strength of nucleotides to GNPs, ranks from high to low is A>C~G. This agrees with previous literatures which stated that adenosine-rich nucleotides possess higher binding strength to GNPs than other bases [70, 71]. Figure 2-6C indicates the structure difference of the aggregated GNPs.

A

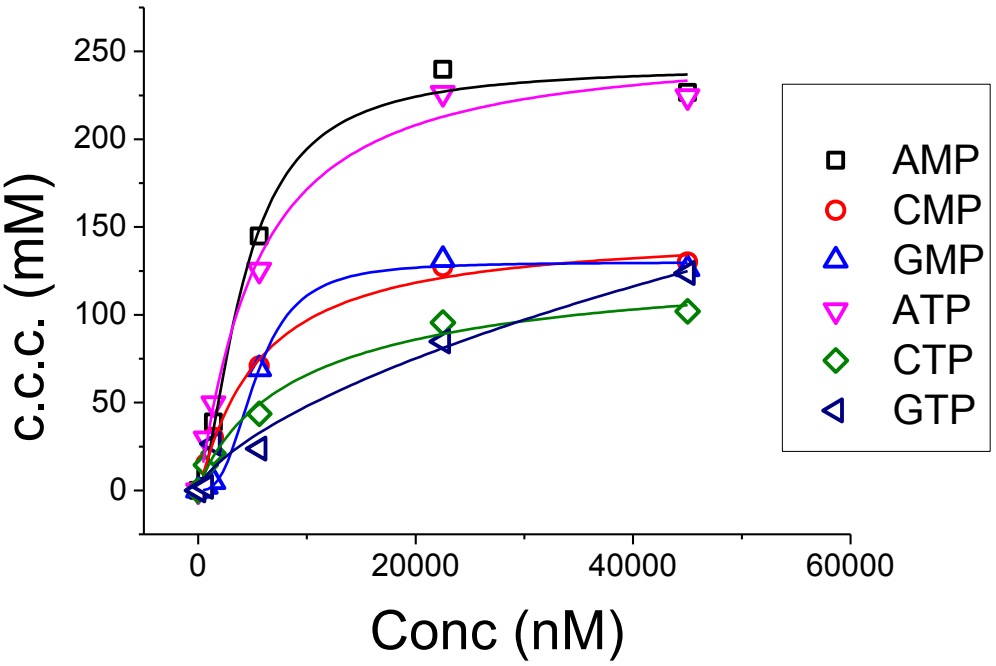
c.c.c. (mM)
Conc (nM)
0
50
100
150
200
250
0
20000
40000
60000
AMP
CMP
GMP
ATP
CTP
GTP

B

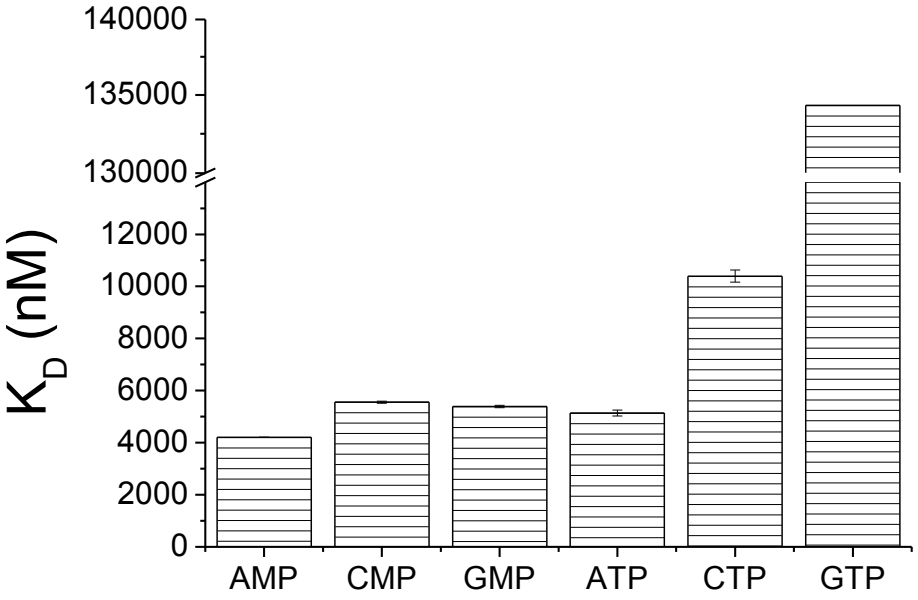
K_D (nM)
0
2000
4000
6000
8000
10000
12000
130000
135000
140000
AMP
CMP
GMP
ATP
CTP
GTP

C

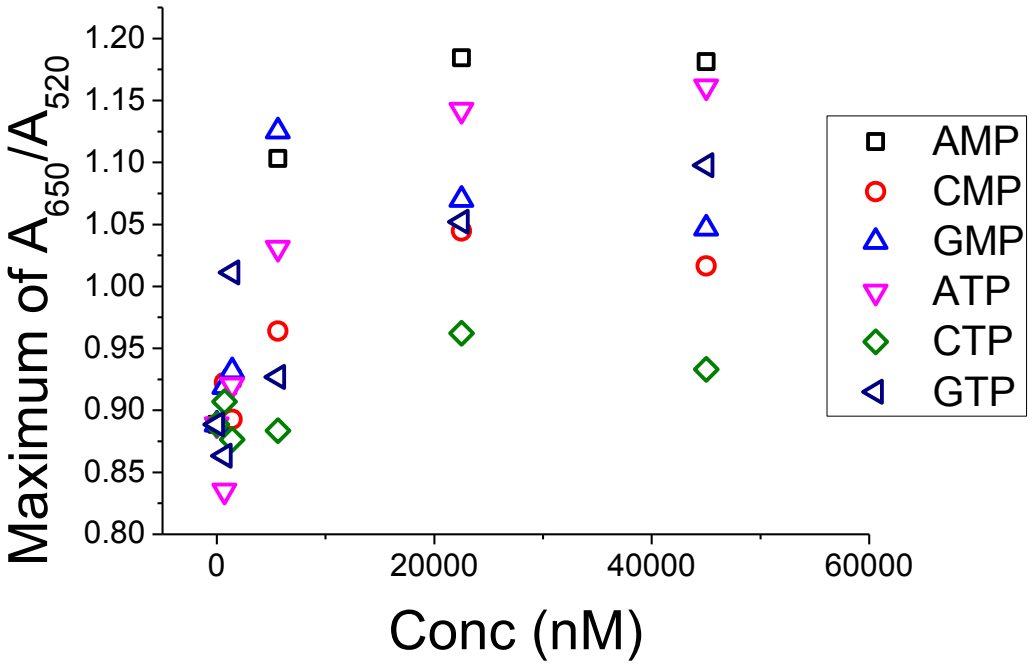

Figure 2-6 Titration results of interactions between GNPs and nucleotides. (A) c.c.c. (B) K_D (C) Maximum color change

2.4 Conclusion

In this Chapter, we investigated the binding strength of different nucleobases, deoxynucleosides, ribonucleosides, deoxynucleoside monophosphate and triphosphate to GNP surfaces. It was demonstrated that the nonspecific adsorption of these molecules interacting with GNPs in aqueous solutions, either stabilize GNPs or aggregate GNPs, depends on whether they have negatively charged phosphate backbone or not. It was also found that the interactions strongly dependent on base type. A have the strongest binding strength to GNPs and T have the weakest binding strength to GNPs. The structures of GNPs aggregated by different molecules are dissimilar.

Chapter 3 Thermodynamics Study of Interactions between GNPs and DNA

3.1 Literature Review and Introduction

A great deal of efforts has been made toward elucidating the surface coverage, structure and function of oligonucleotides on gold nanoparticles, mostly for the use in the development of biosensor applications. Techniques including electrochemistry, XPS, and surface plasmon resonance spectroscopy, fluorescence based method have been used to characterize such interaction systems [71-77]. The thermodynamics of DNA bound to GNPs has been investigated and studied in the past several years [52, 53, 78-81]. Some researchers have reported the length dependency on the binding of DNA to GNPs [82, 83]. It has been reported that pentamers have higher steric hindrance effect to GNPs than that of monomers [70]. Yang and coworkers [57] determined the relative strengths of mononucleotides and polynucleotides for 5 nm GNPs by measuring the stability of mono- or polynucleotide-stabilized GNPs in salt solutions of different concentrations. They reported that the order from the poly nucleotides, with the strength decreasing as poly A ~ poly C ~ poly T > poly G. Some [84] characterized the adsorption ex-situ using Fourier transform infrared spectroscopy and X-ray photoelectron spectroscopy and found that the homo-oligonucleotides adsorb on gold with relative strength ranking as A > C ~ G > T. Table 3-1 shows a list of articles on interactions between gold and DNAs.

Table 3-1 List of literatures on interactions between gold and DNAs.

Literature	Method	Gold	Nucleic acid	Ranking
Wolf, 2004 [85]	Surface plasmon resonance spectroscopy (SPR)	Gold films	Initial adsorption rates (25-mer)	A>C>T
			Long-time (>0.1h) adsorption rates (25-mer)	T>C>A
Kimura-Suda, 2003 [84]	Fourier transform infrared spectroscopy (FTIR) and X-ray photoelectron spectroscopy (XPS)	Gold substrate in aqueous solutions	Homo-oligonucleotides	A>C≥G>T
Parak, 2003 [86]	Electrophoretic mobility	10 nm GNPs	Thiol-oligonucleotides	C>G>A>T
Yang, 2007 [57]	Melting transition measurements	5 nm GNPs	polynucleotides	A>C>T>G
Brown, 2008 [87]	Coverage analysis using mercaptohexanol displacement (MCH)	7.46 nm GNPs	15-mer oligonucleotides (thiol modified)	A,C>G,T

However, none of them studied sequence dependency, length dependency and conformation dependency in the same experimental system. Therefore, the binding strength trend obtained from one cannot be used to infer the trend in another, or vice versa. It urged us to do a systematic study in the same experimental system on sequence, length and conformation dependency in the interactions between DNA and GNPs. In this chapter thermodynamic study was conducted to compare the stabilizing ability and binding strength of various DNAs to GNPs.

3.2 Materials and Methods

The DNAs used in our experiments are purchased from Integrated DNA Technologies® (IDT). All DNA sequences were tested in DINAmelt web server to ensure that no undesired structures (self-structure or self-dimer) exist. DNAs were dissolved in deionized water to 100 μM and then stored at -20 °C. Hybridization condition for ssDNA

was in 1 X buffer (0.1xPBS, 15 mM NaCl and 5 mM KCl) for 24 hours. DNAs used in the experiments were diluted in 1 X buffer. DNA sequences that are used in this chapter are listed in the table below.

Table 3-2 DNA sequences used in Chapter 3.

Name	Length (nt)	Sequence (5'-3')
A-5	5	5 x (A)
A-10	10	10 x (A)
A-15	15	15 x (A)
A-20	20	20 x (A)
A-30	30	30 x (A)
A-50	50	50 x (A)
T-5	5	5 x (T)
T-10	10	10 x (T)
T-15	15	15 x (T)
T-20	20	20 x (T)
T-30	30	30 x (T)
T-50	50	50 x (T)
T-100	100	100 x (T)
C-5	5	5 x (T)
C-10	10	10 x (C)
C-15	15	15 x (C)
C-20	20	20 x (C)
G-5	5	5 x (G)
G-10	10	10 x (G)
G-15	15	15 x (G)
G-20	20	20 x (G)
com1	30	GAC CTT AGA CTT GAC ATG CTT CTC GAC GAC
com2	30	GTC GTC GAG AAG CAT GTC AAG TCT AAG GTC
c1.3	35	GTC GTC GAG AAG CAT GTC AAG TCT AAG GTC **AAA AA**
c2.3	40	GTC GTC GAG AAG CAT GTC AAG TCT AAG GTC **AAA AAA AAA A**
c3.3	45	GTC GTC GAG AAG CAT GTC AAG TCT AAG GTC **AAA AAA AAA AAA AAA**
c1.5	35	**AAA AA** GTC GTC GAG AAG CAT GTC AAG TCT AAG GTC
c2.5	40	**AAA AAA AAA A** GTC GTC GAG AAG CAT GTC AAG TCT AAG GTC
c3.5	45	**AAA AAA AAA AAA AAA** GTC GTC GAG AAG CAT GTC AAG TCT AAG GTC

C2A	35	**AAA AA** GTC GTC GAG AAG CAT GTC AAG TCT AAG GTC
C2C	35	**CCC CC** GTC GTC GAG AAG CAT GTC AAG TCT AAG GTC
C2G	35	**GGG GG** GTC GTC GAG AAG CAT GTC AAG TCT AAG GTC
C2T	35	**TTT TT** GTC GTC GAG AAG CAT GTC AAG TCT AAG GTC
M7	30	TAT GTC GAG AAG CAT GTC AAG TCT AAG GTC
M8	30	GTC GTC GAG AAG CAT TAT AAG TCT AAG GTC
M9	30	GTC GTC GAG AAG CAT GTC AAG TCT AAG TAT
M10	30	GTC TTC GAG AAG CAA GTC AAG TTT AAG GTC
M1.1	30	GTC GTC GAG AAG AAT GTC AAG TCT AAG GTC
M1.2	30	GTC GTC GAG AAG AGT GTC AAG TCT AAG GTC
M1.3	30	GTC GTC GAG AAG AGC GTC AAG TCT AAG GTC
M1.5	30	GTC GTC GAG AAG AGC TAC AAG TCT AAG GTC
MC1	30	GTC GTC GAG CCG CAT GTC AAG TCT AAG GTC
MG1	30	GTC GTC GAG GGG CAT GTC AAG TCT AAG GTC
MT1	30	GTC GTC GAG TTG CAT GTC AAG TCT AAG GTC

*Bold is overhang and underline is mismatch

c.c.c. titration experiments are done the same as in Chapter 2 for ssDNA. Incubation for ssDNA and GNPs was 48 hours. For matched dsDNA, dsDNA with overhangs and dsDNA with mismatches, hybridization time for dsDNA was 24 hours and the incubation time for DNA and GNPs was 1.5 hours instead of 48 hours. In this chapter, the c.c.c. value is a characteristic parameter to indicate the stabilizing effect of DNA to GNPs.

3.3 Results of Interactions between GNPs and Single-Stranded DNA (ssDNA)

3.3.1 Sequence Dependency of ssDNA

To study the sequence dependency in the interactions of DNA with gold nanoparticles in binding strength, we compared 15 nt (nucleotides) homo-oligonucleotides (poly) with only base A, C, G or T. They are named A-15, C-15, G-15 and T-15 respectively. Results

from titration experiments are shown in Figure 3-1. The concentration of DNA increases, c.c.c. value increases for all the sequences (Figure 3-1A). The binding strength of 15 nt homo-oligonucleotides to GNPs, ranks from high to low is A>T>C>G (Figure 3-1B). Some literatures have reported the ranking of sequence comparisons of DNAs to be A>C>G>T or C>G>A>T [57, 84, 85]. The differences are caused by different experimental conditions, such as incubation time, GNPs properties and salt concentration. From the value of maximum of A_{650}/A_{520}, it was concluded that not only sequence type but also DNA concentration would affect the structure of DNA stabilized (Figure 3-1C).

A

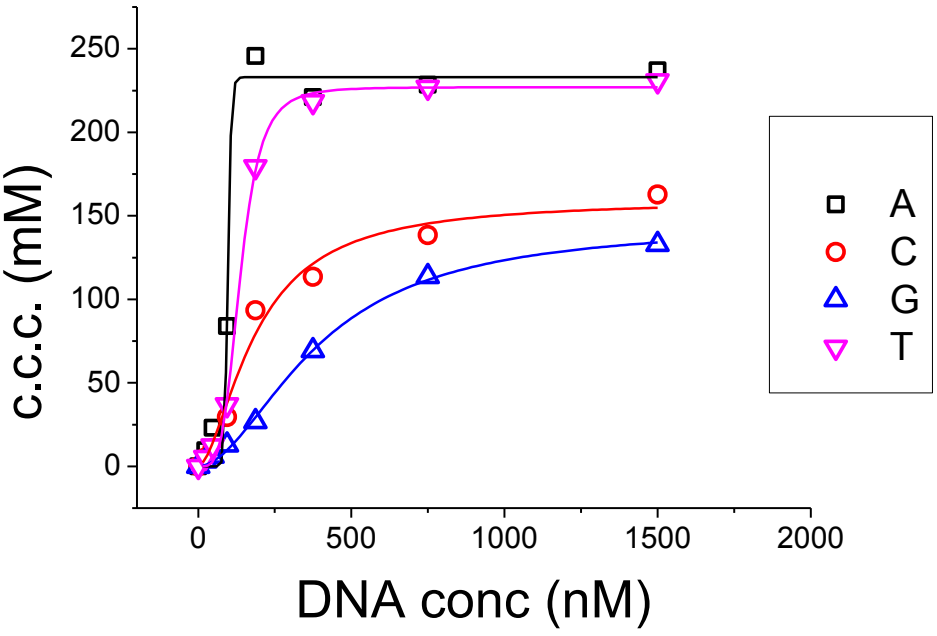

B

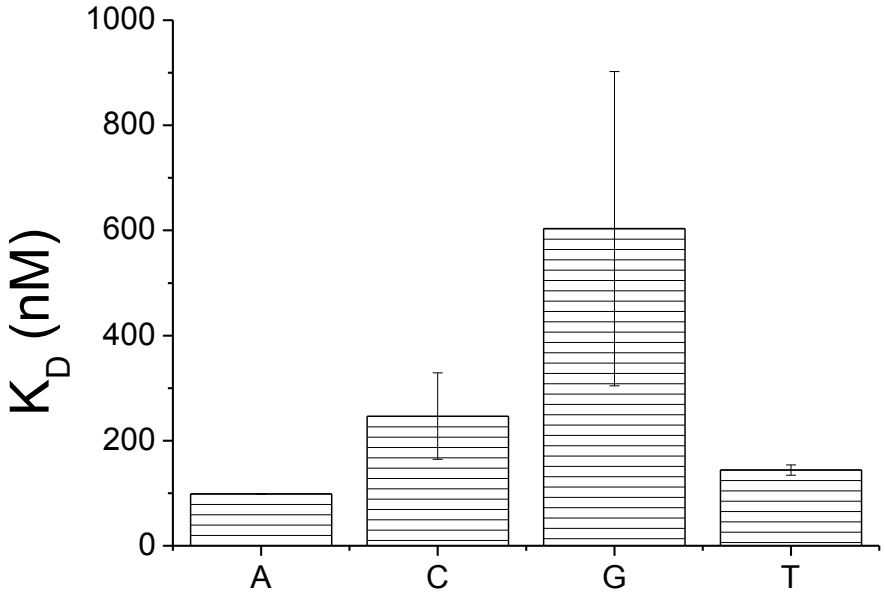

C

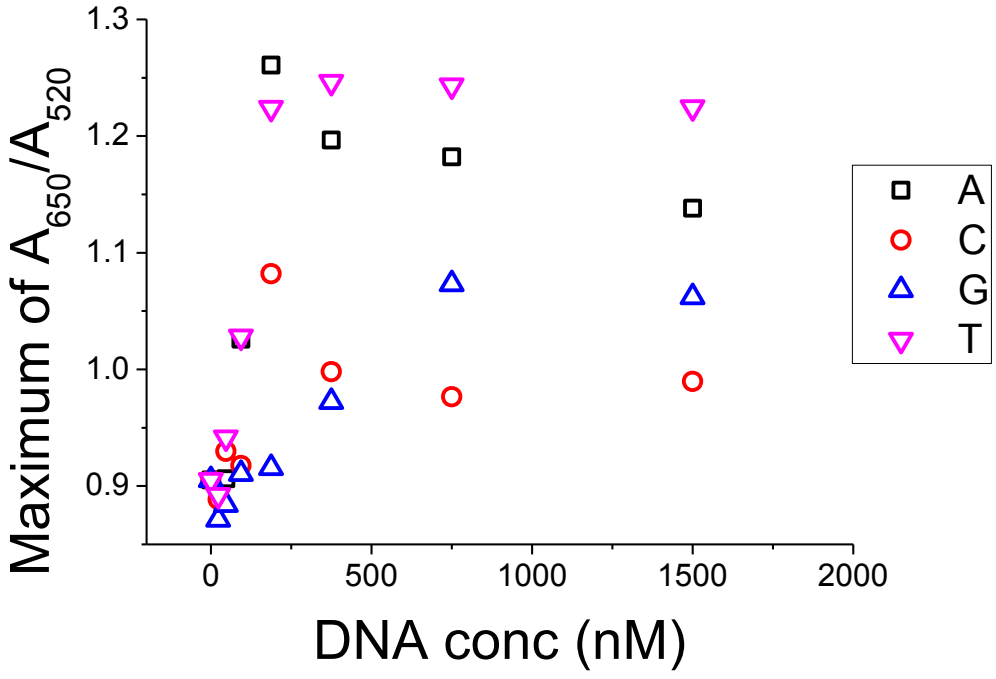

Figure 3-1 Titration results of interactions between GNPs and poly-15 DNAs. (A) c.c.c. (B) K_D (C) Maximum color change

Table 3-3 shows zeta potential of mixture of GNPs and different concentrations of A-15. The mixture was the same as in titration experiments. Zeta potential was tested for 3

times by Delsa Nano C® to test for zeta potential. As DNA concentration increases, the c.c.c. value increases dramatically while zeta potential does not. Similarly, Table 3-4 shows that for different sequences, correlation between c.c.c. and zeta potential is not obvious. There are two possible mechanisms of DNAs at stabilizing GNPs: one is steric stabilization due to the formation of a polymer layer on GNPs surfaces and the other is electrostatic stabilization due to negatively charged backbone of DNAs. These results indicate that for homo-oligonucleotides, the effect of steric stabilization, other than electrostatic stabilization, is the dominant mechanism.

Table 3-3 Comparison between zeta potential and c.c.c. for A-15. (GNPs = 3.7 nM, incubation time = 48 hours)

DNA concentration (nM)	Zeta potential (mV)	c.c.c. (mM)
46.875	-47.9 (±0.9)	59.0 (±0.4)
93.75	-49.3 (±1.1)	123.8 (±10.5)
187.5	-62.4 (±3.2)	233.2 (±10.0)
375	-52.3 (±1.9)	231.2 (±0.5)
750	-41.1 (±8.3)	242.2 (±0.1)
1500	-40.1 (±5.6)	249.2 (±0.0)

Table 3-4 Comparison of zeta potential and c.c.c. of poly-15 DNAs. (GNPs = 3.7 nM, DNA = 94 nM, incubation time = 48 hours)

DNA	Zeta potential (mV)	c.c.c. (mM)
A-15	-43.6 (±2.6)	122.4 (±10.2)
C-15	-44.1 (±2.5)	67.8 (±45.2)
G-15	-51.0 (±3.5)	51.2 (±13.3)
T-15	-46.0 (±3.7)	75.2 (±12.6)

3.3.2 Length Dependency of ssDNA

To study the length dependency of DNA in the interactions between DNA and GNPs, poly DNAs were named after their base type and length. For example, A-5 means homo-oligonucleotides with 5 nucleotides of A. A less than 100% yield of each synthetic step

and the occurrence of side reactions set practical limits of the efficiency of the process. Therefore, the maximum length of synthetic DNAs is limited. The reason A and T are chosen instead of C or G is that the length range available on the market for A and T is much larger than C and G. The longest DNA for A is 50 nt and for T is 100 nt. c.c.c. titration experiments were done for A and T (Figure 3-2). With the same DNA concentration, longer DNA binds to GNPs stronger than shorter ones (Figure 3-2A, B, E). This is because longer DNAs have more negative charged backbones and greater volume than shorter ones. Figure 3-2A, B, E were re-plotted in nt concentration (nt concentration = DNA concentration x DNA length) to be Figure 3-2C, D, F. Binding strength in nt would decrease with the increase of DNA length, for both A and T. This indicates that the effect of binding strength per base is stronger for short DNAs. It would allow larger number of nt to absorb on GNPs surfaces (Figure 3-3).

A

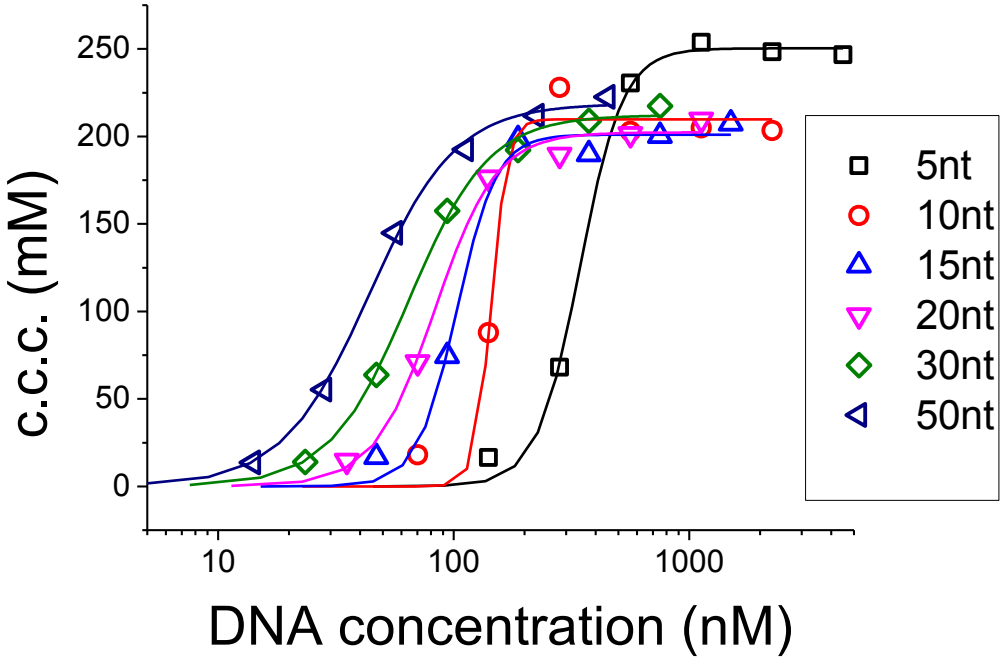

B

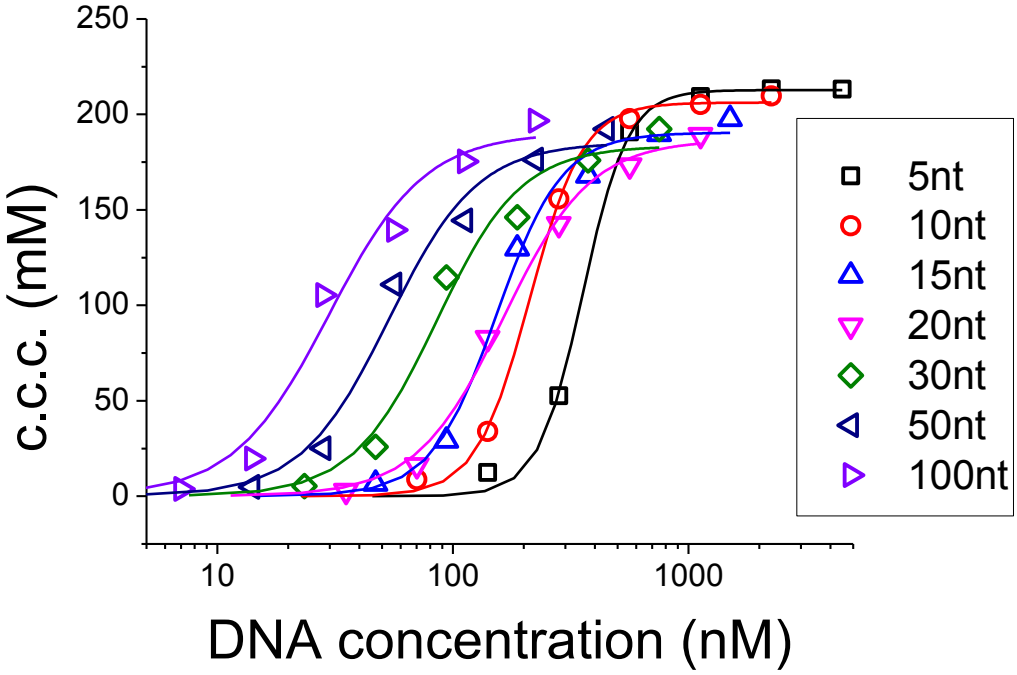
250
200
150
100
50
0
c.c.c. (mM)
10
100
1000
DNA concentration (nM)
5nt
10nt
15nt
20nt
30nt
50nt
100nt

C

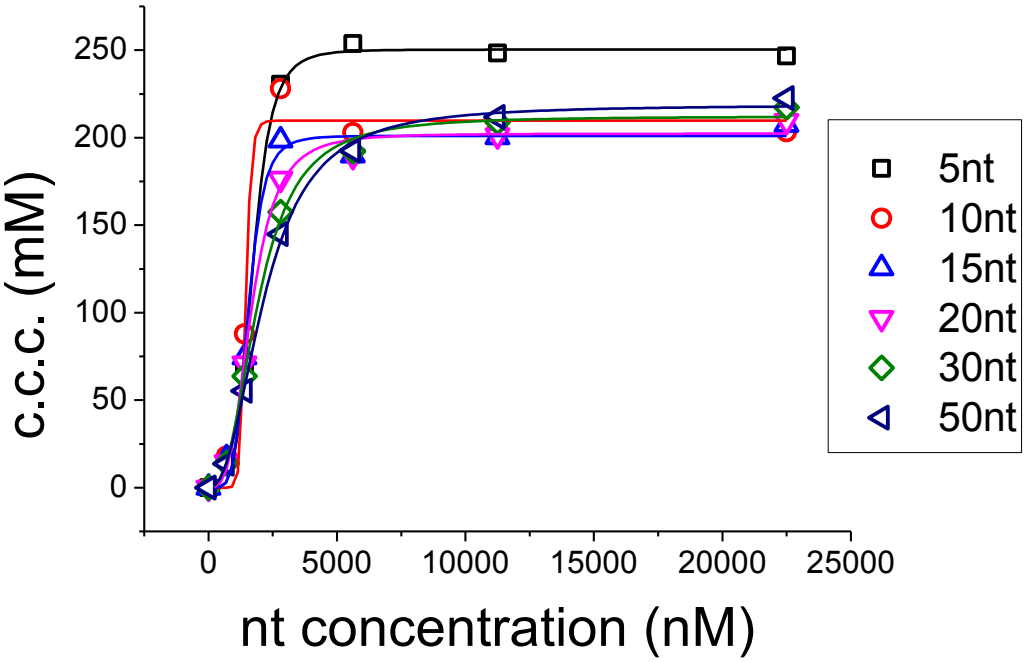
250
200
150
100
50
0
c.c.c. (mM)
0
5000
10000
15000
20000
25000
nt concentration (nM)
5nt
10nt
15nt
20nt
30nt
50nt

D

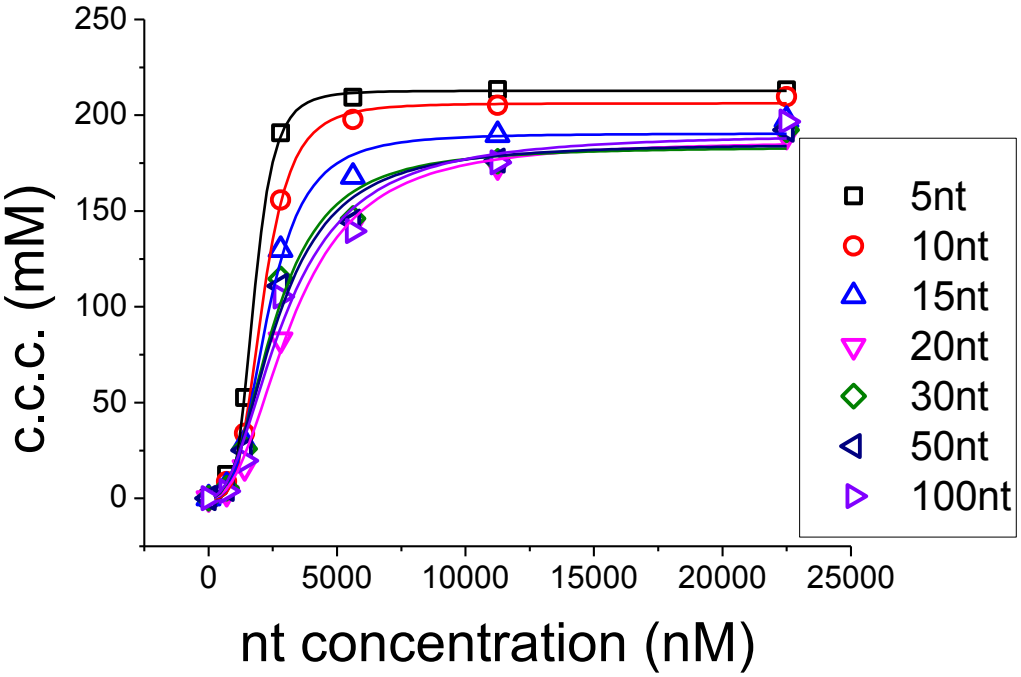
250
200
150
100
50
0
c.c.c. (mM)
0
5000
10000
15000
20000
25000
nt concentration (nM)
5nt
10nt
15nt
20nt
30nt
50nt
100nt

E

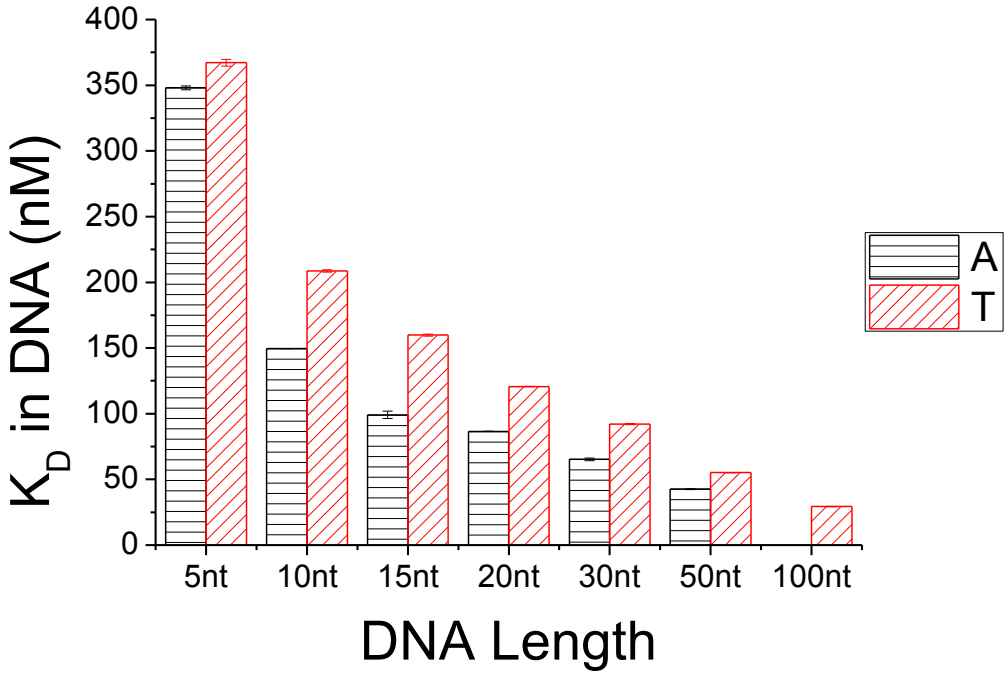
400
350
300
250
200
150
100
50
0
K_D in DNA (nM)
5nt
10nt
15nt
20nt
30nt
50nt
100nt
DNA Length
A
T

F

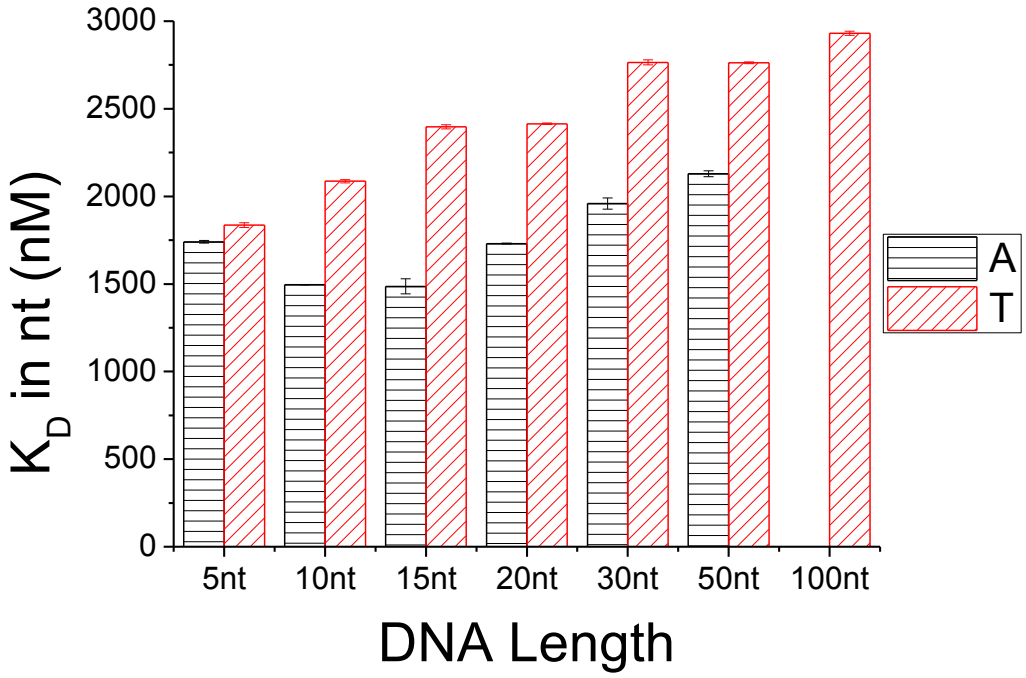

Figure 3-2 Interactions between GNPs and poly DNAs. (A) c.c.c. of poly A in DNA concentration (B) c.c.c. of poly T in DNA concentration (C) c.c.c. of poly A in nt concentration (D) c.c.c. of poly T in nt concentration (E) K_D in DNA concentration (F) K_D in nt concentration

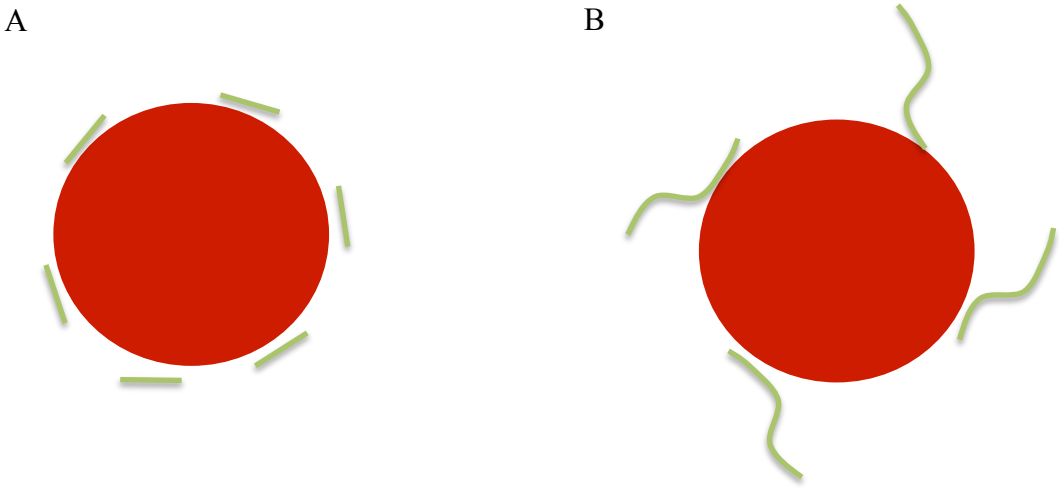

Figure 3-3 Schematic illustration for the binding between DNA and GNPs. (A) Short DNAs (B) Long DNAs

It was found that the maximum of A_{650}/A_{520} values to be different between A and T. Different length of DNA binds to GNPs in a different way and thus would generate different binding structures (Figure 3-4). The maximum color change in nt concentration is not obvious (Figure 3-4A, B) while in DNA concentration is obvious (Figure 3-4C, D). The zeta potential of poly-A in different lengths was tested (Table 3-5). No big difference in zeta potential was observed with the change of DNA length. c.c.c. value is highly length dependent. It suggests that steric stabilization is the dominant factor that DNAs stabilize GNPs.

A

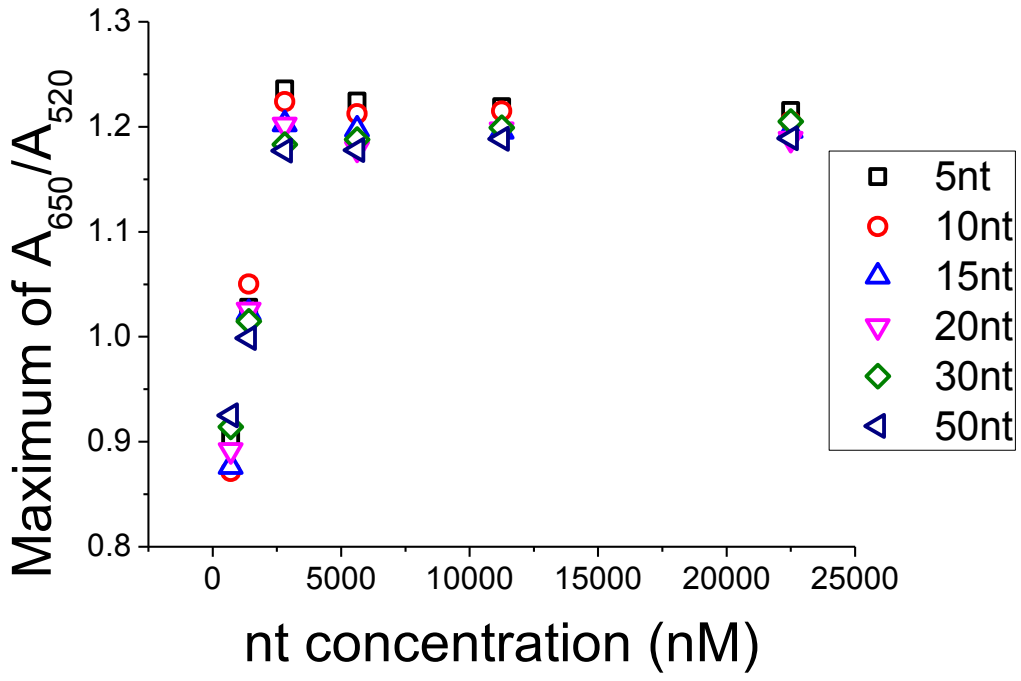

B

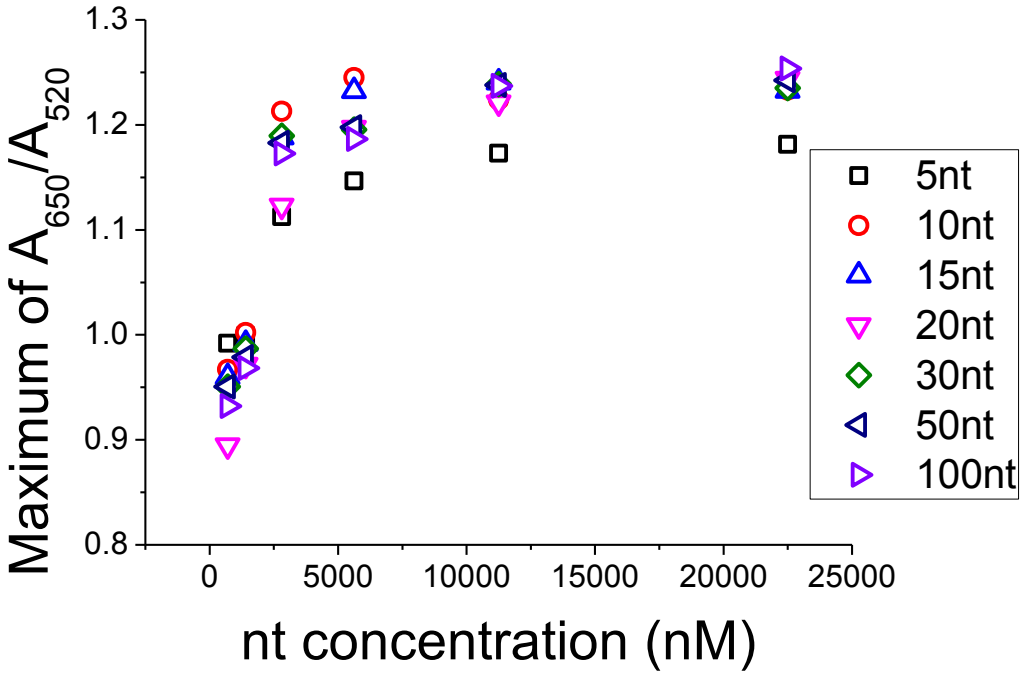
Maximum of A_{650}/A_{520}
1.3
1.2
1.1
1.0
0.9
0.8
0
5000
10000
15000
20000
25000
nt concentration (nM)
5nt
10nt
15nt
20nt
30nt
50nt
100nt

C

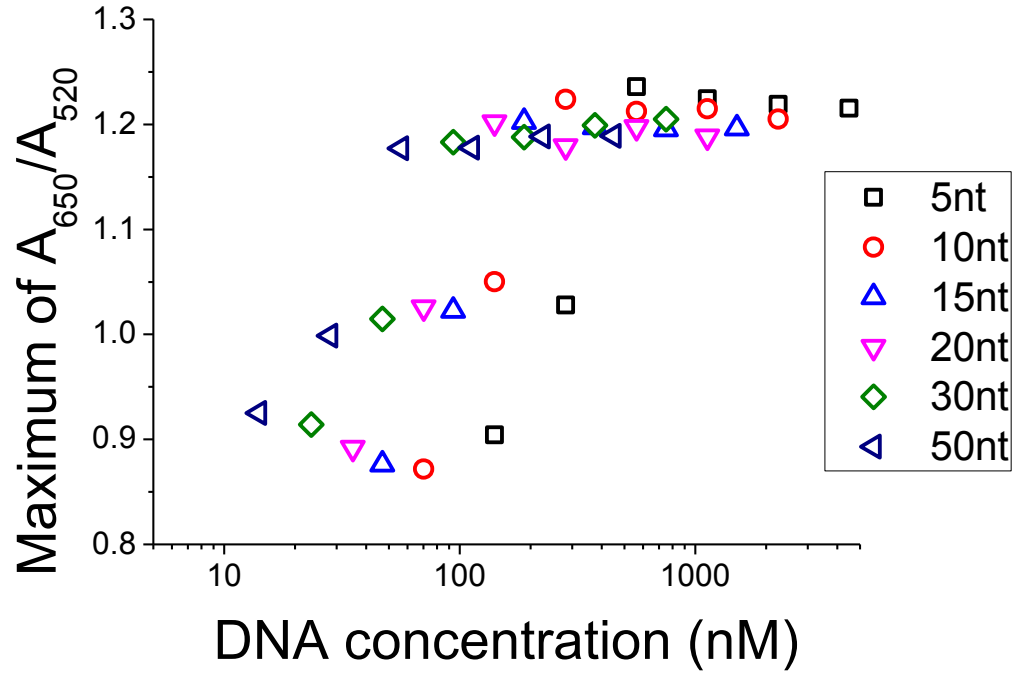
Maximum of A_{650}/A_{520}
1.3
1.2
1.1
1.0
0.9
0.8
10
100
1000
DNA concentration (nM)
5nt
10nt
15nt
20nt
30nt
50nt

D

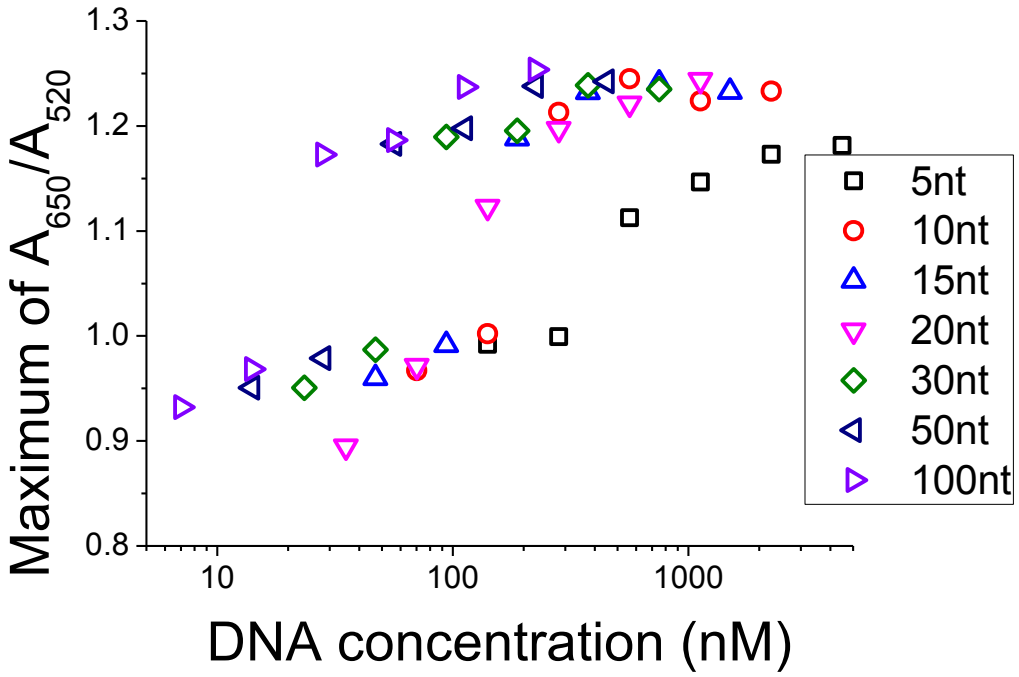

Figure 3-4 Maximum color change of interactions between GNPs and poly DNAs. (A) Poly A in nt concentration (B) Poly T in nt concentration (C) Poly A in DNA concentration (D) Poly T in DNA concentration

Table 3-5 Comparison of zeta potential and c.c.c. of poly A in different length. (GNPs = 3.7 nM, DNA = 2812 nM in nt and incubation time = 48 hours)

DNA Length	Zeta potential (mV)	c.c.c. (mM)
A-5	-43.4 (±3.8)	270.5 (±2.6)
A-10	-49.2 (±5.4)	264.9 (±6.9)
A-15	-40.9 (±4.9)	233.2 (±10.0)
A-20	-44.6 (±4.6)	210.5 (±11.1)
A-30	-47.5 (±6.3)	194.1 (±7.4)
A-50	-49.1 (±3.9)	183.1 (±5.1)

3.3.3 Sequence and Length Dependency of ssDNA

To study the sequence and length dependency of ssDNA, poly DNAs were used. Figure 3-5 shows the results from titration experiments of different DNAs in various lengths. G acts abnormal is because they could form complex self-structures, or called

quartet, with itself if the DNA is too long [88]. In molecular biology, G-quartet are nucleic acid sequences that are rich in guanine and are capable of forming a four-stranded structure [89]. Except for DNAs of 1 nt, it was observed that c.c.c. value decreases with the length of DNA increases for A, C and T. Sequence dependency of stabilization effect of DNA on interactions between GNPs and DNA ranks as A>T>C. 1 nt DNAs would not provide steric repulsion to GNPs. Therefore, 5 nt DNAs could stabilize GNPs better than 1 nt DNAs. 5 nt and longer DNAs would provide steric repulsions so they follow the length dependency trend as in previous section. Figure 3-6 shows the maximum color change. The pattern of poly A and poly T changes by length was not obvious. For poly C and poly G, structure differences were observed in the aggregation complex of DNA-GNPs through the change of DNA length.

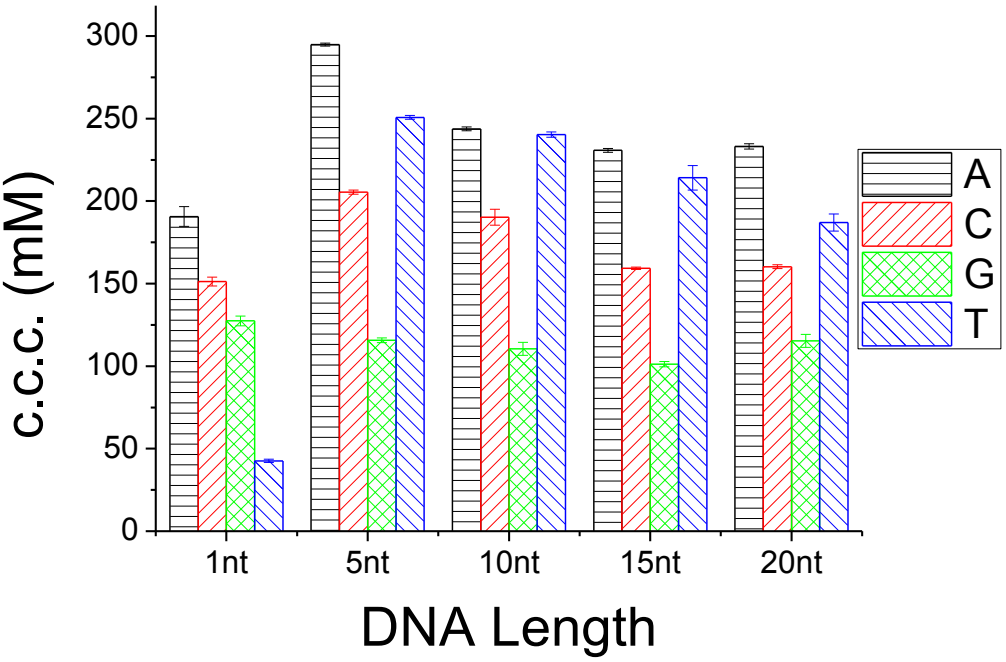

Figure 3-5 c.c.c. of interactions between GNPs and poly A, C, G, T (5625 nM in nt).

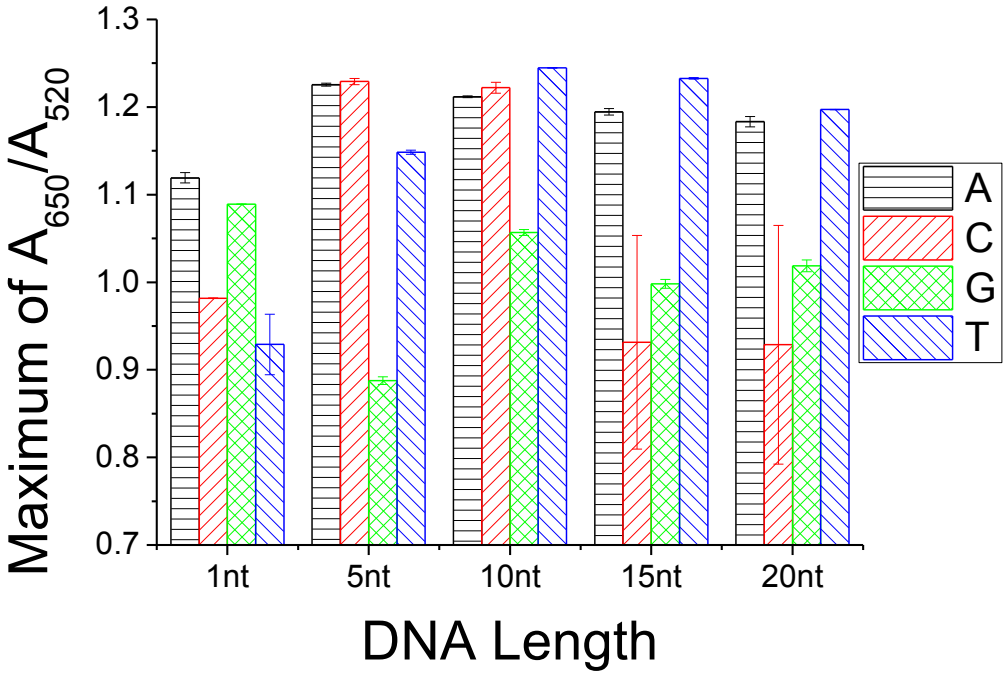

Figure 3-6 Maximum color change of interactions between GNPs and poly A, C, G, T (5625 nM in nt).

3.4 Results of Interactions between GNPs and DNA of Different Conformations

3.4.1 Completely Matched Double-Stranded DNA (dsDNA)

To study interactions between GNPs and ssDNA or dsDNA, we designed two sets of completely matched dsDNA. One of them is 30 nt DNAs of mixed bases, named com1 and com2. The other is also 30 nt, which is composed of homo-oligonucleotides A (A-30) and T (T-30). Experiments were done on different incubation time and 1.5 hours was selected due to big difference between ssDNA and dsDNA. The binding constants for dsDNA in this dissertation were apparent binding constant instead of true K_D.

Figure 3-7A shows that com1 and com2 has higher c.c.c. than dsDNA com1-2. When concentration is low, difference between ssDNA and dsDNA is small. When concentration increases, difference between ssDNA and dsDNA gets big. When concentration approaches saturation, differences become small. Figure 3-7B shows that A-30 has higher c.c.c. than ss DNA AT-30. Small c.c.c. of T is because the reaction speed between T and GNPs is very slow (as demonstrated in Chapter 4). The difference of com1-2 and AT-30 could be related to the difference in binding energy which is listed Table 3-6. At the incubation time of DNAs with GNPs 1.5 hours, the binding strength of ssDNA at stabilizing GNPs is much better than double stranded dsDNA (Figure 3-7C). Figure 3-8 Maximum color change shows the results of maximum color change. It suggests that the binding structures of different DNAs to GNPs are different. Generally speaking, there are two major differences between ssDNA and dsDNA in their interactions between GNPs [90]. One is that ssDNA has exposed nitrogen-containing bases, which have been shown to bind exceptionally strong with aqueous GNPs through hydrogen bond. The other is that ssDNA has flexible structures while dsDNA has rigid double helix structures. Some researchers reported that small gold nanoparticles (5 nm) could inhibit the hybridization of DNA but large gold nanoparticles (17 nm) would not [91]. Moreover, dsDNA with its nitrogen bases hidden by the double helix structure would have to be dehybridized to adsorb to GNPs, locally or globally [70].

A

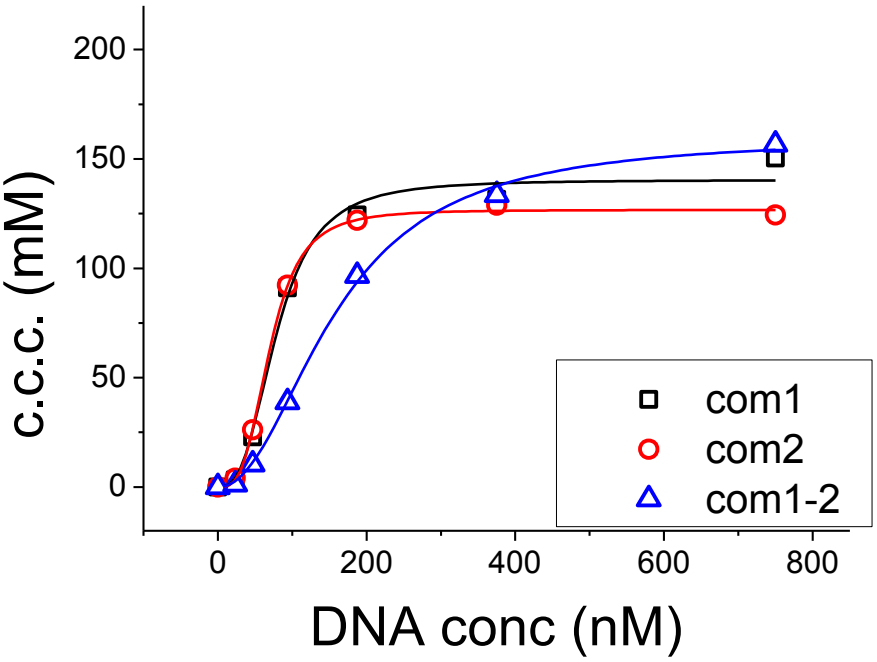
200
150
100
50
0
c.c.c. (mM)
0
200
400
600
800
DNA conc (nM)
com1
com2
com1-2

B

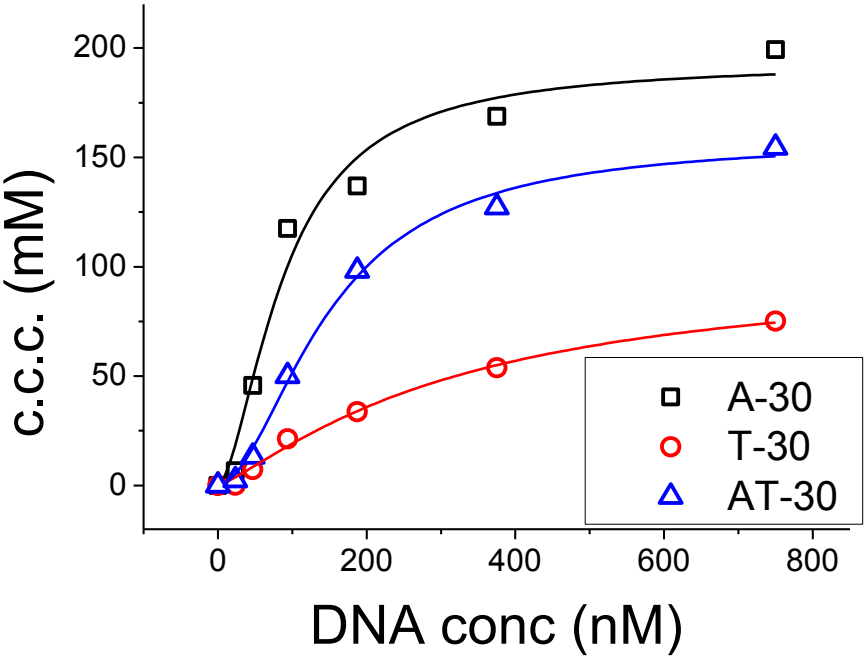
200
150
100
50
0
c.c.c. (mM)
0
200
400
600
800
DNA conc (nM)
A-30
T-30
AT-30

C

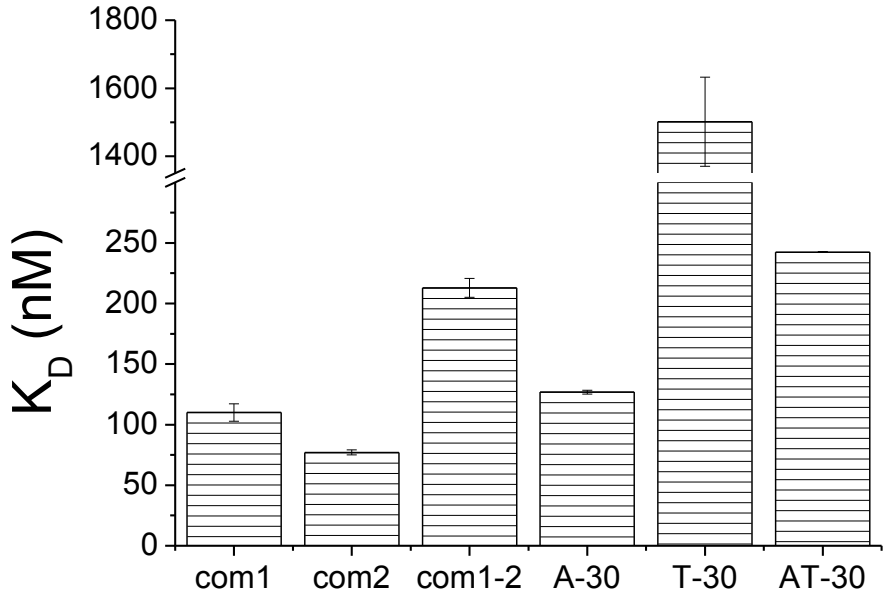

Figure 3-7 Interactions of GNPs and completely matched dsDNA. (A) c.c.c. of com1 and com2 (B) c.c.c. of A-30 and T-30 (C) K_D

Table 3-6 Binding energy of matched dsDNA.

	com1-2	AT-30
ΔG (kcal/mol)	-34.7	-15.3

A

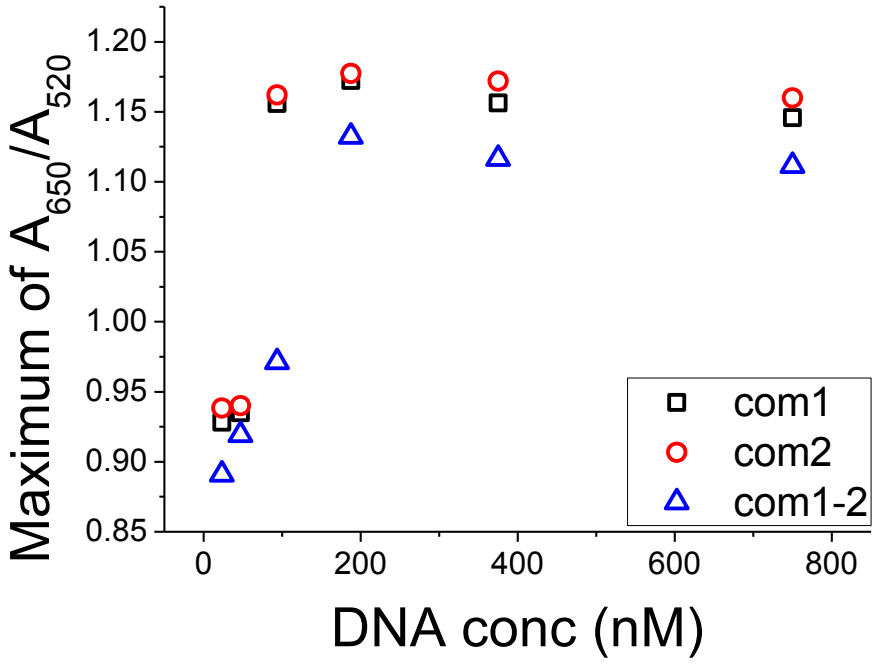

B

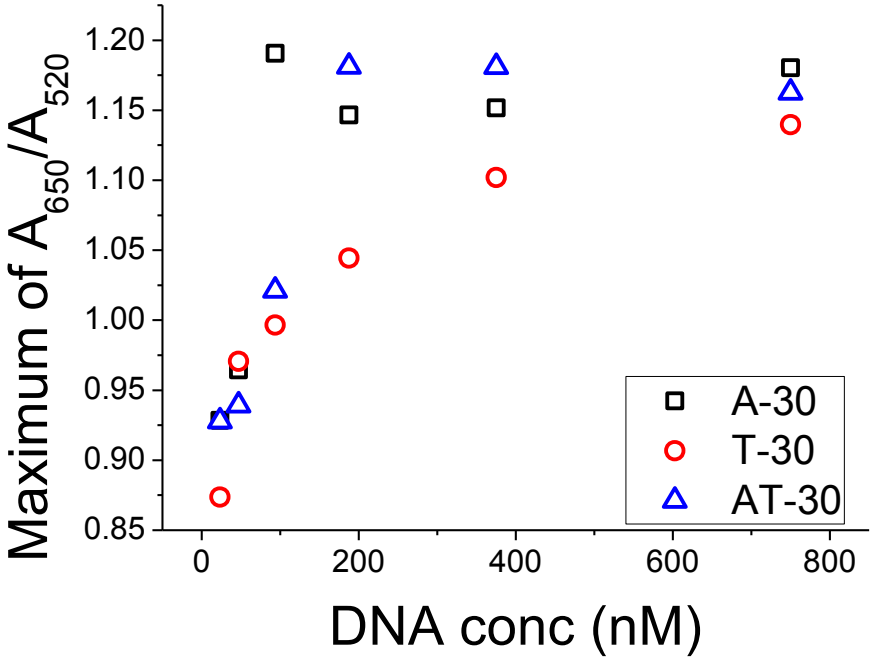

Figure 3-8 Maximum color change of interactions of GNPs and completely matched dsDNA. (A) com1 and com2 (B) A-30 and T-30

3.4.2 dsDNA with Overhangs

To study the interactions between GNPs and ssDNAs with extended oligonucleotides on one end (overhangs), we designed two sets of DNAs based on com2, one for studying length dependency of the overhang oligonucleotides and the other for studying sequence dependency of the overhang oligonucleotides.

Schematics for overhangs in different length are shown in Figure 3-9, including c1.3, c2.3, c3.3, c1.5, c2.5 and c3.5. The number of nucleotide 'A' added to the end of com2, c1 means 5 nt, c2 means 10 nt and c3 means 15 nt.

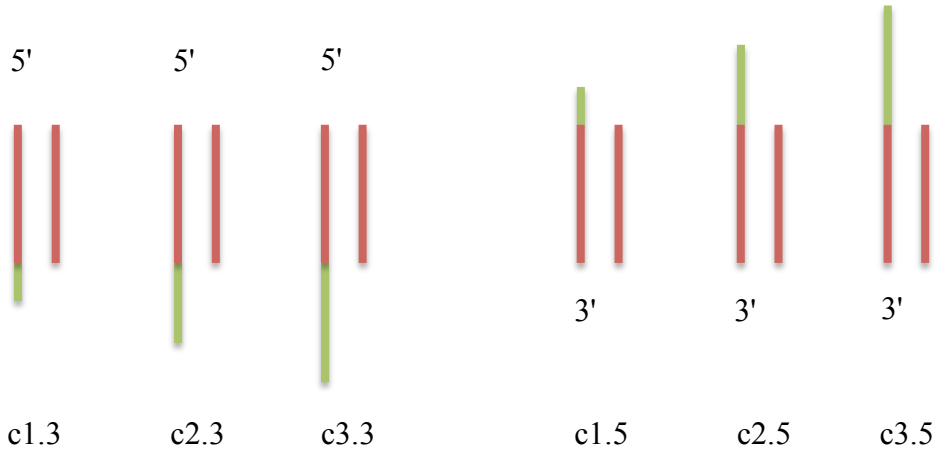

Figure 3-9 Schematic illustration of dsDNA with overhangs in different lengths.

Figure 3-10A shows that modified ssDNAs have bigger c.c.c. values than com2. Figure 3-10B shows that c.c.c. values of dsDNA with overhangs are bigger than those of matched dsDNA. Figure 3-10C shows that the difference between ssDNA and dsDNA with overhangs is smaller than between ssDNA matched DNA. The binding strengths of different overhangs are length dependent and position dependent. The longer the DNA, the more stable the solution. GNPs with dsDNA with overhangs on 3' are more stable than 5'. There are two possible explanations for the differences between those overhangs,

one is that dsDNA was dehybridized by GNPs from its extended tail and the other is that the tail absorbed on GNP surfaces. Table 3-7 shows that the binding energies of those overhangs are almost the same. Most likely the difference is mainly due to the absorption of overhangs to GNP surfaces. Figure 3-11 indicates that the structure of the aggregated GNPs differs with different types of overhangs.

A

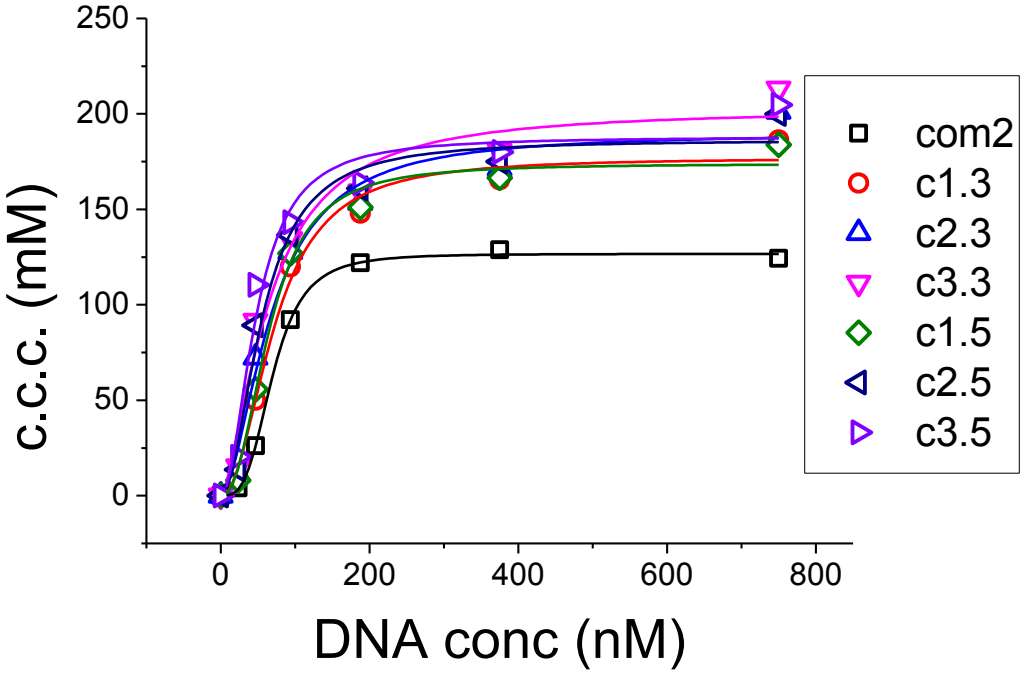

B

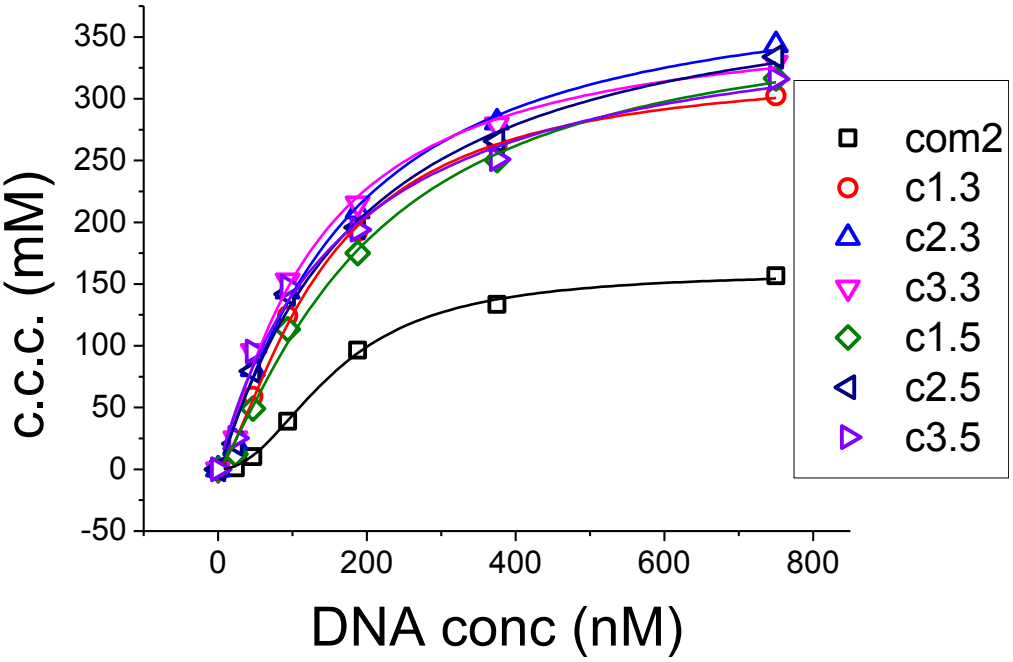

C

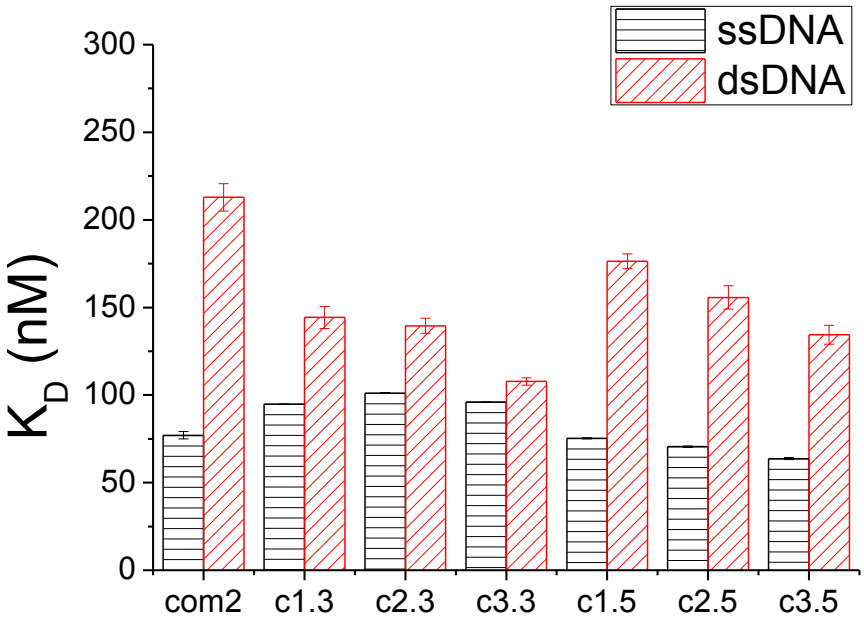

Figure 3-10 Effect of length on interactions between GNPs and dsDNA with overhangs. (A) c.c.c. of ssDNA (B) c.c.c. of dsDNA (C) K_D

Table 3-7 Binding energy of dsDNA with overhangs in different length.

	$\Delta G_{Secondary\ Structure}$ (kcal/mol)	$\Delta G_{Hybridization}$ (kcal/mol)
com2	0.7	-34.7
c1.3	0.7	-35.2
c2.3	0.7	-35.2
c3.3	0.7	-35.2
c1.5	0.7	-35.2
c2.5	0.7	-35.2
c3.5	0.7	-35.2

A

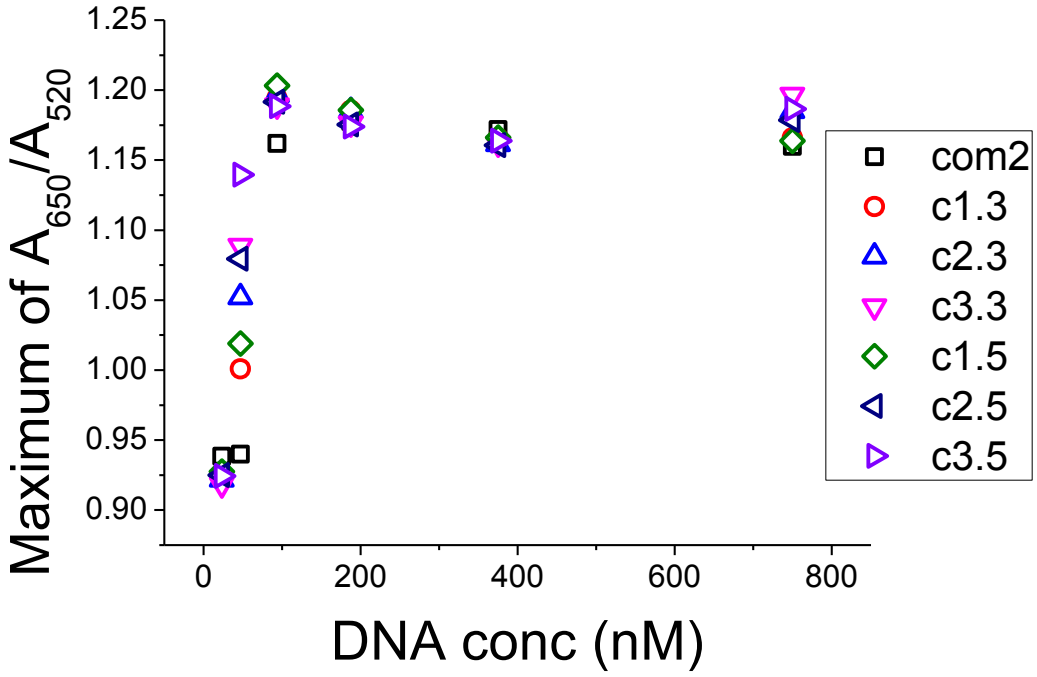

B

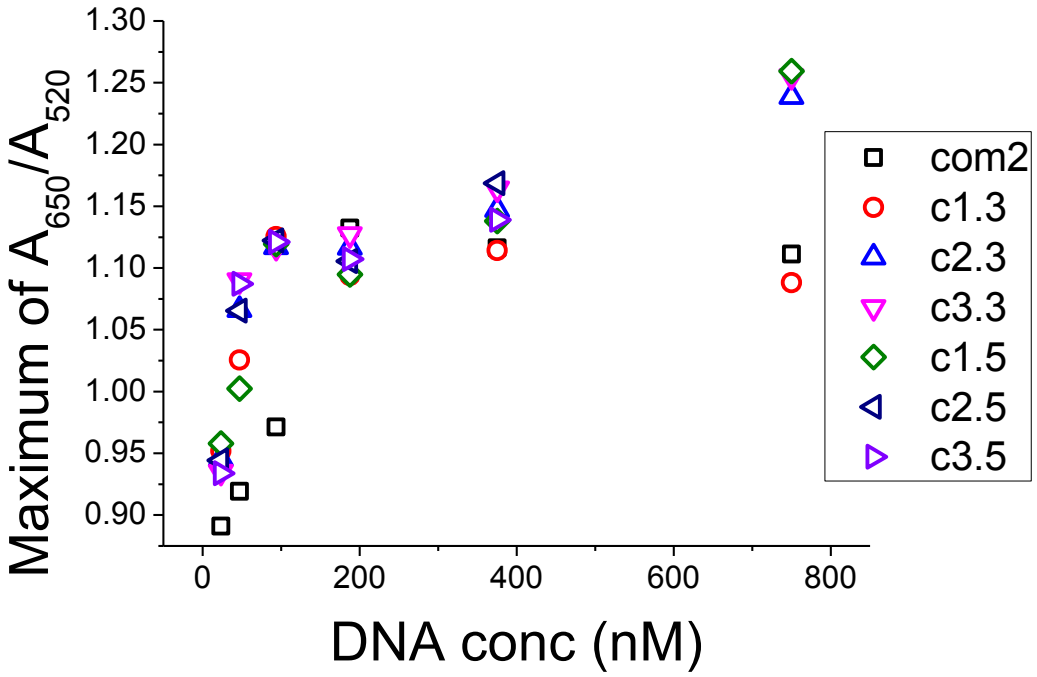

Figure 3-11 Effect of length on interactions between GNPs and dsDNA. (A) Maximum color change of ssDNA (B) Maximum color change of dsDNA

Figure 3-12 shows schematics for overhangs with different sequence. C2A is c1.5. It has five 'A' nucleotides attached to the 5' end of com2. The five 'A' nucleotides was replaced with five 'C', 'G' or 'T' nucleotides. They were named after sequence type, as shown in Figure 3-12.

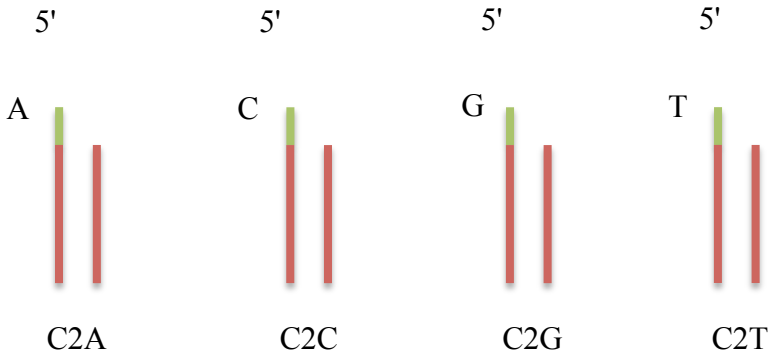

Figure 3-12 Schematic illustration of dsDNA with overhangs in different sequence at 5'.

It was suggested from Figure 3-13 that the c.c.c. values and K_D of these overhangs are very different dependent on sequence type. ssDNA binds to GNPs stronger than dsDNA, except for C2G which is due to the Quadra duplex structure that formed by continues G bases. The binding strength of these dsDNA ranks from high to low is C2C>C2T>C2G>C2A>com2. In addition, the difference between ssDNA and dsDNA on overhangs is smaller than that between ssDNA and matched dsDNA. The binding energies of those dsDNA were very close to each other (Table 3-8). Again, it confirmed the assumption that the stabilization is mainly caused by the extended tail. The structure difference of GNPs aggregation with different DNAs could be confirmed from the maximum of A_{650}/A_{520} (Figure 3-13C).

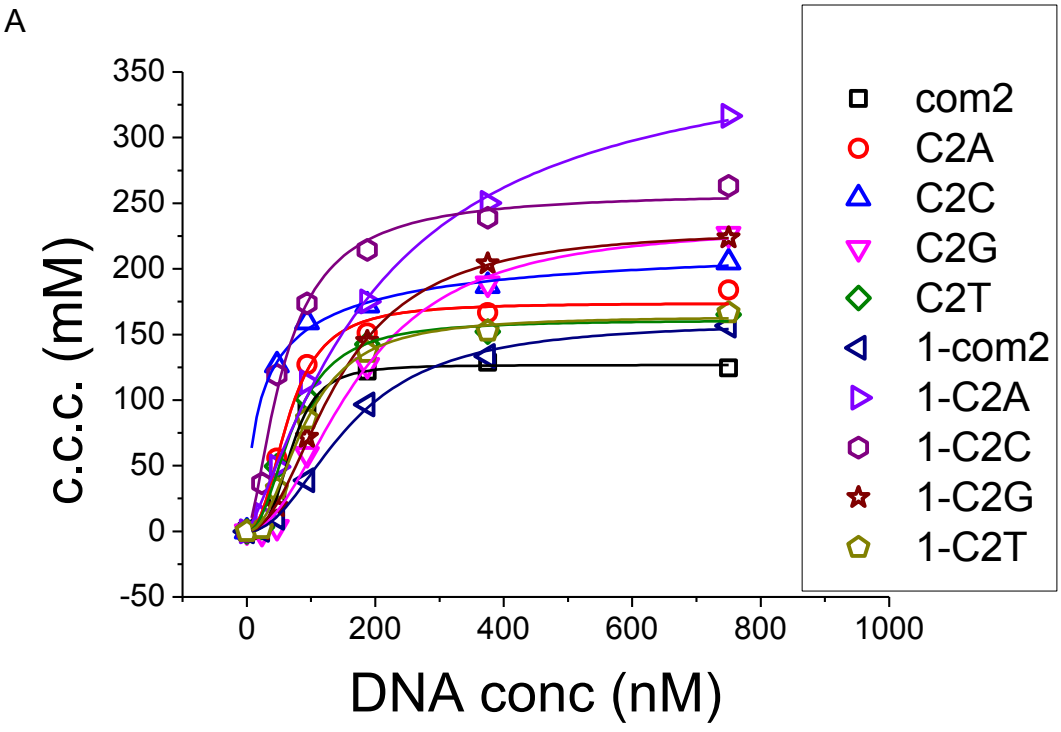

B

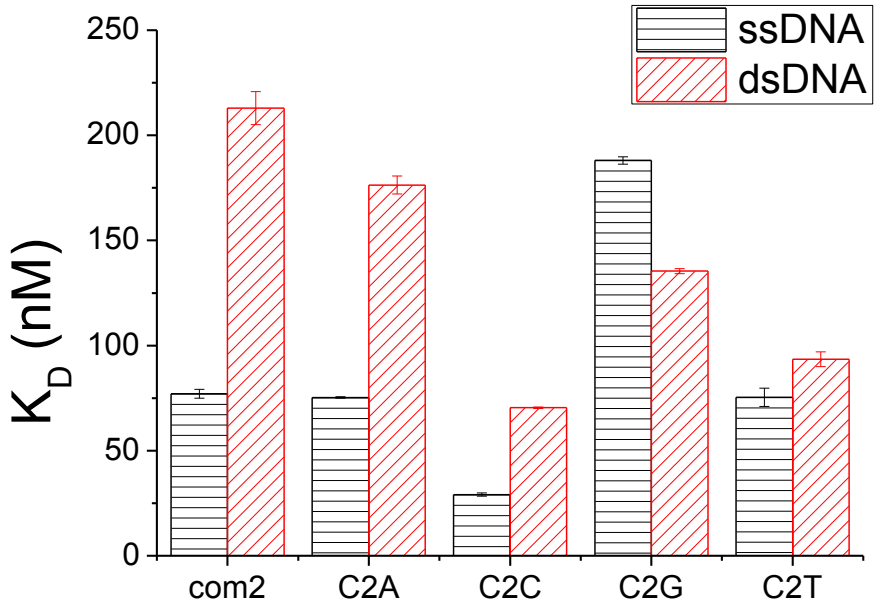

C

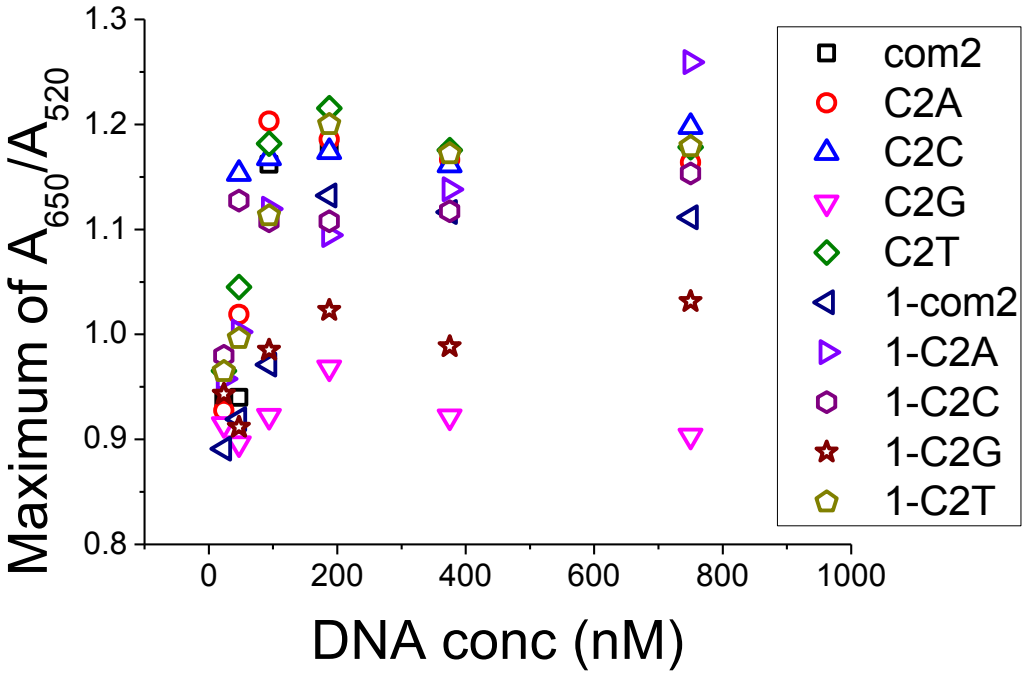

Figure 3-13 Effect of sequence on interactions between GNPs and dsDNA with overhangs. (A) c.c.c. (B) K_D (C) Maximum color change

Table 3-8 Binding energy of dsDNA with overhangs in different sequence.

	$\Delta G_{Secondary\ Structure}$ (kcal/mol)	$\Delta G_{Hybridization}$ (kcal/mol)
com2	0.7	-34.7
C2A	0.7	-35.2
C2C	-1.1	-35.0
C2G	0.7	-35.2
C2T	0.7	-35.3

3.4.3 dsDNA with Mismatches

To study the interactions between GNPs and dsDNA with mismatches, we designed three sets of DNAs with mismatches. The first set is for studying position of the mismatches including mismatches are on one end of the DNA or at the middle or scattered different position. The second set is for studying number of mismatches. The last set is for studying sequence dependency of mismatches.

Schematics of the mismatches in different positions are shown in Figure 3-14. Three nucleotides (GTC) on com2 at different positions were replaced by mismatches (TAT). M7 has the mismatch on 5' end, M8 has the mismatch in the middle, M9 has the mismatch on 3' end and M10 has three mismatches scattered. Figure 3-15 shows that the difference between ssDNA and dsDNA of mismatches is smaller than that between ssDNA and matched DNA. In addition, the binding strength to GNPs of those four dsDNA samples ranks from M7>M8>M10>M9. It means that the position of mismatches is of great importance. The binding energy ranking between dsDNA (M9>M7>M8>M10) shown in Table 3-9 does not agree with binding strength ranking. In addition, the absolute value of Gibb's free energy of dsDNA hybridization is big. Therefore, dsDNA were most likely dehybridized by GNPs locally instead of globally. Figure 3-15C confirms that the structure of GNP aggregation with different mismatches is varied.

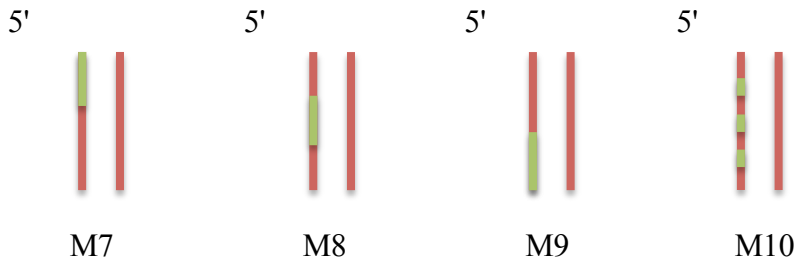

Figure 3-14 Schematic illustration of dsDNA with mismatches on different position.

A

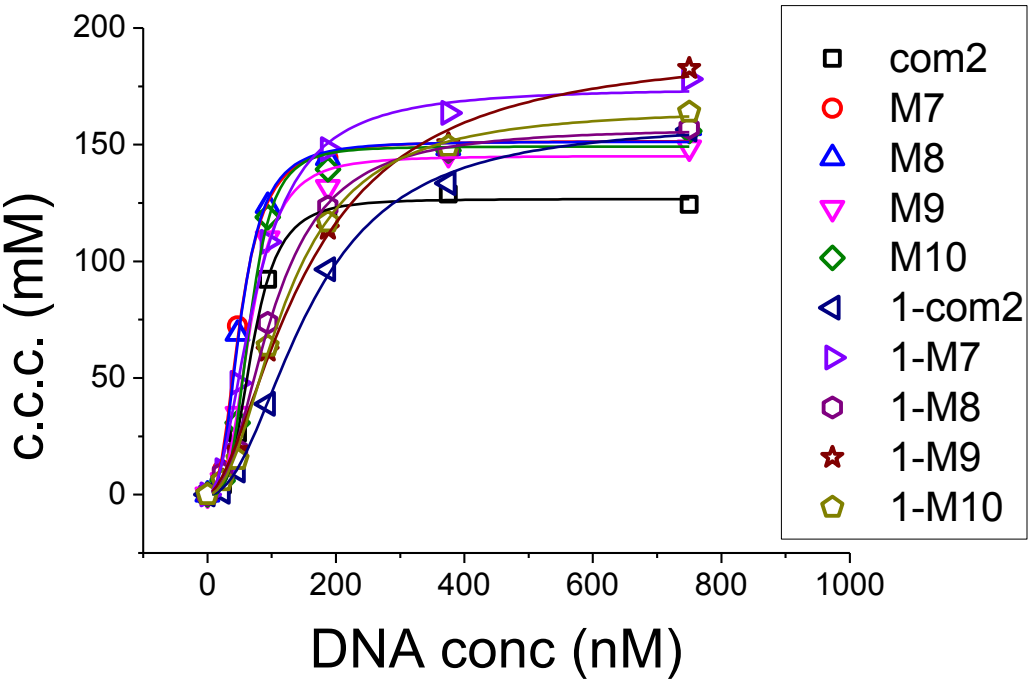

B

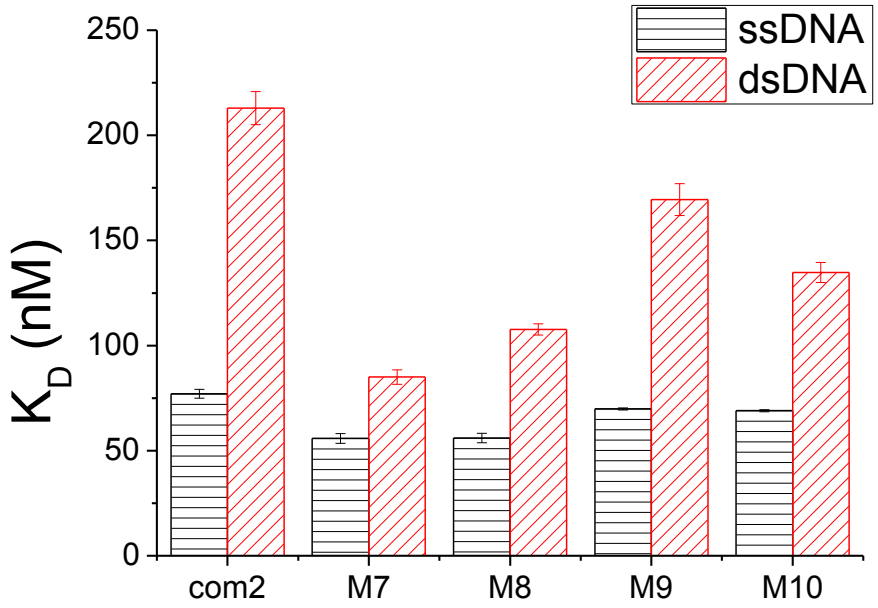

C

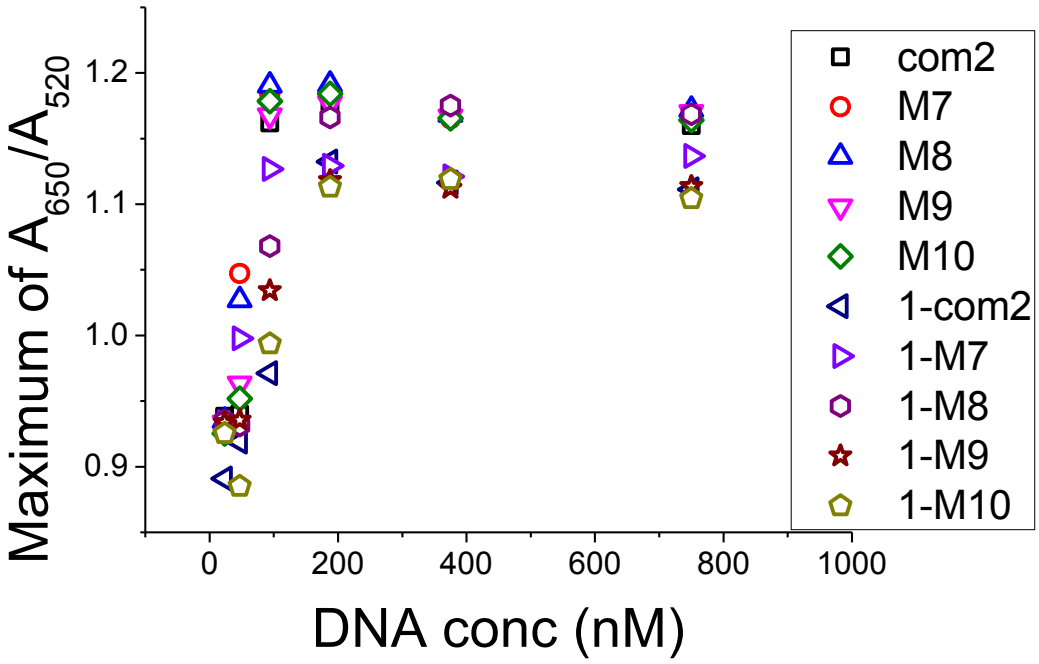

Figure 3-15 Effect of of mismatch position on interactions between GNPs and dsDNA with mismatches. (A) c.c.c. (B) K_D (C) Maximum color change

Table 3-9 Binding energy of dsDNA with mismatches on different position.

	$\Delta G_{Secondary\ Structure}$ (kcal/mol)	$\Delta G_{Hybridization}$ (kcal/mol)
com2	0.7	-34.7
M7	0.0	-30.6
M8	0.7	-25.5
M9	0.7	-31.3
M10	-0.4	-21.5

Figure 3-16 shows schematics of mismatched dsDNA with different number of mismatches. Mismatches of 1nt (M1.1), 2nt (M1.2), and 5nt (M1.5) are investigated. Mismatch position was selected at the middle of the sequence. All mismatches were modified based on com2, and com1 is fixed in all experiments. Figure 3-17A shows that before saturation, ssDNA could stabilize GNPs better than dsDNA. Figure 3-17B shows that the binding strength difference between ssDNA and dsDNA of mismatched dsDNA is smaller than that between ssDNA and matched DNA. In addition, the more mismatches the better the corresponding dsDNA could stabilize GNPs. The binding strength ranking we got from K_D agrees with binding energy ranking as shown in Table 3-10. It indicates that the dehybridization of dsDNA with mismatches by GNPs were locally instead of globally. Figure 3-17C indicates that the structures of GNPs aggregation are different with different DNAs.

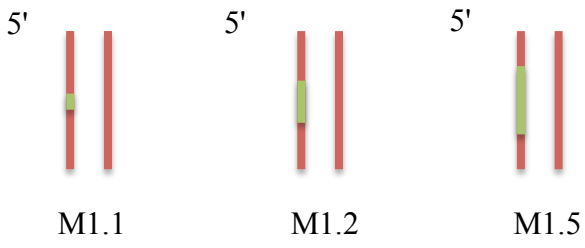

Figure 3-16 Schematic illustration of dsDNA with mismatches of different mismatch bases.

A

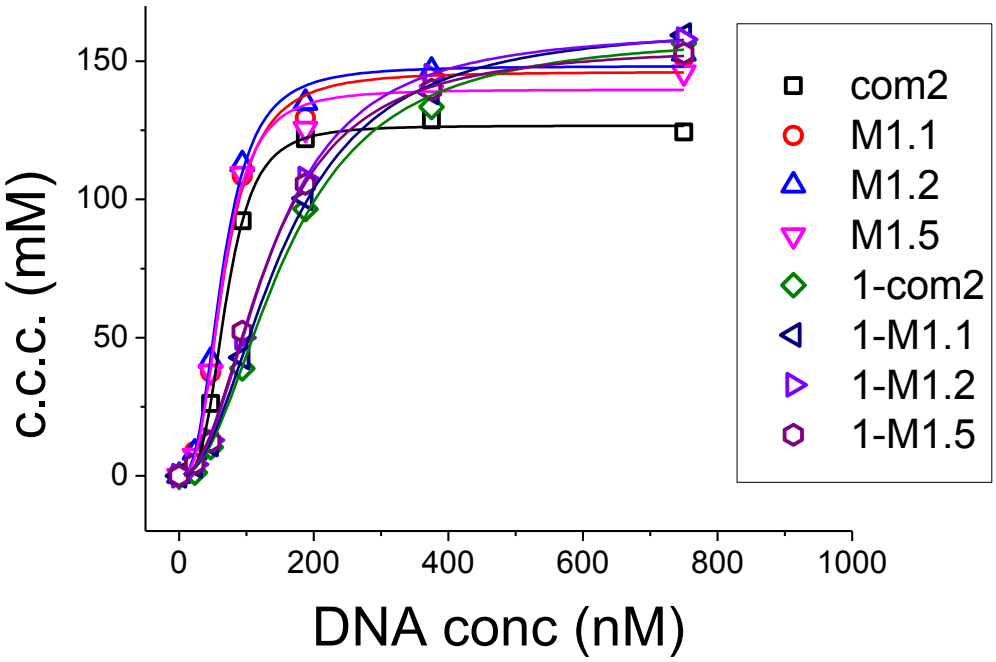
c.c.c. (mM)
DNA conc (nM)
0
50
100
150
0
200
400
600
800
1000
com2
M1.1
M1.2
M1.5
1-com2
1-M1.1
1-M1.2
1-M1.5

B

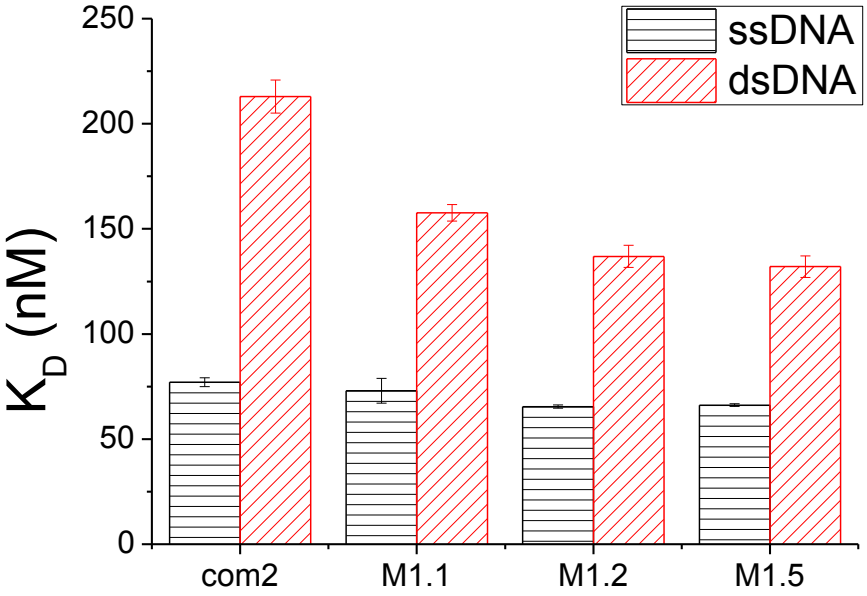
K_D (nM)
0
50
100
150
200
250
com2
M1.1
M1.2
M1.5
ssDNA
dsDNA

C

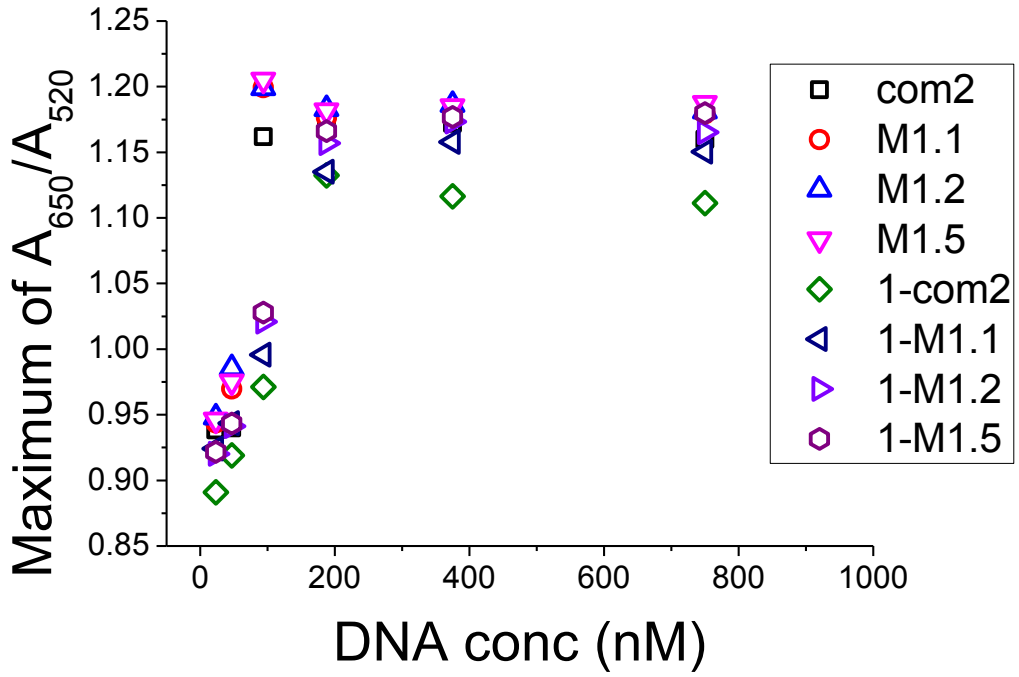

Figure 3-17 Effect of mismatch bases on interactions between GNPs and dsDNA with mismatches. (A) c.c.c. (B) K_D (C) Maximum color change

Table 3-10 Binding energy of dsDNA with mismatches of different mismatch bases.

	$\Delta G_{Secondary\ Structure}$ (kcal/mol)	$\Delta G_{Hybridization}$ (kcal/mol)
com2	0.7	-34.7
M1.1	0.6	-29.9
M1.2	0.6	-28.5
M1.5	-0.2	-21.9

Schematics of sequence dependency on mismatches are shown in Figure 3-18. It is for the sequence dependency of mismatches. In the middle of com2 sequence there are two adjacent bases ‘A’, we replaced the sequence of AA with CC, GG and TT and got the 30 nt DNAs MC1, MG1 and MT1, respectively. Figure 3-19 shows that MG1 acts abnormal due to its higher order self-structure. In addition, the difference between ssDNA and dsDNA of mismatched dsDNA is smaller than that between ssDNA and matched dsDNA. Moreover, the interactions between GNPs and mismatched dsDNA are

slightly sequence dependent. No significant difference of K_D between dsDNA with mismatches with different sequences was observed under this experimental condition, as shown in Table 3-11. Therefore, base dependency in mismatch is not strong in the interaction of GNPs and DNAs. Figure 3-19C indicates that the structures of GNPs aggregation are different with different DNAs.

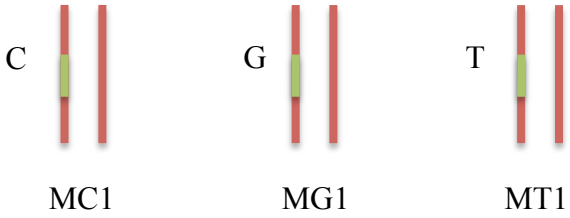

Figure 3-18 Schematic illustration of dsDNA with mismatches of different sequence.

A

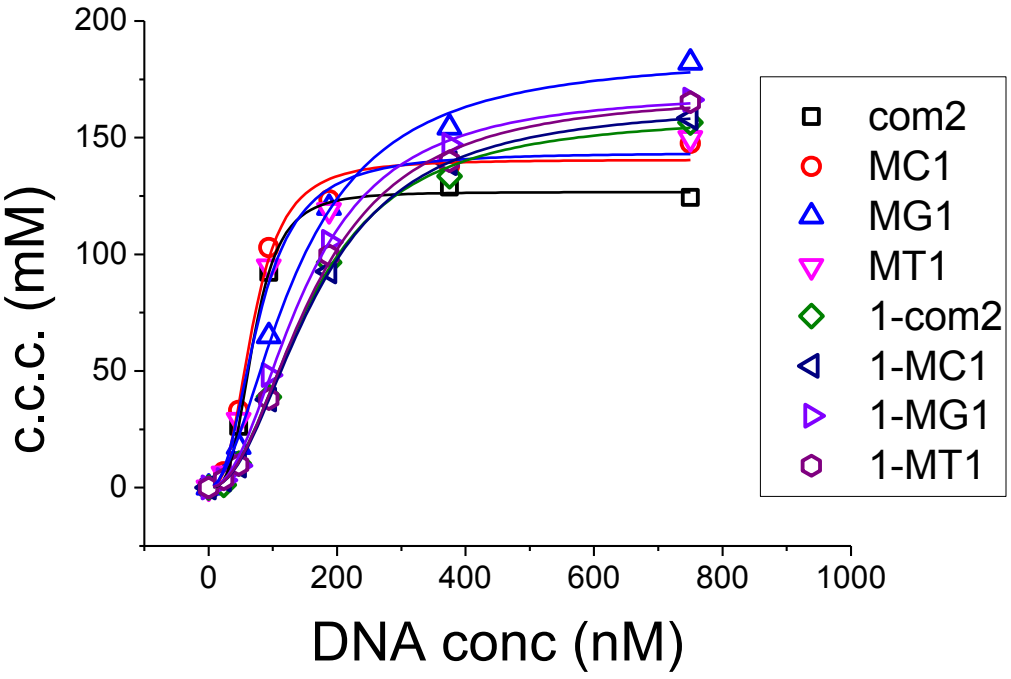

B

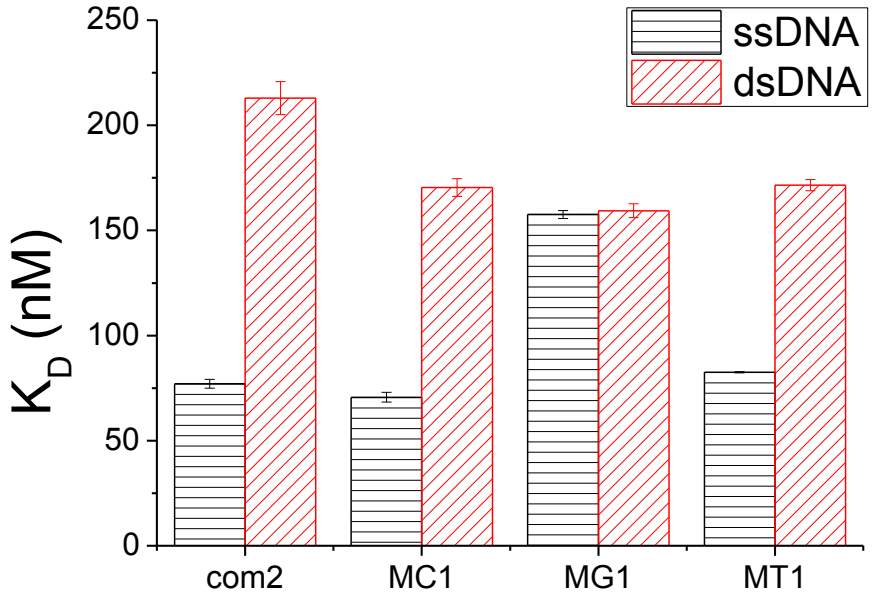

C

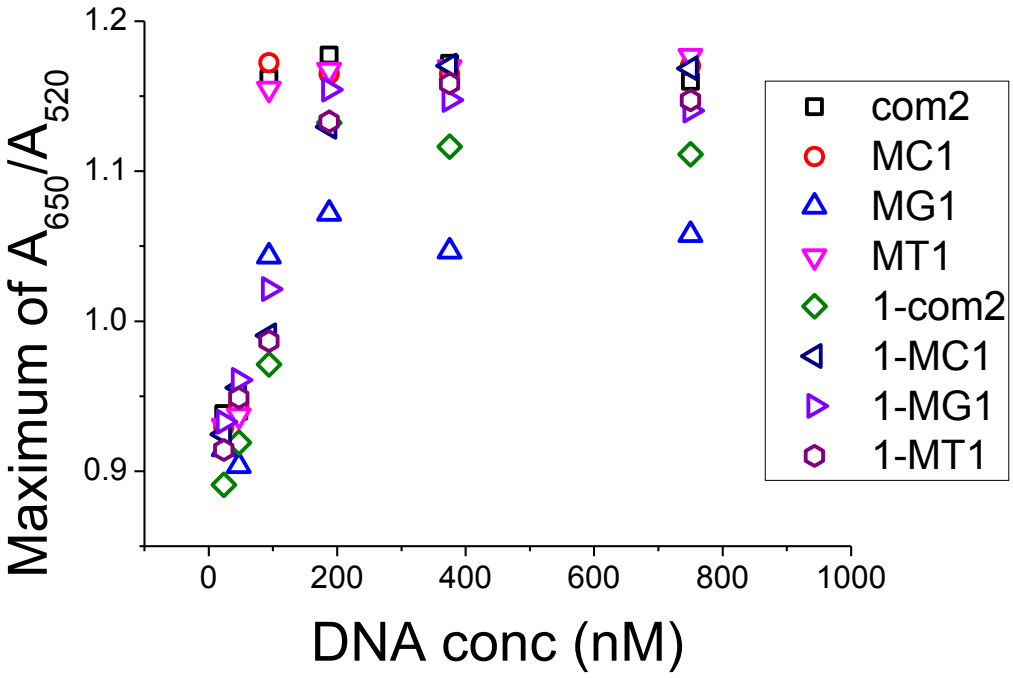

Figure 3-19 Effect of mismatch sequence on interactions between GNPs and dsDNA with mismatches. (A) c.c.c. (B) K_D (C) Maximum color change

Table 3-11 Binding energy of dsDNA with mismatches of different sequence.

	$\Delta G_{Secondary\ Structure}$ (kcal/mol)	$\Delta G_{Hybridization}$ (kcal/mol)
com2	0.7	-34.7
MC1	0.5	-29.0
MG1	1.1	-29.6
MT1	-1.6	-29.4

3.5 Conclusions

It was demonstrated in this chapter that the binding thermodynamics of DNAs to GNPs is strongly sequence dependent, length dependent and conformation dependent. Sequence dependency is due to the difference in binding of nucleobases to GNP surface, as demonstrated in Chapter 2. Length dependency is caused by binding structure difference of DNA bound to GNPs. The effect of binding strength per base is stronger for short DNAs. It would allow larger number of nt to absorb on GNPs surfaces. Conformation dependency could be explained by the difference in propensity of ssDNA and dsDNA to adsorb on GNPs. dsDNA could hardly bind to GNPs in colloidal solution because of its strongly negatively charged phosphate backbone and rigid double helix structures. dsDNA with different overhangs and mismatches were also tested for the purpose of investigating possible improvements on the selectivity and sensitivity of detection methods based on interactions of GNPs and DNAs. dsDNA with overhangs would bind to GNP surfaces through the extended tail. dsDNA with mismatches were dehybridized by GNPs, at least locally.

Chapter 4 Kinetics Study and Effect of Salt on Interactions between GNPs and DNA

4.1 Literature Review and Introduction

In recent years, analysis of the kinetics and effect of salt on interactions between DNA and GNPs has been studied [85, 92-94]. Some found that the interactions between GNPs and DNA under certain NaCl concentrations ranges, the higher the ionic strength, the more DNAs bound to GNPs [71, 95, 96]. It was noticed that it takes around 10 minutes for a 50 nt DNA to bind and stabilize GNPs [92]. However, there is no systematical study on how time and salt concentration affect the binding of DNAs to GNPs using the same experimental system. Therefore, we will use colorimetric method and fluorescent method to discover the effect of time and ionic strength on interactions between DNAs and GNPs.

4.2 Materials and Methods

4.2.1 Material

DNAs in fluorescent study was labeled with 56-FAM (6-carboxyfluorescein), which is a single isomer derivative of fluorescein. Fluorophore labeled DNAs was synthesized and processed by HPLC (high performance liquid chromatography) by IDT. Table 4-1 shows the DNAs that used in this chapter.

Table 4-1 DNA sequences used in Chapter 4.

Name	Length (nt)	Sequence (5'-3')
A-30	30	AAA AAA AAA AAA AAA AAA AAA AAA AAA AAA
T-30	30	TTT TTT TTT TTT TTT TTT TTT TTT TTT TTT
com1	30	GAC CTT AGA CTT GAC ATG CTT CTC GAC GAC
com2	30	GTC GTC GAG AAG CAT GTC AAG TCT AAG GTC
F-A15	15	/56-FAM/AAA AAA AAA AAA AAA
F-C15	15	/56-FAM/CCC CCC CCC CCC CCC
F-T15	15	/56-FAM/TTT TTT TTT TTT TTT
Fcom1	30	GAC CTT AGA CTT GAC ATG CTT CTC GAC GAC/56-FAM/
Fcom2	30	GTC GTC GAG AAG CAT GTC AAG TCT AAG GTC/56-FAM/

* /56-FAM/ is fluorophore dye

4.2.2 Colorimetric Experiments

The titration experiments are similar to that in Chapter 3. The difference will be introduced specifically if needed. There are two titration methods, one is adding NaCl gradually (Figure 4-1A) and the other is adding NaCl at once (Figure 4-1B). For the adding NaCl gradually group, 100 μL DNA were mixed with 200 μL GNPs and incubated for 48 hours. Then 100 μL mixtures were loaded into half-area wells. The titration was done by adding 5 μL NaCl each time. Absorbance was scanned after 5 minutes of incubation. Repeat until the solution has turned deep blue and there was no significant color change between two titrations. For adding NaCl at once group, the procedure was the same as introduced Chapter 3.

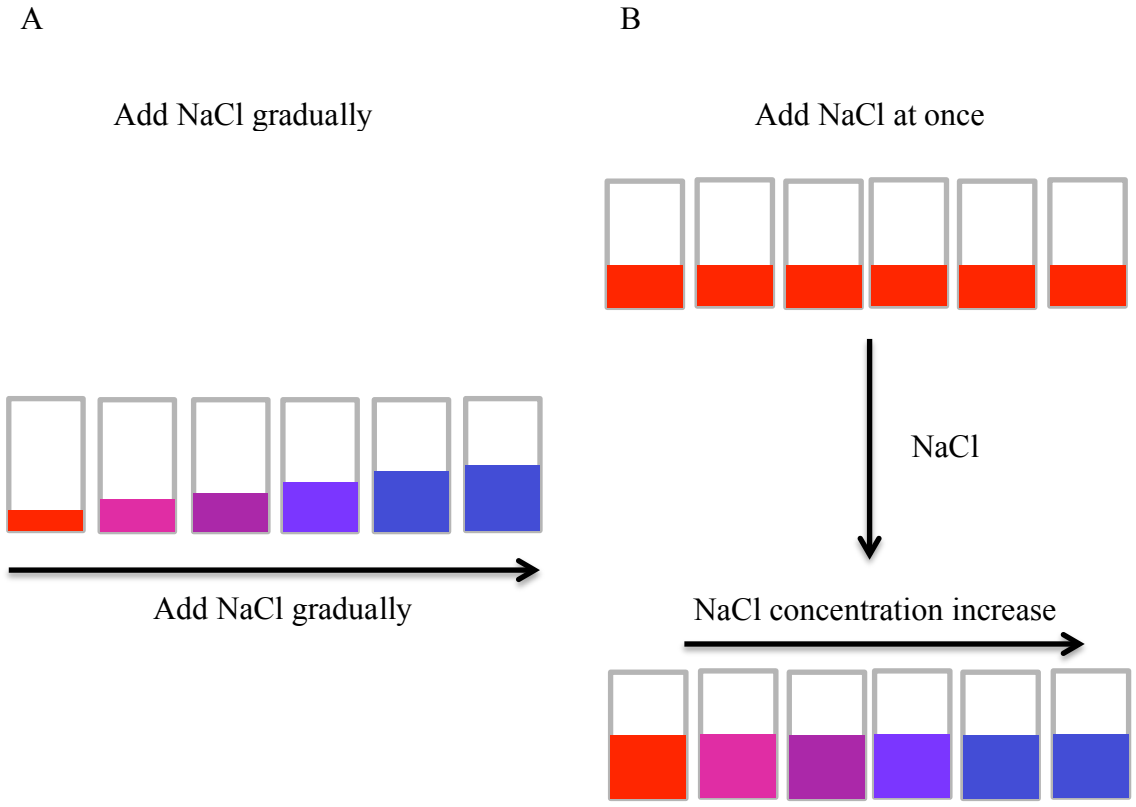

Figure 4-1 Schematic illustration of different titration methods. (A) Gradually (B) At once

4.2.3 Fluorescent Quenching Experiments and Determination of Time Constant

Because it needs more than half of an hour to get a set of results on one time point with colorimetric method, fluorescent method was introduced for kinetic study. Fluorescent method takes seconds to obtain one data point, and the sample amount needed is 1/8 of that need in colorimetric method. The fluorescent method is based on fluorescence quenching effect of GNPs on fluorophore when fluorophore modified DNA is absorbed on GNP surfaces. A typical fluorescent experiment was done by adding 20 μL DNA in 1 X buffer (0.1xPBS, 15 mM NaCl and 5 mM KCl) to 40uL GNPs. Fluorescence intensity (excitation 485 nm, emission 528 nm) was scanned by Synergy2

microplate reader. The scanning was usually done continuously in 2 minutes intervals for 1 hour, and then in 10 minutes intervals for 4 hours.

Figure 4-2 shows the experimental data of 94 nM F-A15. Function ExpDec1 in Origin® was used to fit the data. The equation is stated as:

$$y = y_0 + Ae^{-x/t} \tag{4-1}$$

where y is fluorescence intensity, x is time, y_0, A and t are constants. t is time constant, y_0 is the value of y when time at infinite and A is the difference between y at x = 0 and y_0. The parameter time constant used in this study was used to characterize the binding kinetics between DNA to GNPs [97]. Time constant indicates how rapidly the binding of DNA to GNPs happens [98]. The smaller the time constant is, the faster the binding between DNA and GNPs.

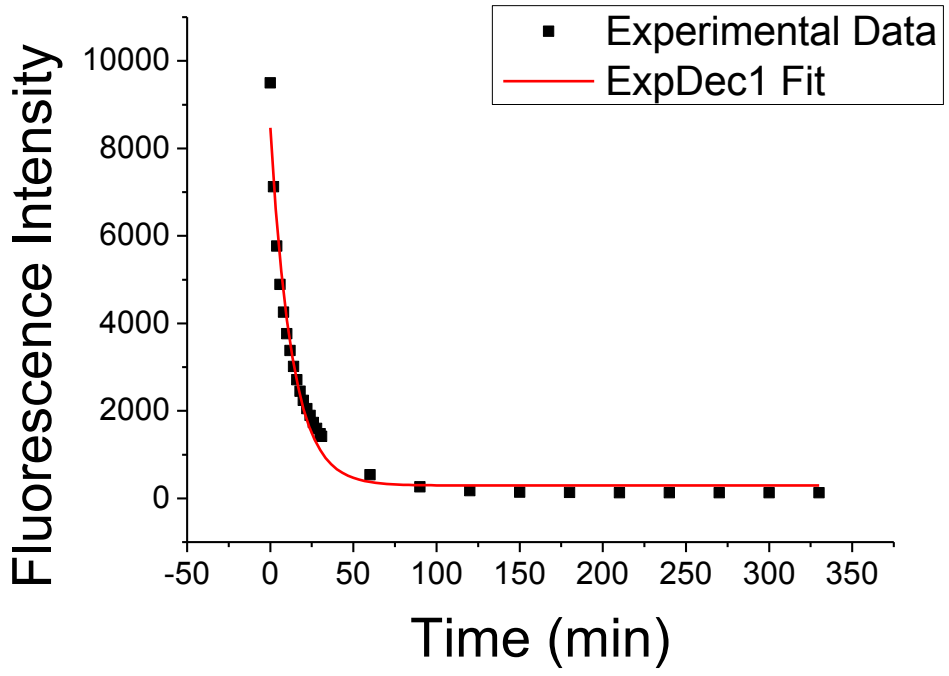

Figure 4-2 Experimental data and time constant fitting for 94 nM F-A15.

4.3 Kinetics Results and Effect of Salt on Interactions between GNPs and ssDNA

4.3.1 Colorimetric Study

Colorimetric method was used to investigate the kinetics of interaction between GNPs and ssDNA from two aspects. One is the way of adding NaCl in titration. Another is binding kinetics effect of salt on base dependency on binding kinetics with GNPs. Last is the comparison on the buffer in DNA dilution.

To study the way of adding NaCl in titration experiments, we compared two ways to add NaCl in the titration step, gradually or at once. Figure 4-3A shows that the c.c.c. ranking of adding NaCl gradually or at once are all A>T>C>G. Figure 4-3B shows that the ranking of binding strength of different homo-oligonucleotides to GNPs is A>T>C>G, for both titration methods. It indicates that adding NaCl gradually would make GNPs more stable than adding NaCl at once, except for G due to its higher order self-structure. NaCl have two effects on GNPs. One aggregation effect is to screen the charge on GNP surfaces and DNA backbone, thus making the binding of GNPs of ssDNA easier. The other effect is to decrease the electric double layer of GNPs. The formal effect stabilizes GNPs while the latter destabilizes GNPs. We could conclude that the dominant effect of salt here is to enhance the binding of DNA to GNPs. Figure 4-3C indicates that the structures of aggregated GNPs are different.

A

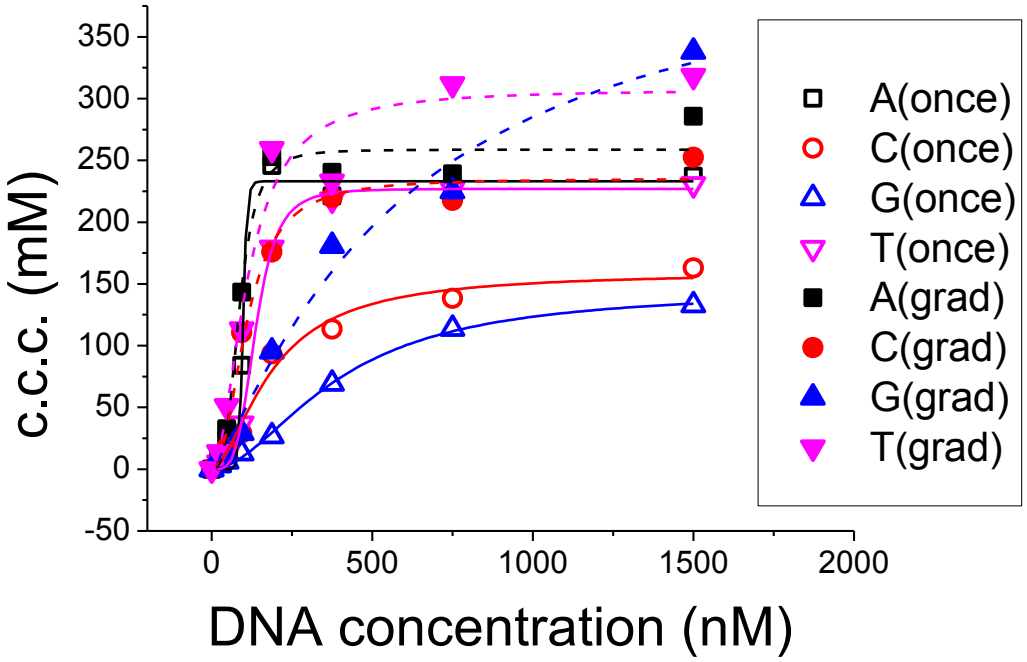
c.c.c. (mM)
DNA concentration (nM)
A(once)
C(once)
G(once)
T(once)
A(grad)
C(grad)
G(grad)
T(grad)

B

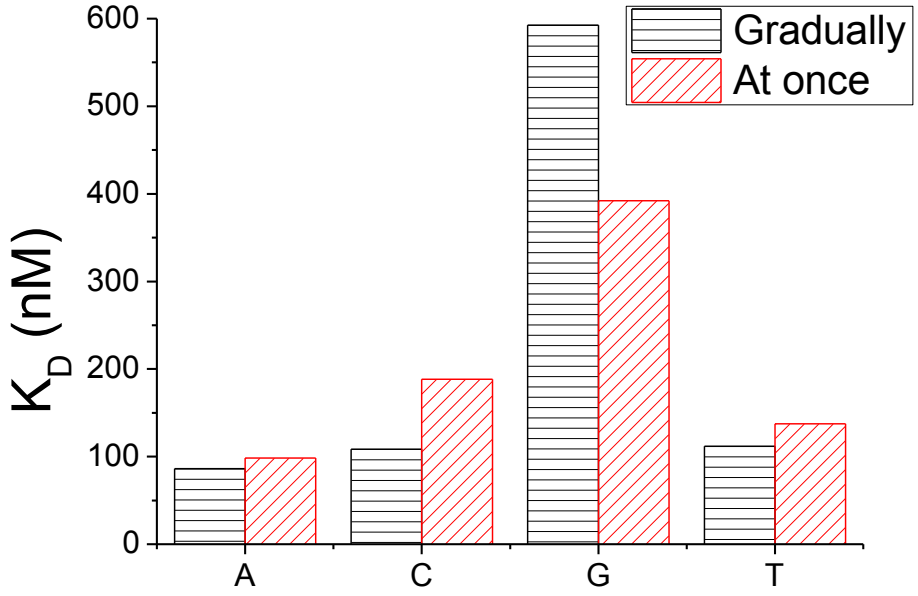
K_D (nM)
Gradually
At once
A
C
G
T

C

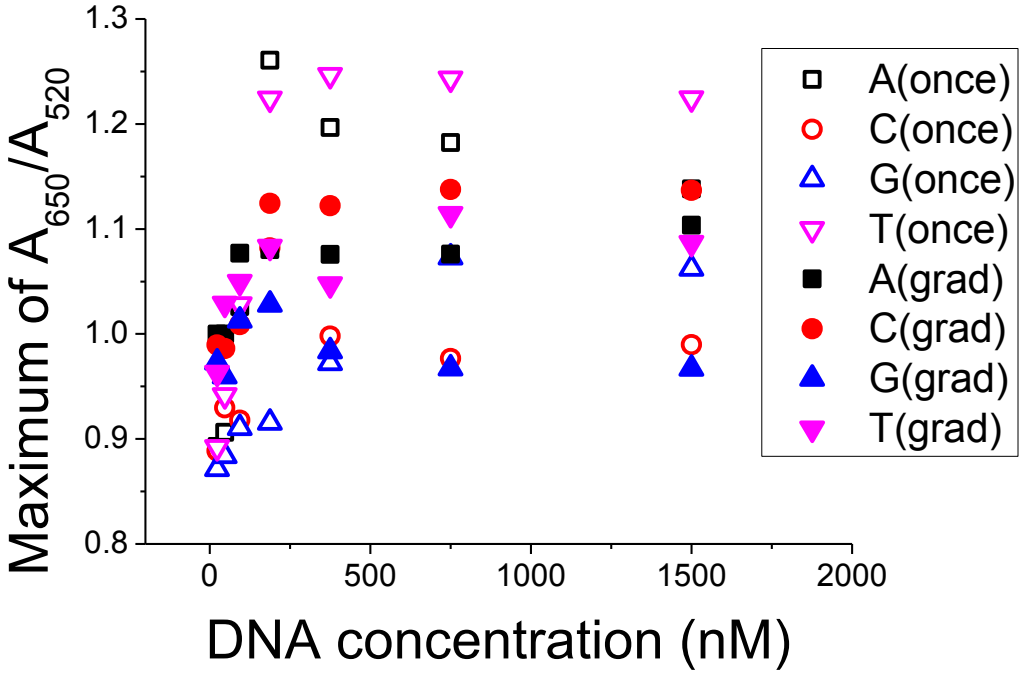

Figure 4-3 Interactions between GNPs and poly-15 DNAs studied by colorimetric method. (A) c.c.c. (B) K_D (C) Maximum color change

To study the effect of salt in ssDNA dilution, ssDNA in different NaCl (0 mM, 7.5 mM, 15 mM, 30 mM and 60 mM) to study the effect of NaCl. Interaction time between DNA and GNPs for 1.5 hours or 48 hours were used the effect of time. The titration method used here is adding NaCl at once.

Figure 4-4A and B shows c.c.c of the titration results using 750nM 15 nt homo-oligonucleotides at incubation time of 1.5 hours, with NaCl in buffer not considered or considered. The DNA concentration is close to saturation as indicated by c.c.c.. The ability of ssDNAs at stabilizing GNPs increases as the concentration of NaCl in buffer increases. This confirms that NaCl would enhance the binding of ssDNA to GNPs. In addition, sequence dependency is stronger on low NaCl concentrations. Figure 4-5A and B shows c.c.c of the titration results using 750nM 15 nt homo-oligonucleotides at incubation time of 48 hours. The trend for 48 hours is similar to that of 1.5 hours.

Moreover, binding kinetics of DNA to GNPs is sequence dependent. For example, the c.c.c. values remain to be close for A and C between incubation time of 1.5 hours and 48 hours, and c.c.c. increased dramatically at 48 hours for G and T. at 48 hours, when NaCl is 60 mM, sequence dependency is negligible. The structure of aggregated GNPs in different incubation times is of big difference, except for A-15 (Figure 4-4C and Figure 4-5C).

A

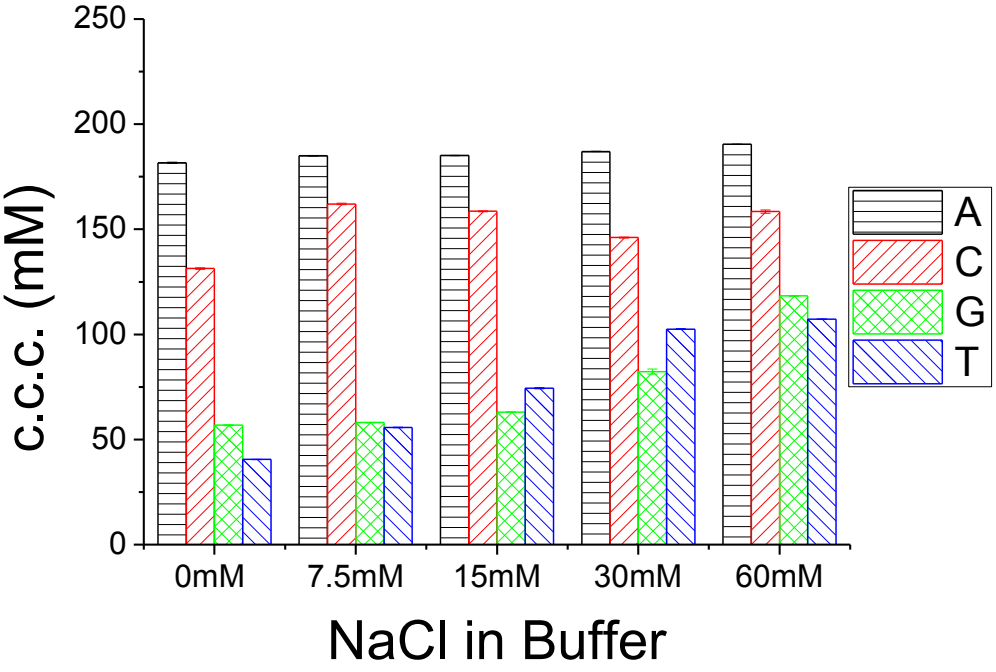

B

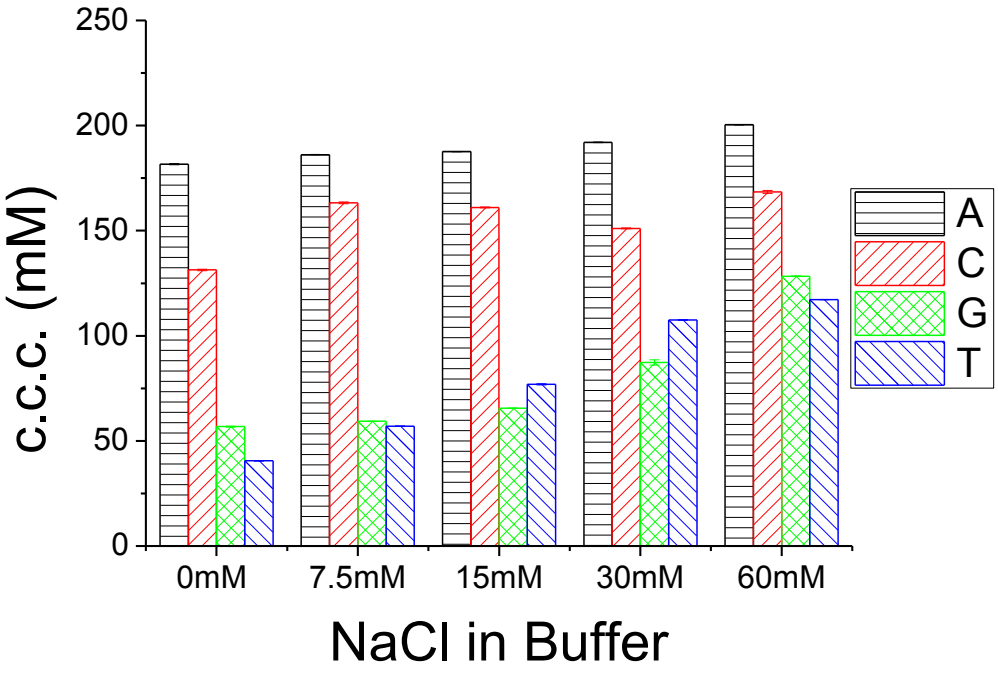

C

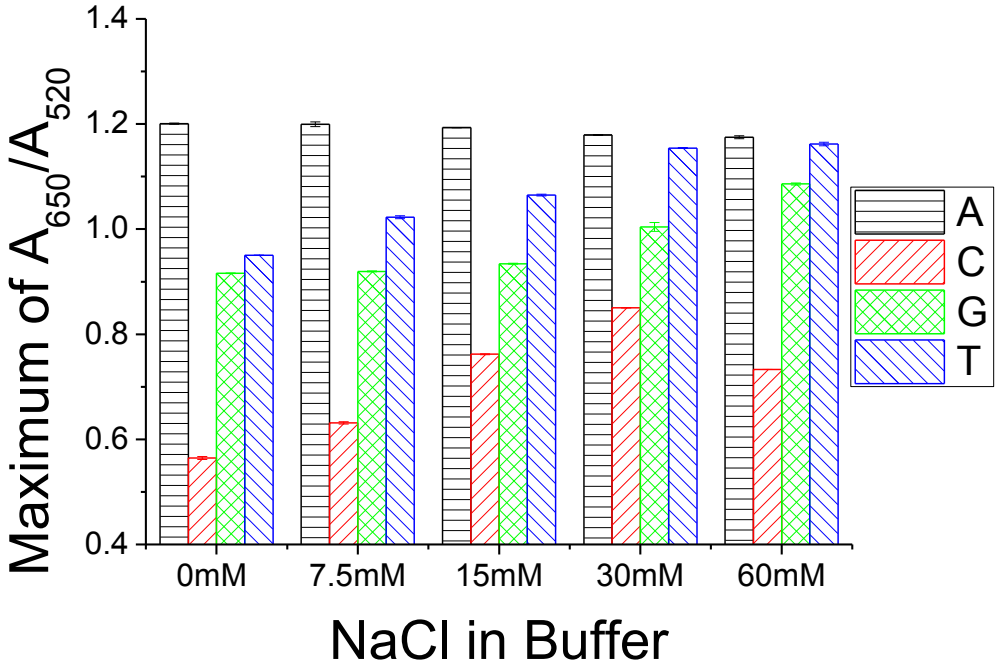

Figure 4-4 Interactions between GNPs and poly-15 DNAs at incubation time 1.5 hours studied by colorimetric method. (A) c.c.c. calculated when NaCl in buffer not considered (B) c.c.c. calculated when NaCl in buffer considered (C) Maximum color change

A

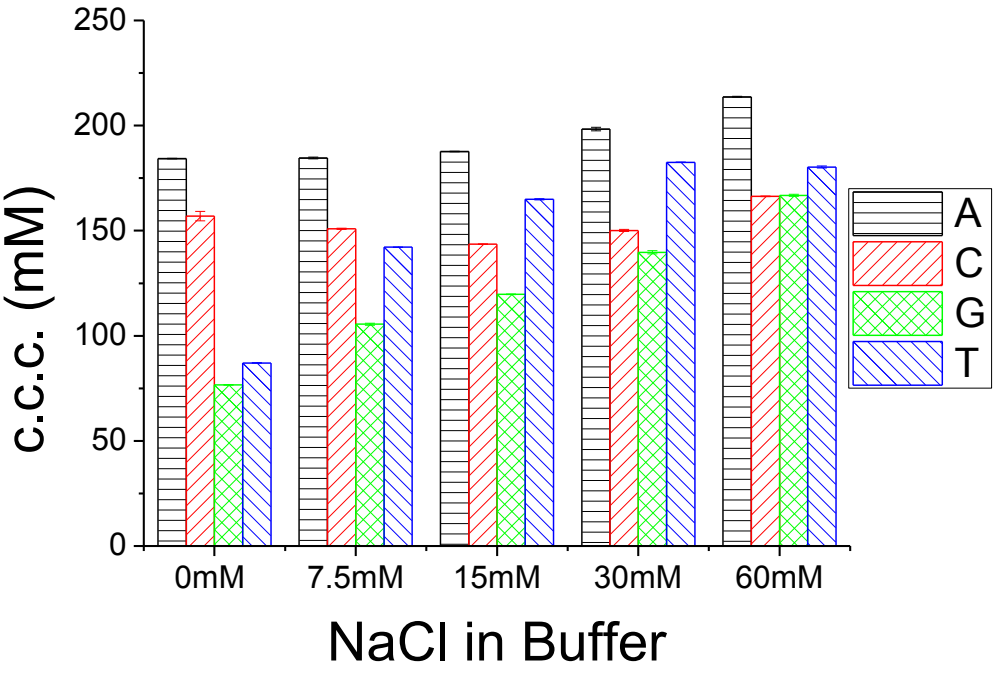
250
200
150
100
50
0
c.c.c. (mM)
0mM
7.5mM
15mM
30mM
60mM
NaCl in Buffer
A
C
G
T

B

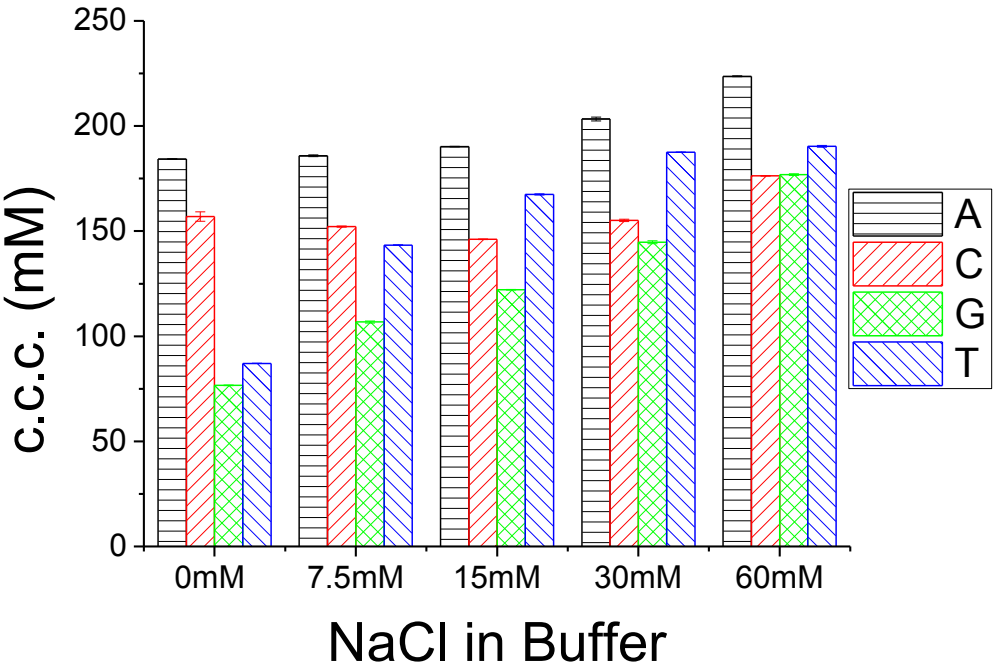
250
200
150
100
50
0
c.c.c. (mM)
0mM
7.5mM
15mM
30mM
60mM
NaCl in Buffer
A
C
G
T

C

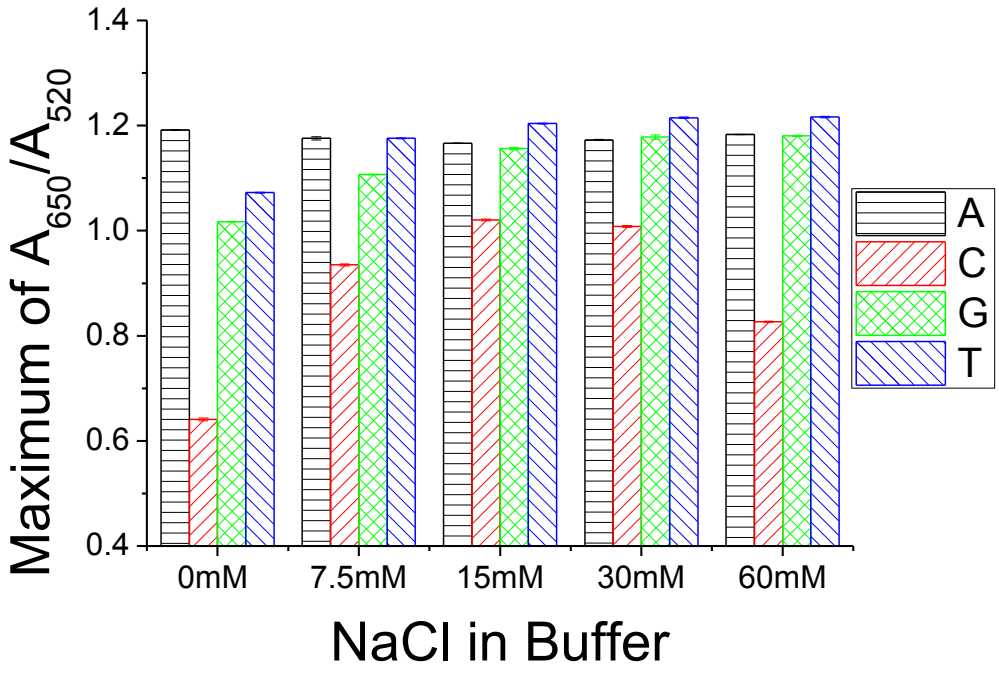

Figure 4-5 Interactions between GNPs and poly-15 DNAs at incubation time 48 hours studied by colorimetric method. (A) c.c.c. calculated when NaCl in buffer not considered (B) c.c.c. calculated when NaCl in buffer considered (C) Maximum color change

4.3.2 Fluorescent Study

The binding kinetics of F-15 DNAs in 1 X buffer to GNPs was investigated (Figure 4-6). F-G15 is not available due to its higher order self-structure. The time constant of F-A15 is smaller than that of C or T when DNA concentration is low. Time constant of F-A15 is close to that of C and T. It indicates that F-A15 binds to GNPs in a faster rate than C or T, at a low DNA concentration. However, A, C and T binds to GNPs similar at high DNA concentration.

Figure 4-7 shows that to study the effect of NaCl in DNA dilution buffer, 1 X buffer was replaced with different concentrations of NaCl. Figure 4-7 shows time constants of DNA in different concentrations mixed with GNPs for all DNA concentrations. Time

constant decreases with the increasing of NaCl concentration, for all base types and DNA concentrations. This indicates NaCl plays a significant role in the binding kinetics of ssDNA and GNPs NaCl would screen the negatively charged GNPs surface and make it easier for ssDNA to bind to GNP surface. DNAs with nucleotides T binds to GNPs surfaces much slower than those with A or C. That's why the binding strength of ssDNA T-30 to GNPs is weaker than dsDNA AT-30 at incubation time for DNA and GNPs of 1.5 hours, as in Figure 3-7. Some reported that the attachment of nucleotides to GNPs took place within 15 minutes [70]. Other researchers have reported that a salt aging step was crucial in obtaining stable oligonucleotide-modified nanoparticles [71, 95, 99]. They found that the increasing of stability of DNA-GNPs in higher salt concentrations is due to higher oligonucleotide surface coverage. It is likely that DNAs lie on GNP surfaces at first, and then stand up on GNP surfaces as NaCl concentration increases [83]. NaCl would screen the negatively charges on GNPs surfaces and DNA backbones. The reduced repulsion forces allow more DNAs to bind to the GNPs surfaces, thus increasing the stability of GNPs.

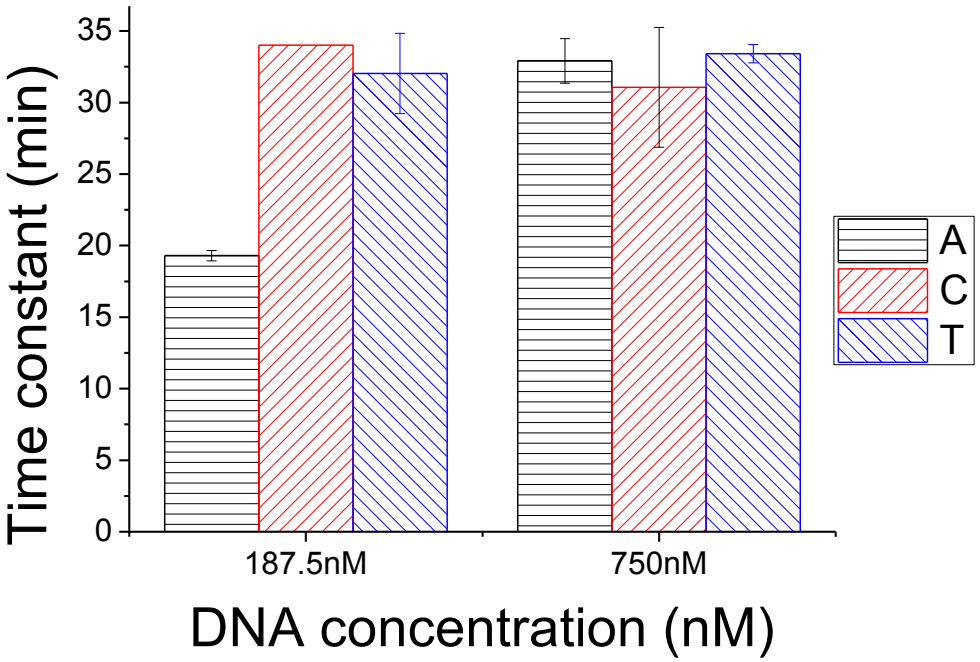

Figure 4-6 Interactions of GNPs and F-15 in 1 X buffer studied by fluorescent method.

A

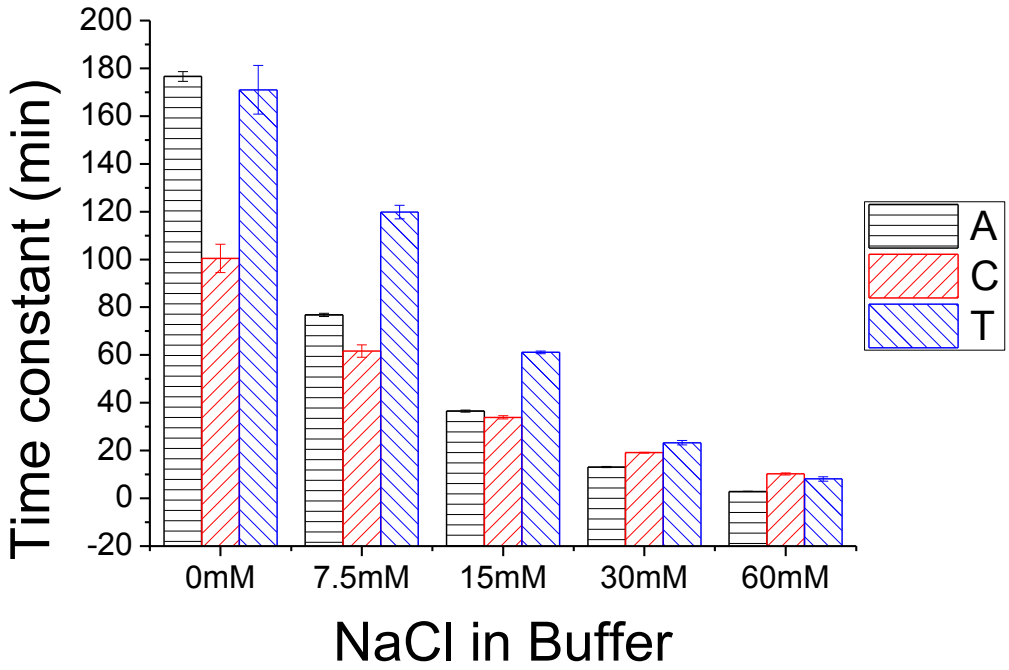

B

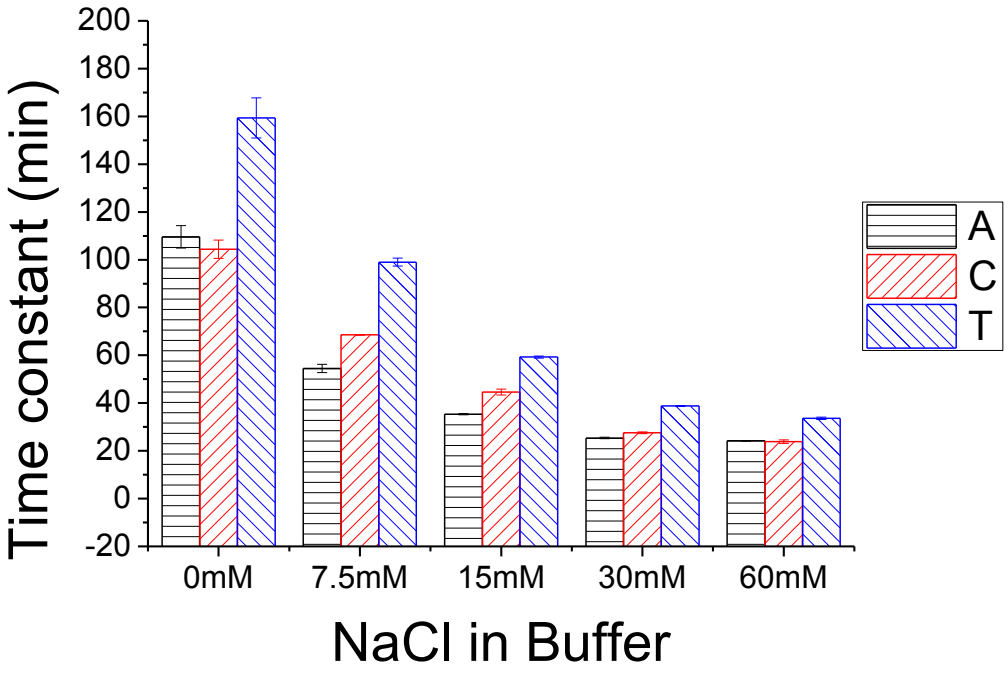

C

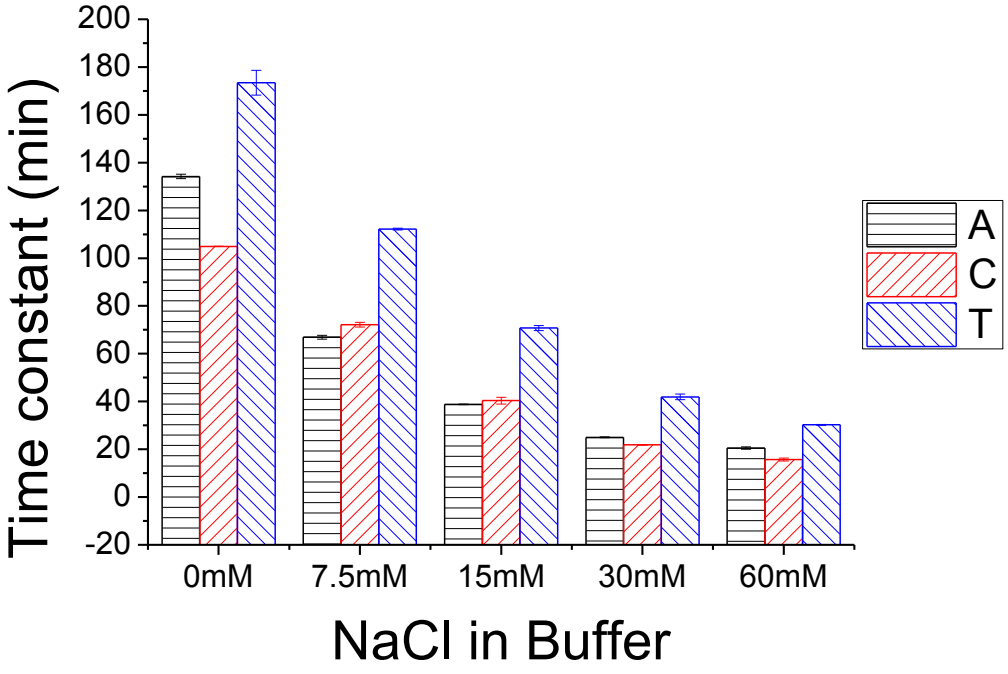

Figure 4-7 Interactions of GNPs and F-15 DNAs in different NaCl studied by fluorescent method. A) Low concentration DNA = 94 nM; B) Intermediate concentration DNA = 187.5 nM; C) High concentration DNA = 375 nM

4.4 Kinetics Results and Effect of Salt on Interactions between GNPs and dsDNA

4.4.1 Colorimetric Study

Two sets of completely complementary DNAs com1 & com2 and A-30 & T-30 were used. Firstly dsDNA was hybridized for 24 hours, and then mixed with GNPs. Titration experiments were done on incubation time of 1.5 hours and 48 hours. Figure 4-8A, B shows that that c.c.c. values of incubation time 48 hours for all samples are larger than that of 1.5 hour. T-30 has a dramatic increase on c.c.c. from incubation time of 1.5 hours to 48 hours. This means the binding between DNAs and GNPs dose not reached equilibrium state within 1.5 hours of incubation. The difference between ssDNA and dsDNA is more obvious at incubation time of 1.5 hours. Therefore, the K_D here is not the real K_D, but a parameter to indicate the extend of DNA binds to GNPs. Figure 4-8C shows that K_D at incubation time of 48 hours is much smaller than that of 1.5 hours. It suggests more DNAs were bound to GNPs at incubation time 48 hours. It indicates that incubation time is a significant factor to be considered in designing GNPs based biosensors. The structures of aggregated DNA-GNP conjugate in different NaCl concentrations are different (Figure 4-9).

A

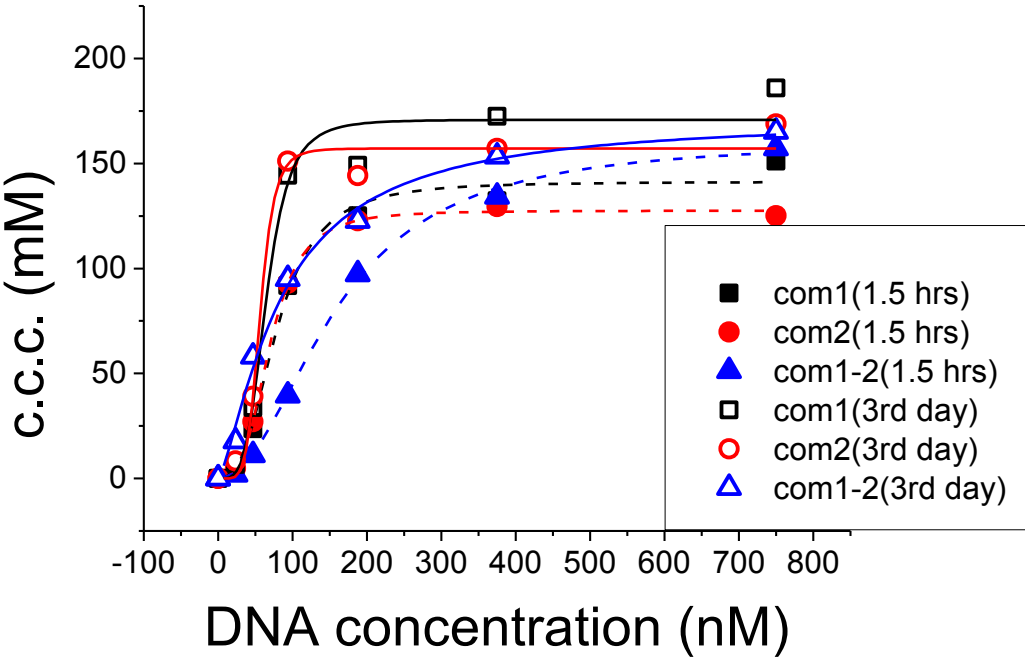
200
150
100
50
0
c.c.c. (mM)
-100
0
100
200
300
400
500
600
700
800
DNA concentration (nM)
com1(1.5 hrs)
com2(1.5 hrs)
com1-2(1.5 hrs)
com1(3rd day)
com2(3rd day)
com1-2(3rd day)

B

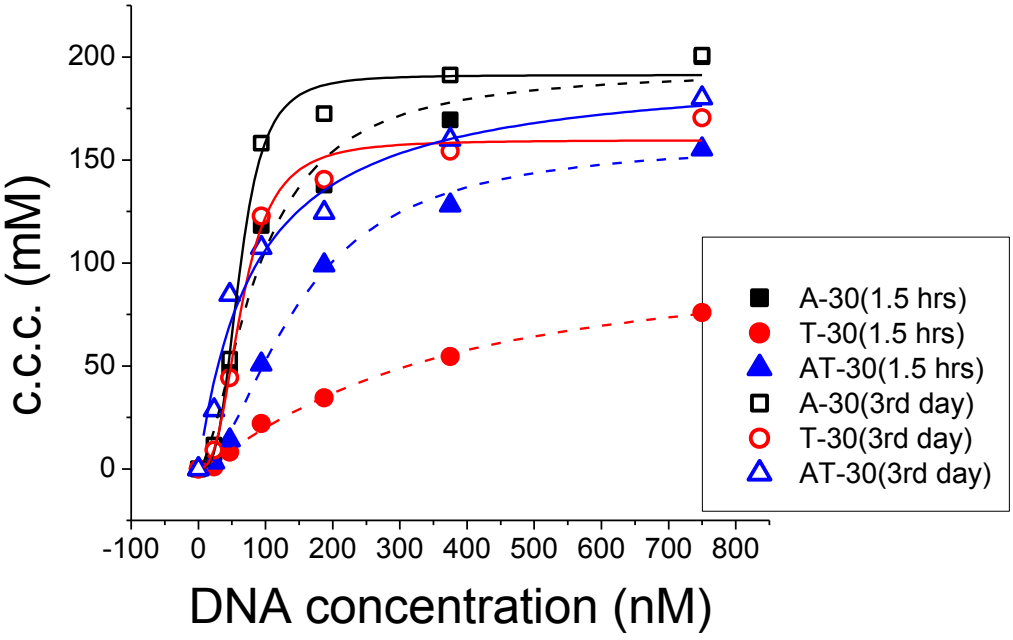
200
150
100
50
0
c.c.c. (mM)
-100
0
100
200
300
400
500
600
700
800
DNA concentration (nM)
A-30(1.5 hrs)
T-30(1.5 hrs)
AT-30(1.5 hrs)
A-30(3rd day)
T-30(3rd day)
AT-30(3rd day)

C

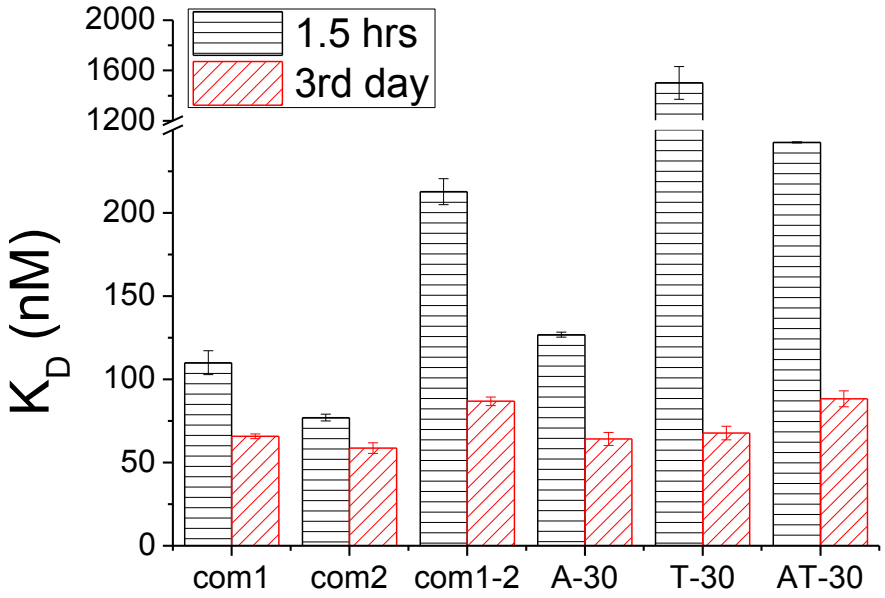

Figure 4-8 Interactions between GNPs and matched dsDNA studied by colorimetric method. (A) c.c.c. of com1 and com2 (B) c.c.c. of A-30 and T-30 (C) K_D

A

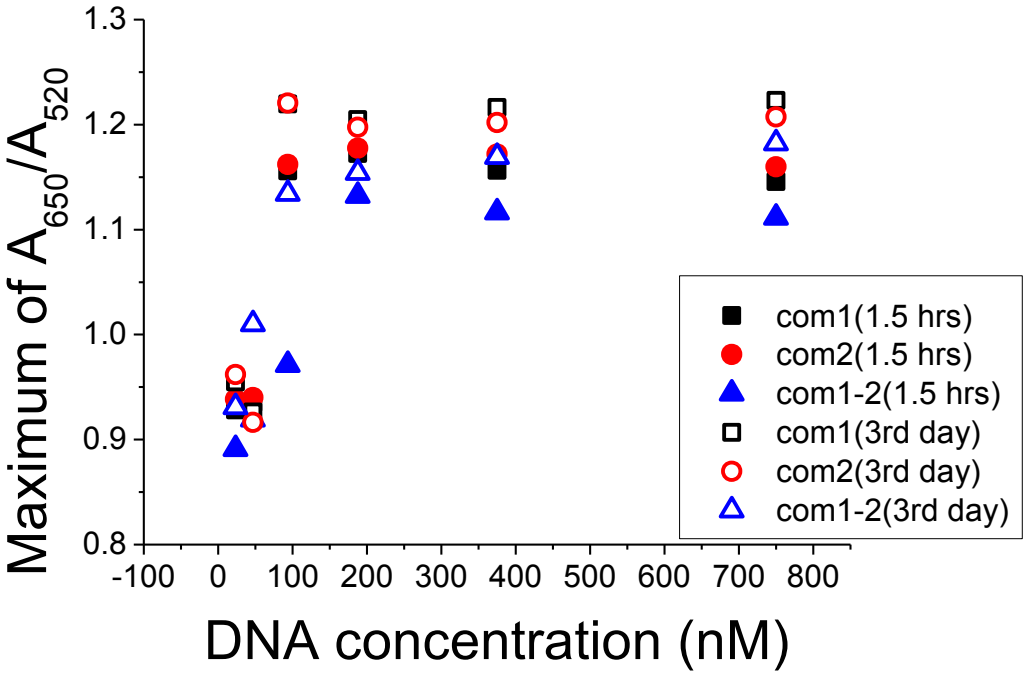

B

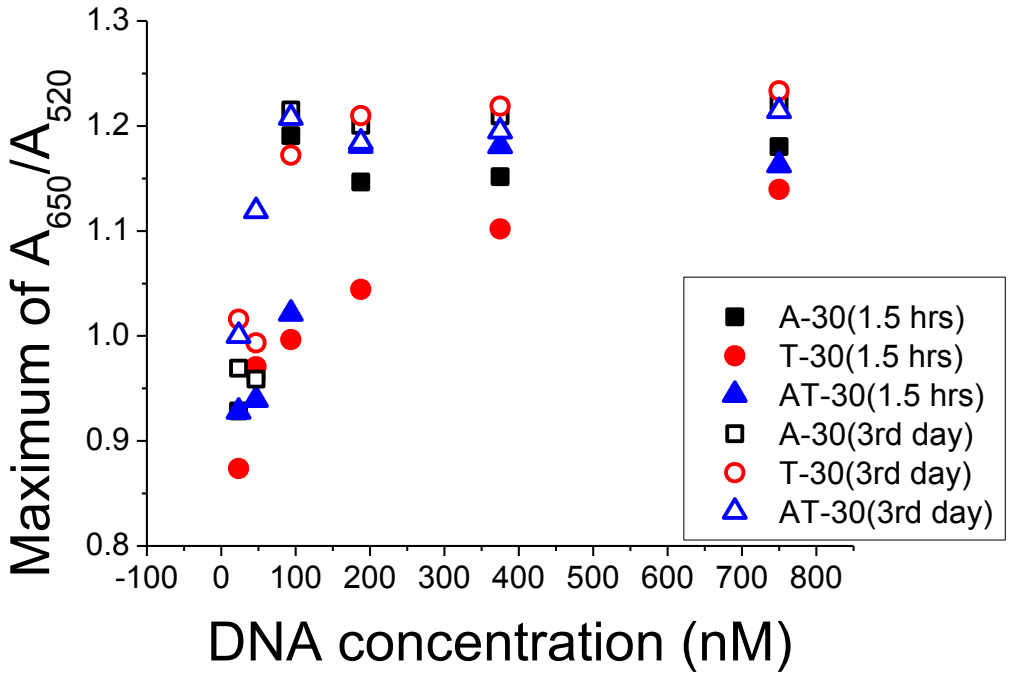

Figure 4-9 Interactions between GNPs and matched dsDNA studied by colorimetric method. (A) Maximum color change of com1 and com2 (B) Maximum color change of A-30 and T-30

4.4.2 Fluorescent Study

To compare the binding kinetics of ssDNA and dsDNA in more details, we did fluorescent study. com1 and com2 were modified with a fluorophore on one end, named Fcom1 (F1) and Fcom2 (F2), respectively. Two sets of experiments were conducted: one is Fcom1 & com2 (F1-2) and the other is com1 & Fcom2 (1-F2). Hybridization buffer of DNAs are 0 mM, 7.5 mM, 15 mM, 30 mM and 60 mM NaCl. Figure 4-10 shows that ssDNAs have smaller time constants than dsDNA, except for those in 0 mM NaCl (DNA not hybridized) and 60 mM NaCl (GNPs aggregated) as hybridization buffer. This means that ssDNAs binds to GNPs faster than dsDNA. In presence of higher NaCl concentration, both ssDNA and dsDNA have smaller time constants. The role of salt in the interaction between dsDNA and GNPs is more complicated than that of ssDNA. One of the effects is

to screen the negative charge on GNPs, which would help the binding of DNA to GNPs and therefore stabilize GNPs. The second effect is to enhance the hybridization efficiency of dsDNA. The third effect is to decrease the electrical double layer of GNPs. The first would stabilize GNPs, the second would stabilize GNPs and the third would destabilize GNPs. It could be concluded that in the range of NaCl concentration from this experiment, the dominant effect of salt is to screen charges on GNPs and enhance the binding of ssDNAs to GNPs, thus stabilizing GNPs.

A

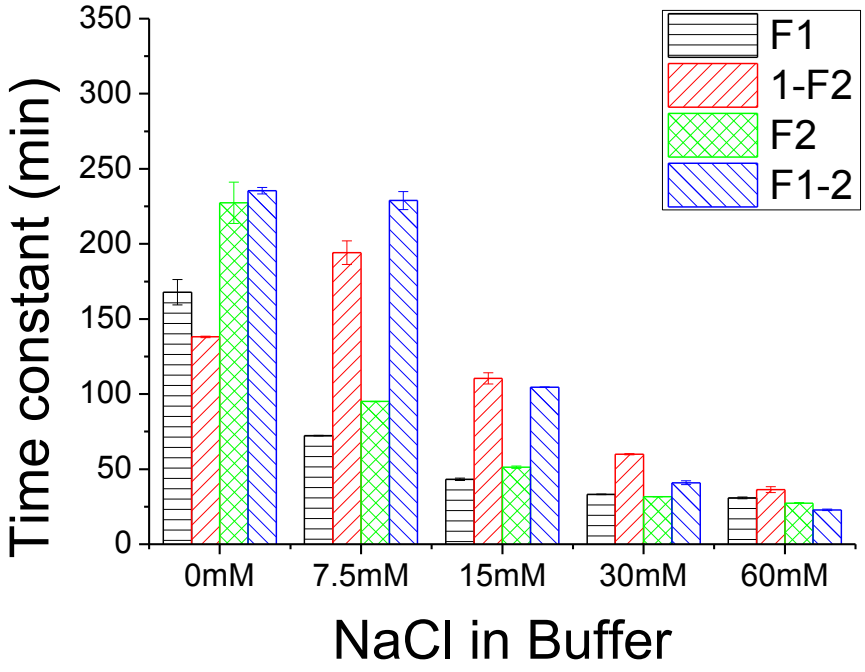

B

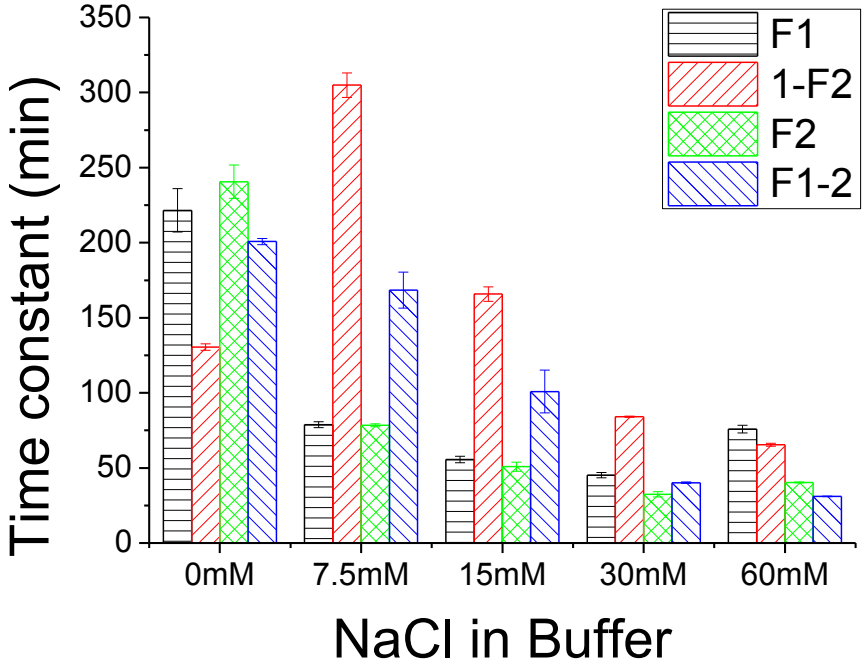

Figure 4-10 Interactions between GNPs and matched dsDNA studied by fluorescent method. (A) DNA concentration 187.5 nM (B) DNA concentration 375 nM

4.5 Conclusions

In this chapter, colorimetric method and fluorescent method were used to investigate the effect of time and salt concentration on interactions between DNAs and GNPs. It was concluded that in salt titration, adding NaCl gradually would make GNPs more stable than adding NaCl at once. Incubation time plays an important role in the binding of DNAs and GNPs. A longer incubation time would enhance the binding of DNAs to GNPs to a greater extent. Effect of salt concentration is shown to be crucial on the binding of DNAs and GNPs. Generally speaking, salt could enhance the binding kinetics, which is mainly due to the screening effect of salt on negative charges GNP surfaces and DNA backbones.

Chapter 5 Computational Study of Interactions between DNA and Target Molecules

5.1 Literature Review and Introduction

Due to its rationalized design, cost and time saving, and easy adaptability, computational methods have many advantages over experimental methods. A lot of thermodynamics-based computational models have been utilized to help rationalize the sequence design of nucleic acid probes. Most of these models are based on ranking of free energy, and these models could provide qualitative comparison between different sequence candidates [100-103]. In recent years, quite a few quantitative computational models have also been reported [104-109]. These quantitative models could calculate equilibrium concentrations of all interacting species. The calculations are based on initial concentrations and thermodynamic parameters. Previous quantitative studies consider two nucleic acids with limited DNA conformations. Recently, a model that considers various interactions between nucleic acids and non-nucleic acid species as well as formation of various nucleic acid self-structures has previously been established [110]. More importantly, all these quantitative methods were inconvenient to use due to a lack of user-friendly platform.

Therefore, we will provide an easy-to-use platform to calculate the equilibrium concentrations of three species, including non-nucleic acid molecules. The platform is based on Microsoft® Excel formulas and VBA (Visual Basic for Applications) macros.

We will develop two Excel spreadsheets. One of which is used for situations involving only nucleic acid species, and the other is used for the situation involving both nucleic acid and non-nucleic acid species.

5.2 Thermodynamics Model

For any nucleic acid species i, five different types of conformations of all nucleic acid species are considered as shown in Figure 5-1. It shows that five conformations could occur in the mixture: random coil (D_i), secondary structure ($D_{i,S}$) formed by a single stranded nucleic acid, self-dimer (D_iD_i) which is formed by two identical nucleic acids, duplex formed with another nucleic acid species j ($D_iD_{j\ (j\neq i)}$), and complex formed with a non-nucleic acid species k (D_i*P_k). Formation of D_i,S, D_iD_i, and D_iD_j is considered.

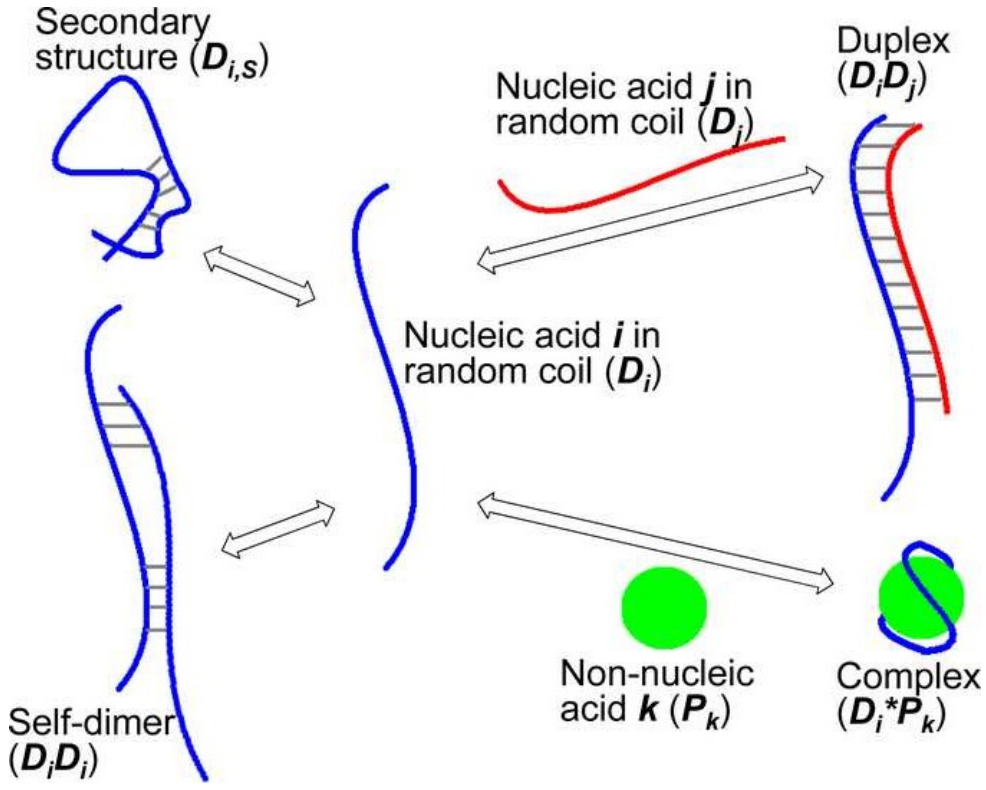

Figure 5-1 Illustration of different conformations considered for each nucleic acid species in the thermodynamic model.

Because of the difference in governing equations between situations with non-nucleic acid species or without non-nucleic species, we dealt with them separately. In Spreadsheet I which considers three nucleic acid molecules, equations need to be solved are as follows:

$$\frac{[D_1]}{[D_{1,S}]} = K_{D_{1,S}} = \exp\left(\frac{\Delta G_{D_{1,S}}}{RT}\right) \tag{5-1}$$

$$\frac{[D_2]}{[D_{2,S}]} = K_{D_{2,S}} = \exp\left(\frac{\Delta G_{D_{2,S}}}{RT}\right) \tag{5-2}$$

$$\frac{[D_3]}{[D_{3,S}]} = K_{D_{3,S}} = \exp\left(\frac{\Delta G_{D_{3,S}}}{RT}\right) \tag{5-3}$$

$$\frac{[D_1]\cdot[D_1]}{[D_1D_1]} = K_{D_1D_1} = \exp\left(\frac{\Delta G_{D_1D_1}}{RT}\right) \tag{5-4}$$

$$\frac{[D_2]\cdot[D_2]}{[D_2D_2]} = K_{D_2D_2} = \exp\left(\frac{\Delta G_{D_2D_2}}{RT}\right) \tag{5-5}$$

$$\frac{[D_3]\cdot[D_3]}{[D_3D_3]} = K_{D_3D_3} = \exp\left(\frac{\Delta G_{D_3D_3}}{RT}\right) \tag{5-6}$$

$$\frac{[D_1]\cdot[D_2]}{[D_1D_2]} = K_{D_1D_2} = \exp\left(\frac{\Delta G_{D_1D_2}}{RT}\right) \tag{5-7}$$

$$\frac{[D_1]\cdot[D_3]}{[D_1D_3]} = K_{D_1D_3} = \exp\left(\frac{\Delta G_{D_1D_3}}{RT}\right) \tag{5-8}$$

$$\frac{[D_2]\cdot[D_3]}{[D_2D_3]} = K_{D_2D_3} = \exp\left(\frac{\Delta G_{D_2D_3}}{RT}\right) \tag{5-9}$$

$$[D_1] + 2[D_1D_1] + [D_{1,S}] + [D_1D_2] + [D_1D_3] = [D_1^{initial}] \tag{5-10}$$

$$[D_2] + 2[D_2D_2] + [D_{2,S}] + [D_1D_2] + [D_2D_3] = [D_2^{initial}] \quad (5\text{-}11)$$

$$[D_3] + 2[D_3D_3] + [D_{3,S}] + [D_1D_3] + [D_2D_3] = [D_3^{initial}] \quad (5\text{-}12)$$

where D_1, D_2 and D_3 represent the three nucleic acid species that are considered in the reaction, [ ] represents equilibrium concentrations, $[D_i^{initial}]$ means the initial concentration of D_i, R is the universal gas constant, T is the absolute temperature, and ΔG is the change in Gibbs free energy. ΔG for interactions between nucleic acid species can be accurately estimated based on nearest neighbor model [111] with web servers (e.g., mfold [112-114]) or standalone software packages (e.g., RNAstructure [115]).

In situation II which considers two nucleic acids and one non-nucleic acid molecule, equations need to be solved are of some difference. For any non-nucleic acid species k, only two types of conformations are considered here: unbound (P_k) and complex formed with a nucleic acid species i (D_i*P_k). In contrast to the interactions between nucleic acid species which could be described with their intrinsic dissociation constant, the interactions between nucleic acid species and non-nucleic acid species commonly request to be described using experimentally determined apparent dissociation constant $K_{D\ i*Pk}^{App}$. Equations need to be solved are as follows:

$$\frac{[D_1]}{[D_{1,S}]} = K_{D_{1,S}} = \exp\left(\frac{\Delta G_{D_{1,S}}}{RT}\right) \quad (5\text{-}13)$$

$$\frac{[D_2]}{[D_{2,S}]} = K_{D_{2,S}} = \exp\left(\frac{\Delta G_{D_{2,S}}}{RT}\right) \quad (5\text{-}14)$$

$$\frac{[D_1]\cdot[D_1]}{[D_1D_1]} = K_{D_1D_1} = \exp\left(\frac{\Delta G_{D_1D_1}}{RT}\right) \tag{5-15}$$

$$\frac{[D_2]\cdot[D_2]}{[D_2D_2]} = K_{D_2D_2} = \exp\left(\frac{\Delta G_{D_2D_2}}{RT}\right) \tag{5-16}$$

$$\frac{[D_1]\cdot[D_2]}{[D_1D_2]} = K_{D_1D_2} = \exp\left(\frac{\Delta G_{D_1D_2}}{RT}\right) \tag{5-17}$$

$$\frac{[D_1^*]\cdot[P_1]}{[D_1^*P_1]} = \frac{\left([D_1]+[D_{1,S}]+2[D_1D_1]\right)\cdot[P_1]}{[D_1^*P_1]} = K_{D_1^*P_1}^{App} \tag{5-18}$$

$$\frac{[D_2^*]\cdot[P_1]}{[D_2^*P_1]} = \frac{\left([D_2]+[D_{2,S}]+2[D_2D_2]\right)\cdot[P_1]}{[D_2^*P_1]} = K_{D_2^*P_1}^{App} \tag{5-19}$$

$$[D_1]+2[D_1D_1]+[D_{1,S}]+[D_1D_2]+[D_1^*P_1] = [D_1^{initial}] \tag{5-20}$$

$$[D_2]+2[D_2D_2]+[D_{2,S}]+[D_1D_2]+[D_2^*P_1] = [D_2^{initial}] \tag{5-21}$$

$$[P_1]+[D_1^*P_1]+[D_2^*P_1] = [P_1^{initial}] \tag{5-22}$$

where D_i* is the nucleic acid species i in unbound conformations, which could be either random coil Di, secondary structure $D_{i,S}$, self-dimer D_iD_i or the combination of any two or three of them, D_1, D_2 represent the two nucleic acid species that are considered in the reaction, P_1 represents the non-nucleic acid species, and $[P_1^{initial}]$is the initial concentration of P_1.

For spreadsheet I, if these equations (5-1) to (5-12) are combined together, we can get a system of three functions which could be solved numerically. From that, other equilibrium concentrations could be obtained. For spreadsheet II, if these equations (5-13)

to (5-22) are combined together, we can get a system of three functions which could be solved numerically. From that, other equilibrium concentrations could be obtained.

5.3 Microsoft® Excel Based Platform

5.3.1 Implementation of the Thermodynamics Model on Excel

It is of great importance to make the thermodynamic model accessible to general scientific researchers who are not expertise in developing thermodynamic model theory or solving numerical equation set. We implement the algorithm of the thermodynamic model using a very commonly adapted and user-friendly platform, Microsoft® Excel. Microsoft Excel is a spreadsheet application developed by Microsoft for Microsoft Windows and Mac OS X [116]. The implementation was achieved by the aid of VBA (Visual Basic for Applications) macros [117]. Two Excel spreadsheets were developed: Spreadsheet I for the applications involving only nucleic acid species, with the number of nucleic acid species no more than three, and Spreadsheet II for the applications involving both nucleic acid and non-nucleic acid species, with the number of nucleic acid species no more than two and the number of non-nucleic acid species no more than one.

There are four modules in both spreadsheets (Figure 5-2). The input module is used to collect species information including DNA sequences, reaction temperature, dissociation constant for non-nucleic acid species, and initial concentrations. Then in the model module, the sequence information is asked to be pasted into DINAMelt web server (http://mfold.rna.albany.edu/?q=DINAMelt) to calculate the change of Gibbs free energy ΔG. The results are collected and then converted into dissociation constants. Then all parameters are combined together to form three equations. In the computation module,

the set of three equations is solved by setting one equation as objective function and other equations as constraints. A parameter named “Reliability” is defined to evaluate the accuracy of the solution. Up to three initial guesses would be used to solve the set of equations until the results meet the requirements of “Reliability”. If reliable solution was found, then the “Reliability” is marked as “Good”; otherwise the “Reliability” is marked as “Poor”. Possible reasons for poor results include but not limited to: the limit of significant digits in Excel’s numerical retain principle [118] and the high sensitivity to initial guesses. Results and all input parameters could be found in the output module.

5.3.2 User Interface of the Excel Spreadsheet

The main users interface in both spreadsheets is very similar to each other (Figure 5-3). A reset button is provided to set all to default. Then species type, name and sequence are collected. There is a pop-up box triggered by a button to collect names and sequences of all molecular species (Figure 5-4). Followed is the temperature section which collects the reaction temperature. The section to retrieve Gibb’s free energy of both self-structure and hybridization of DNAs are provided. By following all the instructions, one could easily obtain Gibb’s free energy. Then dissociation constant is collected, only in Spreadsheet II. After that, a pop-up box will allow users to input up to ten initial concentrations for one of the species while keeping the initial concentrations of the other two species as constant (Figure 5-5). The platform would save users considerable amount of time by processing ten concentrations at a time. By clicking the “Computation” button, one could get the result of equilibrium concentrations.

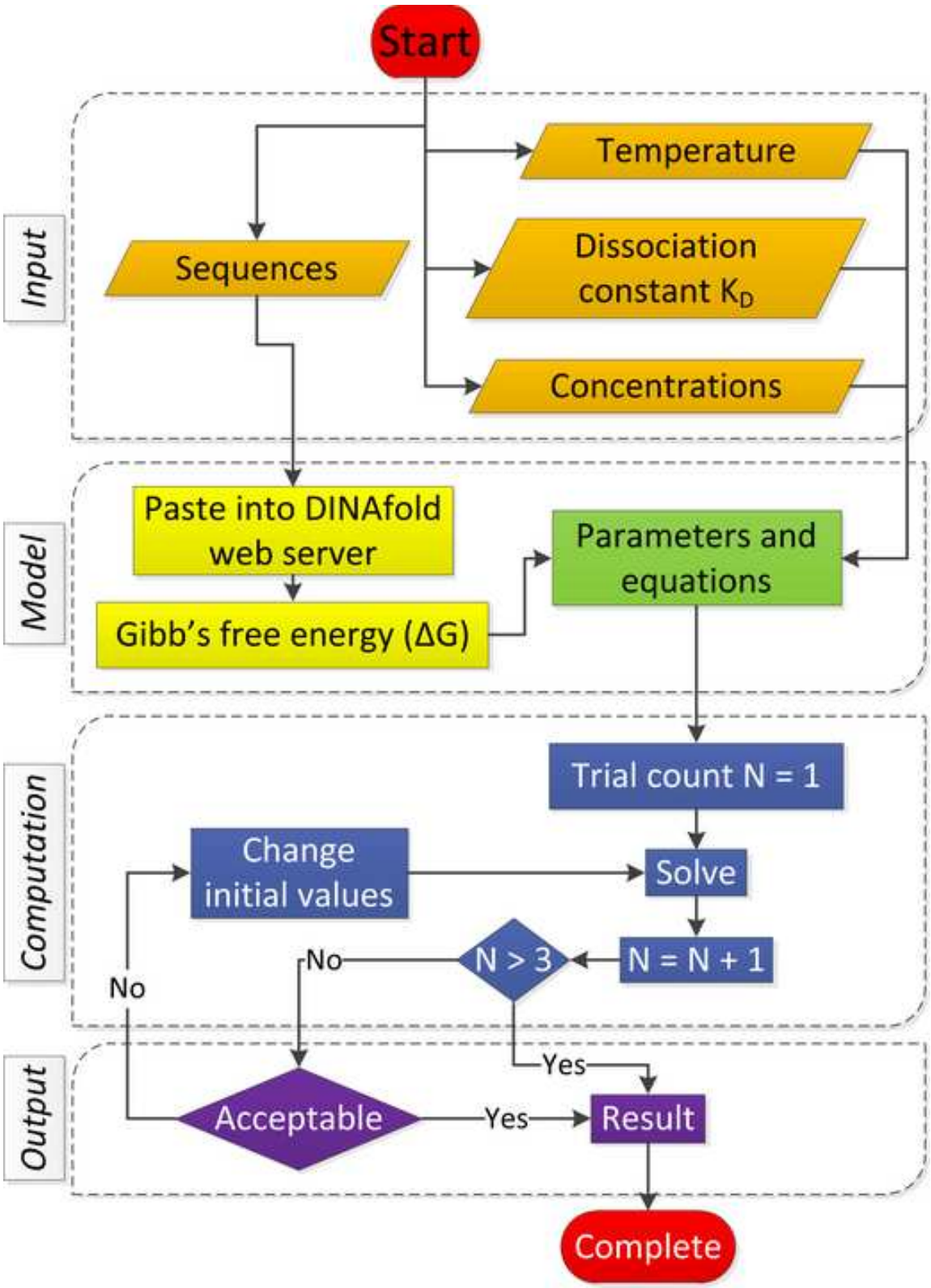

Figure 5-2 Flowchart of the implementation of the thermodynamic modeling on Excel.

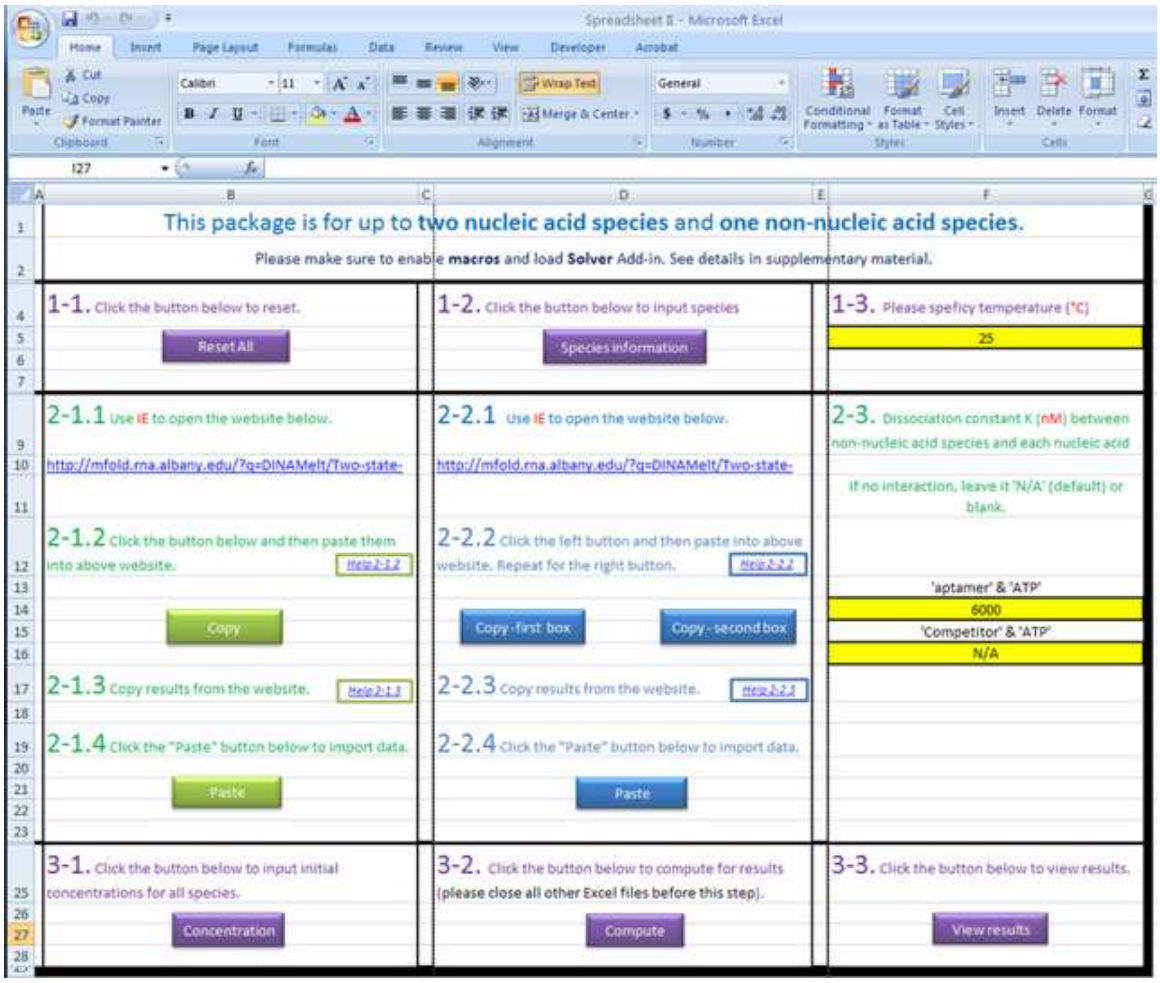

Figure 5-3 Screenshot of the main user interface of spreadsheet II.

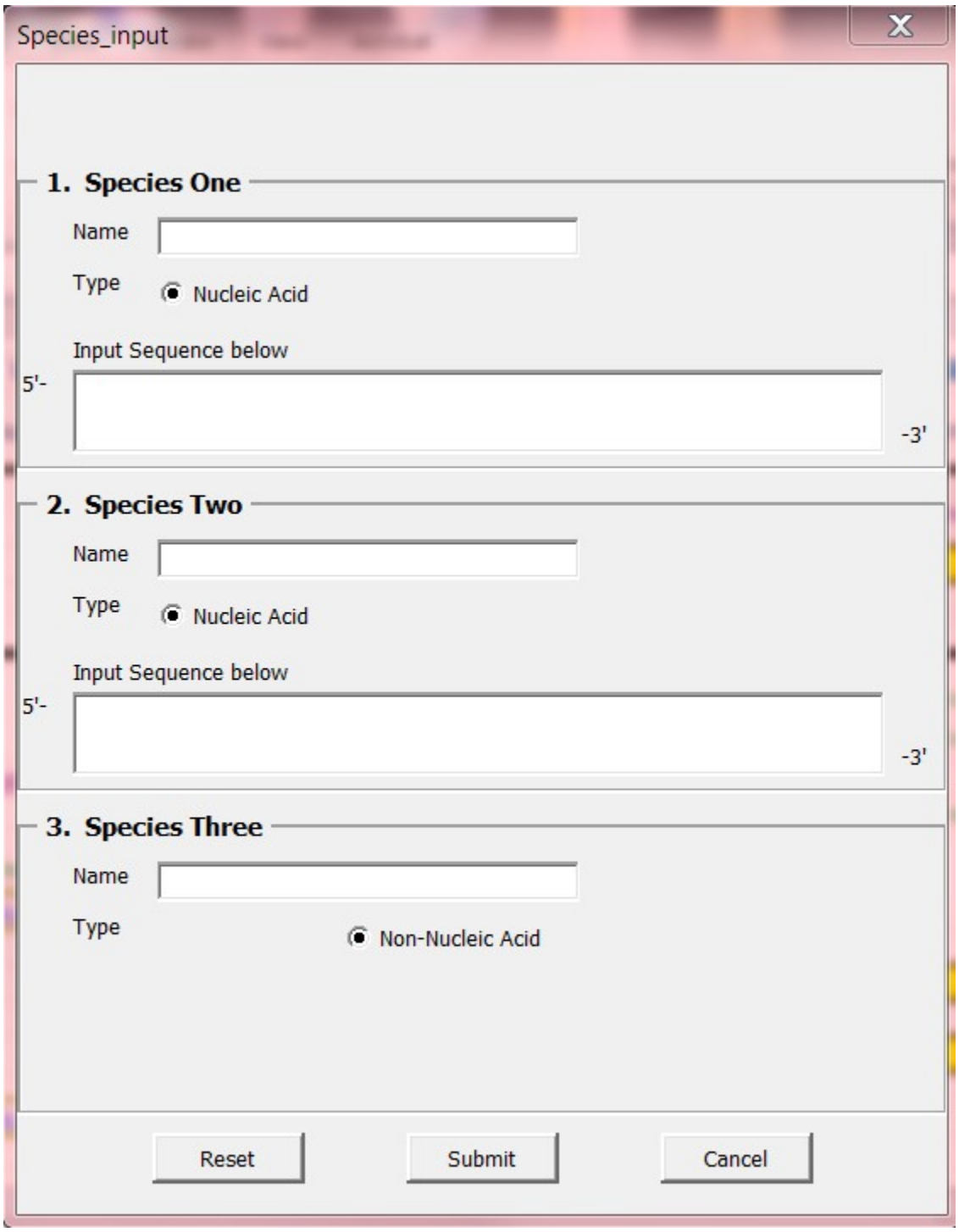

Figure 5-4 Screenshot of the pop-up box for species information in Step 1-2 in Spreadsheet II.

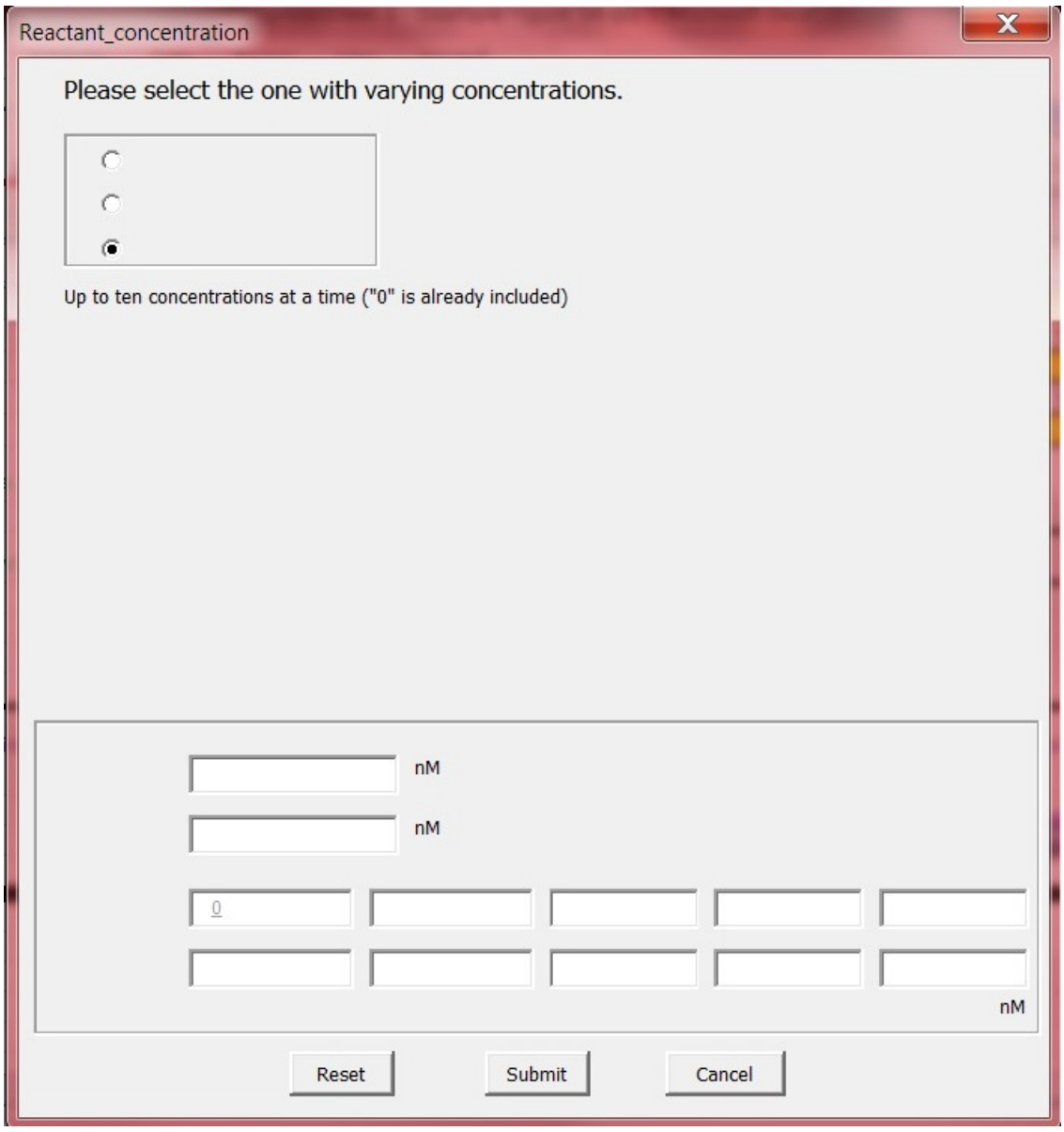

Figure 5-5 Screenshot of pop-up box for concentrations in Step 3-1 in Spreadsheet II

5.4 Testing of the Spreadsheets

The two spreadsheets were tested extensively with various situations to make sure all steps and functions work as well as desired. An example from spreadsheet II is presented here to show how to use this spreadsheet to design the nucleic acid probe sequences and experimental conditions. The example used is aptamer-based competitive nucleic acid

ATP probes reported in our group's previous paper [110, 119]. The detection of ATP is based on the hybridization of the ATP aptamer and the competitor probe. With ATP, the competitor would be free and fluorescence would be quenched. Without ATP, the competitor would hybridize with aptamer and fluorescence intensity is high. Therefore, the amount of duplex formed by competitor and ATP aptamer could represent the fluorescence intensity. The lower the fluorescence intensity the more ATP presents. Figure 5-6A shows the comparison between two competitors under the same conditions (300 mM NaCl). The two ATP nucleic acid probes that used here were designed based on a generic strategy developed by our group [110, 119]. They are named as P1 (5'-ACC TGG GAA TAC TCC CCC-3') and P2 (5'-ACC TTC CTC CGG TTA GAA GGT-3'). The nucleic acid probes are complementary to an anti-ATP DNA aptamer (5'-ACC TGG GGG AGT ATT GCG GAG GAA GGT-3') [119]. The results indicate that probe sequence would significantly affect the performance of biosensor in detection. Figure 5-6B shows the comparison of P2 in different salt concentrations (300 mM NaCl vs. 10 mM NaCl). It suggests that salt concentration is crucial in detection. The above modeling results demonstrate that the Excel platform could be a very usefully tool in guiding the design of nucleic acid probes and experimental conditions in biosensor applications.

A

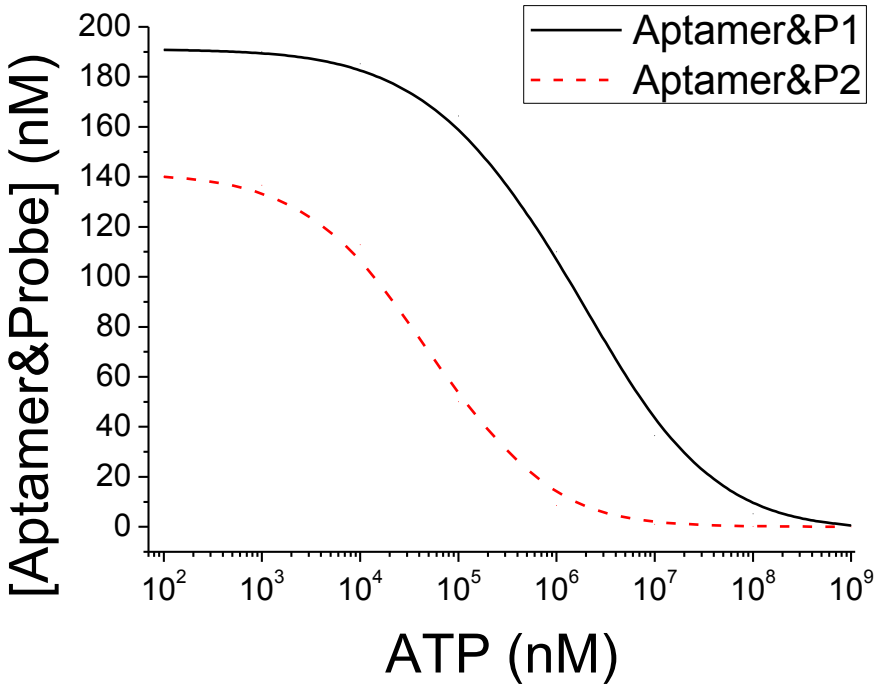

B

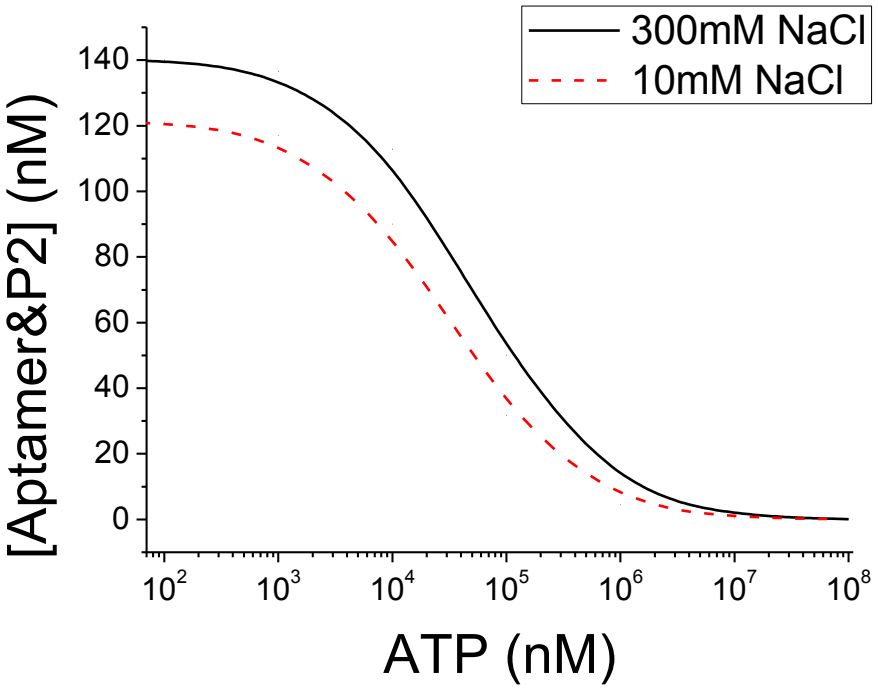

Figure 5-6 Application of Spreadsheet II in optimum design of biosensors. (A) Comparison between P1 and P2 (B) Effect of salt on P2. [Apatmer^{inital}]=200 nM, [Probe^{initial}]=200 nM, 5 mM $MgCl_2$, $K_{aptamer\&ATP}^{App}$ = 6000 nM, 25°C

5.5 Conclusion

We have provided two spreadsheets based on Microsoft® Excel macros and Visual Basic Applications. These spreadsheets could compute for equilibrium concentrations of up to three nucleic acid molecules or two nucleic acid molecules and one non-nucleic acid molecule. It would allow biomedical researchers who are usually not familiar with thermodynamics modeling, numerical methods and computational skills to compute for the equilibrium concentrations of interactions involving up to three molecules. A total of ten sets of concentrations could be obtained in one computation. These spreadsheets are well built and easy-to-use. The buttons and links are designed to be user-friendly. These two spreadsheets have been tested under different conditions. The two Excel spreadsheets will save users great amount of time and budget in designing nucleic acid sequences and experimental condition of biosensors.

Chapter 6 Conclusions and Future Work

6.1 Conclusions

In this dissertation, we have studied the interactions between GNPs and nucleobase, nucleoside, nucleotide, ssDNA and dsDNA. The goal is to aid the design of biosensors based on GNPs and DNA probes to detect DNA oligonucleotides and other molecules. Systematical thermodynamics and kinetics experimental investigations were conducted on the interactions between DNA molecules and GNPs. A platform based on Excel using VBA and macros was provided to quantitatively study the interactions between DNA probes and target molecules, which could be nucleic acids or non-nucleic acid molecules.

Colorimetric method was used to study the interactions between GNPs and nucleobases, nucleosides and nucleotides. It was observed that nucleobases and nucleosides would destabilize GNPs but nucleotides would stabilize GNPs. It was found that molecules containing base T bind to GNPs the weakest, which agrees with previous studies. It was also found that the structures of aggregated GNPs are different with different molecules.

Colorimetric method was used to study the thermodynamics of interactions between GNPs and DNA. It was found that for interactions between GNPs and DNAs, the binding strength and structure strongly depend on sequence, length, conformation. DNAs with more bases A binds to GNPs stronger than DNAs with more base T. Under the condition

of same DNA concentration, longer DNAs bind to GNPs stronger than shorter ones. However, under the condition of same nucleotide concentration, the effect of binding per nucleotide for shorter DNAs is stronger than longer ones. ssDNA was found to bind to GNPs much stronger than dsDNA. dsDNA with overhangs and mismatches was also studied

Colorimetric method and fluorescent method was used to study the binding kinetics and effect of salt on interactions between DNAs and GNPs. It was found that NaCl concentration and incubation time of DNA to GNPs have great effect on binding between DNA and GNPs. Under certain NaCl concentration range, NaCl would enhance the binding of DNAs to GNPs. In addition, the longer the incubation time, the more DNAs bind to GNPs. The binding kinetics was also found to be sequence dependent.

A platform based on Microsoft® Excel formulas and VBA was built to study the interactions between DNA and target molecules. The platform was established on thermodynamics based quantitative model to compute for the equilibrium concentrations. The platform is user-friendly and accessible to scientific researchers who are not familiar with thermodynamics knowledge or computational skills.

In conclusion, the results of this dissertation could be used to help optimize the design of biosensors based on GNPs and DNA probes.

6.2 Future Work

Suggestion for future work can be summarized as following:

1. In this dissertation, only two structures of DNA were considered, random coil and self-structure. Other DNA structures including hair pin structure and higher order self-structure formed by DNAs containing base G could also be considered in future work.

2. The interactions between target molecules and GNPs are not considered in our work. For example, the metal ion K^+ would aggregate GNPs and the protein BSA could prevent GNPs from aggregation. These interactions are of significant importance in the application of biosensors.

3. In the future, methods like transmission electron microscopy (TEM) could be used to investigate the structure of the interactions between GNPs and DNAs, which would give a better understanding on how they interact with each other.

References

1. Wang, J.S. and X.G. Qu, *Recent progress in nanosensors for sensitive detection of biomolecules.* Nanoscale, 2013. **5**(9): p. 3589-3600.

2. Turner, A.P.F., I. Karube, and G.S. Wilson, *Biosensors. Fundamentals and applications*. Biosensors. Fundamentals and applications. 1987: Oxford University Press, Oxford, New York etc. i-xvi, 1-770.

3. Grieshaber, D., et al., *Electrochemical biosensors - Sensor principles and architectures.* Sensors, 2008. **8**(3): p. 1400-1458.

4. Scheller, F.W., et al., *Biosensors - Fundamentals, applications and trends.* Sensors and Actuators B-Chemical, 1991. **4**(1-2): p. 197-206.

5. Saharudin Haron, A.K.R., *Optical biodetection of cadimium and lead ions in water.* Medical Engineering and Physics, 2006. **28**(10): p. 978-981.

6. Pohanka, M., P. Skladal, and M. Kroea, *Biosensors for biological warfare agent detection.* Defence Science Journal, 2007. **57**(3): p. 185-193.

7. Lambrianou, A., S. Demin, and E.H. Hall, *Protein engineering and electrochemical biosensors*, in *biosensing for the 21st Century*, R. Renneberg and F. Lisdat, Editors. 2008, Springer Berlin Heidelberg. p. 65-96.

8. Pohanka, M., D. Jun, and K. Kuca, *Mycotoxin assays using biosensor technology: A review.* Drug and Chemical Toxicology, 2007. **30**(3): p. 253-261.

9. *Optical Biosensors: A Revolution towards quantum nanoscale electronics device fabrication.* Journal of Biomedicine and Biotechnology, 2011. **2011**.

10. Luo, X.-L., et al., *Glucose biosensor based on ENFET doped with SiO< sub> 2</sub> nanoparticles.* Sensors and Actuators B: Chemical, 2004. **97**(2): p. 249-255.

11. Sant, W., et al., *Development of chemical field effect transistors for the detection of urea.* Sensors and Actuators B: Chemical, 2003. **95**(1): p. 309-314.

12. Iqbal, M., et al., *Label-Free biosensor arrays based on silicon ring resonators and high-speed optical scanning instrumentation.* Ieee Journal of Selected Topics in Quantum Electronics, 2010. **16**(3): p. 654-661.

13. Witzens, J. and M. Hochberg, *Optical detection of target molecule induced aggregation of nanoparticles by means of high-Q resonators.* Optics Express, 2011. **19**(8): p. 7034-7061.

14. Narsaiah, K., et al., *Optical biosensors for food quality and safety assurance-a review.* Journal of Food Science and Technology-Mysore, 2012. **49**(4): p. 383-406.

15. Pandey, P., M. Datta, and B.D. Malhotra, *Prospects of nanomaterials in biosensors.* Analytical Letters, 2008. **41**(2): p. 159-209.

16. Njoki, P.N., et al., *Size correlation of optical and spectroscopic properties for gold nanoparticles.* Journal of Physical Chemistry C, 2007. **111**(40): p. 14664-14669.

17. Orendorff, C.J., T.K. Sau, and C.J. Murphy, *Shape-dependent plasmon-resonant gold nanoparticles.* Small, 2006. **2**(5): p. 636-639.

18. Chirea, M., et al., *Size-dependent electrochemical properties of gold nanorods.* Journal of Physical Chemistry C, 2009. **113**(30): p. 13077-13087.

19. Castaneda, M.T., S. Alegret, and A. Merkoci, *Electrochemical sensing of DNA using gold nanoparticles.* Electroanalysis, 2007. **19**(7-8): p. 743-753.

20. Wang, Z. and Y. Lu, *Functional DNA directed assembly of nanomaterials for biosensing.* Journal of Materials Chemistry, 2009. **19**(13): p. 1788-1798.

21. Norman, T.J., et al., *Near infrared optical absorption of gold nanoparticle aggregates.* Journal of Physical Chemistry B, 2002. **106**(28): p. 7005-7012.

22. Kundu, S. and H. Liang, *Polyelectrolyte-mediated non-micellar synthesis of monodispersed 'aggregates' of gold nanoparticles using a microwave approach.* Colloids and Surfaces a-Physicochemical and Engineering Aspects, 2008. **330**(2-3): p. 143-150.

23. Kim, T., et al., *Kinetics of gold nanoparticle aggregation: Experiments and modeling.* Journal of Colloid and Interface Science, 2008. **318**(2): p. 238-243.

24. Link, S., M.B. Mohamed, and M.A. El-Sayed, *Simulation of the optical absorption spectra of gold nanorods as a function of their aspect ratio and the effect of the medium dielectric constant.* Journal of Physical Chemistry B, 1999. **103**(16): p. 3073-3077.

25. Kelly, K.L., et al., *The optical properties of metal nanoparticles: The influence of size, shape, and dielectric environment.* Journal of Physical Chemistry B, 2003. **107**(3): p. 668-677.

26. Xiao, Y., et al., *Shape and color of Au nanoparticles follow biocatalytic processes.* Langmuir, 2005. **21**(13): p. 5659-5662.

27. Lee, K.-S. and M.A. El-Sayed, *Gold and silver nanoparticles in sensing and imaging: Sensitivity of plasmon response to size, shape, and metal composition.* Journal of Physical Chemistry B, 2006. **110**(39): p. 19220-19225.

28. Genevieve, M., et al., *Biofunctionalization of gold nanoparticles and their spectral properties.* Microelectronic Engineering, 2007. **84**(5-8): p. 1710-1713.

29. Huang, H.-C., et al., *Optically responsive gold nanorod-polypeptide assemblies.* langmuir, 2008. **24**(24): p. 14139-14144.

30. Chen, H., et al., *Shape- and size-dependent refractive index sensitivity of gold nanoparticles.* Langmuir, 2008. **24**(10): p. 5233-5237.

31. Liu, S.Q., D. Leech, and H.X. Ju, *Application of colloidal gold in protein immobilization, electron transfer, and biosensing.* Analytical Letters, 2003. **36**(1): p. 1-19.

32. Lakowicz, J.R., *Radiative decay engineering: Biophysical and biomedical applications.* Analytical Biochemistry, 2001. **298**(1): p. 1-24.

33. Campion, A., et al., *Electronic-energy transfer to metal-surfaces - A test of classical image dipole theory at short distances.* Chemical Physics Letters, 1980. **73**(3): p. 447-450.

34. Debye, P.H., E, *The theory of electrolytes. I. Lowering of freezing point and related phenomena.* Physikalische Zeitschrift, 1923. **24**: p. 185-206.

35. Derjaguin, B. and L. Landau, *Theory of the stability of strongly charged lyophobic sols and of the adhesion of strongly charged-particles in solutions of electrolytes.* Progress in Surface Science, 1993. **43**(1-4): p. 30-59.

36. Verwey, E.J., K.v. Nes, and J.T.G. Overbeek, *Theory of the stability of lyophobic colloids*. 1948, New York: Elsevier.

37. Hunter, R.J., *Introduction to modern colloid science*. 1993: Oxford University Press.

38. Mirnik, M., *Schulze-hardy rule and mass action law.* Nature, 1961. **190**(477): p. 689-&.

39. Cosgrove, T., *Colloid science : principles, methods and applications*. 2005, Oxford, UK; Ames, Iowa: Blackwell Pub.

40. Rosi, N.L. and C.A. Mirkin, *Nanostructures in biodiagnostics.* Chemical Reviews, 2005. **105**(4): p. 1547-1562.

41. Sharrna, P., et al., *Nanoparticles for bioimaging.* Advances in Colloid and Interface Science, 2006. **123**: p. 471-485.

42. Marazuela, M. and M. Moreno-Bondi, *Fiber-optic biosensors – an overview.* Analytical and Bioanalytical Chemistry, 2002. **372**(5-6): p. 664-682.

43. Jayasena, S.D., *Aptamers: An emerging class of molecules that rival antibodies in diagnostics.* Clinical Chemistry, 1999. **45**(9): p. 1628-1650.

44. Clark, S.L. and V.T. Remcho, *Aptamers as analytical reagents.* Electrophoresis, 2002. **23**(9): p. 1335-1340.

45. Jenison, R.D., et al., *High-resolution molecular discrimination by RNA.* Science, 1994. **263**(5152): p. 1425-1429.

46. Tombelli, S., A. Minunni, and A. Mascini, *Analytical applications of aptamers.* Biosensors & Bioelectronics, 2005. **20**(12): p. 2424-2434.

47. Hermann, T. and D.J. Patel, *Biochemistry - Adaptive recognition by nucleic acid aptamers.* Science, 2000. **287**(5454): p. 820-825.

48. Li, H.X. and L. Rothberg, *Colorimetric detection of DNA sequences based on electrostatic interactions with unmodified gold nanoparticles.* Proceedings of the National Academy of Sciences of the United States of America, 2004. **101**(39): p. 14036-14039.

49. Kim, C.K., et al., *Gold-nanoparticle-based miniaturized laser-induced fluorescence probe for specific DNA hybridization detection: studies on size-dependent optical properties.* Nanotechnology, 2006. **17**(13): p. 3085-3093.

50. Wang, L., et al., *Unmodified gold nanoparticles as a colorimetric probe for potassium DNA aptamers.* Chemical Communications, 2006(36): p. 3780-3782.

51. Wang, J., et al., *A gold nanoparticle-based aptamer target binding readout for ATP assay.* Advanced Materials, 2007. **19**(22): p. 3943-+.

52. Lang, B., *Hybridization thermodynamics of DNA bound to gold nanoparticles.* Journal of Chemical Thermodynamics, 2010. **42**(12): p. 1435-1440.

53. Storhofff, J.J., et al., *Sequence-dependent stability of DNA-modified gold nanoparticles.* Langmuir, 2002. **18**(17): p. 6666-6670.

54. Gourishankar, A., et al., *Isothermal titration calorimetry studies on the binding of DNA bases and PNA base monomers to gold nanoparticles.* Journal of the American Chemical Society, 2004. **126**(41): p. 13186-13187.

55. Demers, L.M., et al., *Thermal desorption behavior and binding properties of DNA bases and nucleosides on gold.* Journal of the American Chemical Society, 2002. **124**(38): p. 11248-11249.

56. Zhao, W., et al., *Tunable stabilization of gold nanoparticles in aqueous solutions by mononucleotides.* Langmuir, 2007. **23**(13): p. 7143-7147.

57. Yang, J., et al., *Dissociation of double-stranded DNA by small metal nanoparticles.* Journal of Inorganic Biochemistry, 2007. **101**(5): p. 824-830.

58. Kimling, J., et al., *Turkevich method for gold nanoparticle synthesis revisited.* Journal of Physical Chemistry B, 2006. **110**(32): p. 15700-15707.

59. Khlebtsov, N.G., *Determination of size and concentration of gold nanoparticles from extinction spectra.* Analytical Chemistry, 2008. **80**(17): p. 6620-6625.

60. Gittings, M.R. and D.A. Saville, *The determination of hydrodynamic size and zeta potential from electrophoretic mobility and light scattering measurements.* Colloids and Surfaces a-Physicochemical and Engineering Aspects, 1998. **141**(1): p. 111-117.

61. Pusey, P.N. and W. Vanmegen, *Dynamic light-scattering by non-ergodic media.* Physica A, 1989. **157**(2): p. 705-741.

62. Brown, J.C., et al., *Light-scattering study of dynamic and time-averaged correlations in dispersions of charged-particles.* Journal of Physics a-Mathematical and General, 1975. **8**(5): p. 664-682.

63. Minton, A.P., *The influence of macromolecular crowding and macromolecular confinement on biochemical reactions in physiological media.* Journal of Biological Chemistry, 2001. **276**(14): p. 10577-10580.

64. Zhou, H.-X., G. Rivas, and A.P. Minton, *Macromolecular crowding and confinement: Biochemical, biophysical, and potential physiological consequences*, in *Annual Review of Biophysics*. 2008. p. 375-397.

65. Digiano, F.A., et al., *Simplified competitive equilibrium adsorption model.* Chemical Engineering Science, 1978. **33**(12): p. 1667-1673.

66. Sheindorf, C., M. Rebhun, and M. Sheintuch, *A freundlich-type multicomponent isotherm.* Journal of Colloid and Interface Science, 1981. **79**(1): p. 136-142.

67. Jaroniec, M., A. Derylo, and A. Marczewski, *The langmuir-freundlich equation in adsorption from dilute-solutions on solids.* Monatshefte Fur Chemie, 1983. **114**(4): p. 393-397.

68. Levan, M.D. and T. Vermeulen, *Binary langmuir and freundlich isotherms for ideal adsorbed solutions.* Journal of Physical Chemistry, 1981. **85**(22): p. 3247-3250.

69. Hunter, R.J. and L.R. White, *Foundations of colloid science*. 1987, Oxford [Oxfordshire]; New York: Clarendon Press ; Oxford University Press.

70. Zhao, W., L. Lin, and I.M. Hsing, *Nucleotide-mediated size fractionation of gold nanoparticles in aqueous solutions.* Langmuir, 2010. **26**(10): p. 7405-7409.

71. Demers, L.M., et al., *A fluorescence-based method for determining the surface coverage and hybridization efficiency of thiol-capped oligonucleotides bound to gold thin films and nanoparticles.* Analytical Chemistry, 2000. **72**(22): p. 5535-5541.

72. Hartwich, G., et al., *Electrochemical study of electron transport through thin DNA films.* Journal of the American Chemical Society, 1999. **121**(46): p. 10803-10812.

73. Steel, A.B., T.M. Herne, and M.J. Tarlov, *Electrochemical quantitation of DNA immobilized on gold.* Analytical Chemistry, 1998. **70**(22): p. 4670-4677.

74. Herne, T.M. and M.J. Tarlov, *Characterization of DNA probes immobilized on gold surfaces.* Journal of the American Chemical Society, 1997. **119**(38): p. 8916-8920.

75. Peterlinz, K.A., et al., *Observation of hybridization and dehybridization of thiol-tethered DNA using two-color surface plasmon resonance spectroscopy.* Journal of the American Chemical Society, 1997. **119**(14): p. 3401-3402.

76. Piscevic, D., et al., *Oligonucleotide hybridization observed by surface-plasmon optical techniques.* Applied Surface Science, 1995. **90**(4): p. 425-436.

77. Levicky, R., et al., *Using self-assembly to control the structure of DNA monolayers on gold: A neutron reflectivity study.* Journal of the American Chemical Society, 1998. **120**(38): p. 9787-9792.

78. Haick, H., *Chemical sensors based on molecularly modified metallic nanoparticles.* Journal of Physics D-Applied Physics, 2007. **40**(23): p. 7173-7186.

79. Lytton-Jean, A.K.R. and C.A. Mirkin, *A thermodynamic investigation into the binding properties of DNA functionalized gold nanoparticle probes and molecular fluorophore probes.* Journal of the American Chemical Society, 2005. **127**(37): p. 12754-12755.

80. Stevenson, K.A., et al., *Covalent attachment of gold nanoparticles to DNA templates.* Journal of Nanoscience and Nanotechnology, 2002. **2**(3-4): p. 397-404.

81. Thaxton, C.S., D.G. Georganopoulou, and C.A. Mirkin, *Gold nanoparticle probes for the detection of nucleic acid targets.* Clinica Chimica Acta, 2006. **363**(1-2): p. 120-126.

82. Steel, A.B., et al., *Immobilization of nucleic acids at solid surfaces: Effect of oligonucleotide length on layer assembly.* Biophysical Journal, 2000. **79**(2): p. 975-981.

83. Sandstrom, P., M. Boncheva, and B. Akerman, *Nonspecific and thiol-specific binding of DNA to gold nanoparticles.* Langmuir, 2003. **19**(18): p. 7537-7543.

84. Kimura-Suda, H., et al., *Base-dependent competitive adsorption of single-stranded DNA on gold.* Journal of the American Chemical Society, 2003. **125**(30): p. 9014-9015.

85. Wolf, L.K., Y. Gao, and R.M. Georgiadis, *Sequence-dependent DNA immobilization: Specific versus nonspecific contributions.* Langmuir, 2004. **20**(8): p. 3357-3361.

86. Parak, W.J., et al., *Conformation of oligonucleotides attached to gold nanocrystals probed by gel electrophoresis.* Nano Letters, 2003. **3**(1): p. 33-36.

87. Brown, K.A., S. Park, and K. Hamad-Schifferli, *Nucleotide-surface interactions in DNA-modified Au-nanoparticle conjugates: Sequence effects on reactivity and hybridization.* Journal of Physical Chemistry C, 2008. **112**(20): p. 7517-7521.

88. Burge, S., et al., *Quadruplex DNA: sequence, topology and structure.* Nucleic Acids Research, 2006. **34**(19): p. 5402-5415.

89. Campbell, N.H. and S. Neidle, *G-quadruplexes and metal ions.* Metal ions in life sciences, 2012. **10**: p. 119-34.

90. Loweth, C.J., et al., *DNA-based assembly of gold nanocrystals.* Angewandte Chemie-International Edition, 1999. **38**(12): p. 1808-1812.

91. Yang, J., et al., *Single stranded DNA stabilization and assembly of Au nanoparticles of different sizes.* Chemical Physics, 2006. **323**(2-3): p. 304-312.

92. Li, H., et al., *Assays based on differential adsorption of single-stranded and double-stranded DNA on unfunctionalized gold nanoparticles in a colloidal suspension.* Plasmonics, 2007. **2**(4): p. 165-171.

93. Bishop, J., et al., *Competitive displacement of DNA during surface hybridization.* Biophysical Journal, 2007. **92**(1): p. L10-L12.

94. Chavez, J.L., et al., *Colorimetric detection with aptamer-gold nanoparticle conjugates: effect of aptamer length on response.* Journal of Nanoparticle Research, 2012. **14**(10).

95. Elghanian, R., et al., *Selective colorimetric detection of polynucleotides based on the distance-dependent optical properties of gold nanoparticles.* Science, 1997. **277**(5329): p. 1078-1081.

96. Chiu, C.S. and S. Gwo, *Quantitative surface acoustic wave detection based on colloidal gold nanoparticles and their bioconjugates.* Analytical Chemistry, 2008. **80**(9): p. 3318-3326.

97. Liptak, B.G., *Instrument engineers' handbook, Fourth Edition, Volume Two: Process Control and Optimization*. 2010: Taylor & Francis.

98. Lewis, R.W., P. Nithiarasu, and K. Seetharamu, *Fundamentals of the Finite Element Method for Heat and Fluid Flow*. 2004: Wiley.

99. Storhoff, J.J., et al., *One-pot colorimetric differentiation of polynucleotides with single base imperfections using gold nanoparticle probes.* Journal of the American Chemical Society, 1998. **120**(9): p. 1959-1964.

100. Hall, B., J.R. Hesselberth, and A.D. Ellington, *Computational selection of nucleic acid biosensors via a slip structure model.* Biosensors & Bioelectronics, 2007. **22**(9-10): p. 1939-1947.

101. Dirks, R.M., et al., *Paradigms for computational nucleic acid design.* Nucleic Acids Research, 2004. **32**(4): p. 1392-1403.

102. Penchovsky, R. and R.R. Breaker, *Computational design and experimental validation of oligonucleotide-sensing allosteric ribozymes.* Nature Biotechnology, 2005. **23**(11): p. 1424-1433.

103. Monroe, W.T. and F.R. Haselton, *Molecular beacon sequence design algorithm.* Biotechniques, 2003. **34**(1): p. 68-+.

104. Meserve, D., et al., *A double-stranded molecular probe for homogeneous nucleic acid analysis.* Analyst, 2008. **133**(8): p. 1013-1019.

105. Ragan, C., M. Zuker, and M.A. Ragan, *Quantitative prediction of miRNA-mRNA interaction based on equilibrium concentrations.* Plos Computational Biology, 2011. **7**(2): p. 11.

106. Gelfand, C.A., et al., *A quantitative method for evaluating the stabilities of nucleic acids.* Proceedings of the National Academy of Sciences of the United States of America, 1999. **96**(11): p. 6113-6118.

107. Tsourkas, A., et al., *Hybridization kinetics and thermodynamics of molecular beacons.* Nucleic Acids Research, 2003. **31**(4): p. 1319-1330.

108. Vallee-Belisle, A., F. Ricci, and K.W. Plaxco, *Thermodynamic basis for the optimization of binding-induced biomolecular switches and structure-switching biosensors.* Proceedings of the National Academy of Sciences of the United States of America, 2009. **106**(33): p. 13802-13807.

109. Bonnet, G., et al., *Thermodynamic basis of the enhanced specificity of structured DNA probes.* Proceedings of the National Academy of Sciences of the United States of America, 1999. **96**(11): p. 6171-6176.

110. Li, N., *Detection of non-nucleic acid targets with an unmodified aptamer and a fluorogenic competitor.* Jala, 2010. **15**(3): p. 189-197.

111. SantaLucia, J., *A unified view of polymer, dumbbell, and oligonucleotide DNA nearest-neighbor thermodynamics.* Proceedings of the National Academy of Sciences of the United States of America, 1998. **95**(4): p. 1460-1465.

112. Markham, N.R. and M. Zuker, *DINAMelt web server for nucleic acid melting prediction.* Nucleic Acids Research, 2005. **33**: p. W577-W581.

113. Markham, N.R. and M. Zuker, *UNAFold: software for nucleic acid folding and hybridization.* Methods in molecular biology (Clifton, N.J.), 2008. **453**: p. 3-31.

114. Zuker, M., *Mfold web server for nucleic acid folding and hybridization prediction.* Nucleic Acids Research, 2003. **31**(13): p. 3406-3415.

115. Reuter, J.S. and D.H. Mathews, *RNAstructure: software for RNA secondary structure prediction and analysis.* Bmc Bioinformatics, 2010. **11**.

116. de Levie, R., *Advanced excelR for excientific data analysis*. 2004: Oxford University Press, Incorporated.

117. Bovey, R., et al., *Professional Excel Development: The definitive guide to developing applications using microsoft excel and VBA, and .NET*. 2009: Addison Wesley Professional.

118. Yalta, A.T., *The accuracy of statistical distributions in Microsoft (R) Excel 2007.* Computational Statistics & Data Analysis, 2008. **52**(10): p. 4579-4586.

119. Li, N. and C.-M. Ho, *Aptamer-based optical probes with separated molecular recognition and signal transduction modules.* Journal of the American Chemical Society, 2008. **130**(8): p. 2380-2381.